JUSTUS-LIEBIG-UNIVERSITÄT GIESSEN

INSTITUT FÜR ANORGANISCHE UND ANALYTISCHE CHEMIE

REACTION BEHAVIOR OF IRON AND COPPER COMPLEXES TOWARDS DIOXYGEN

Inaugural-Dissertation

zur Erlangung des Doktorgrades
der Naturwissenschaften
im Fachbereich Biologie und Chemie
der Justus-Liebig-Universität Gießen

vorgelegt von

Jörg Astner

aus
Erlangen

JUSTUS-LIEBIG-UNIVERSITÄT GIESSEN

INSTITUT FÜR ANORGANISCHE UND ANALYTISCHE CHEMIE

REACTION BEHAVIOR OF IRON AND COPPER COMPLEXES TOWARDS DIOXYGEN

Inaugural-Dissertation

zur Erlangung des Doktorgrades
der Naturwissenschaften
im Fachbereich Biologie und Chemie
der Justus-Liebig-Universität Gießen

vorgelegt von

Jörg Astner

aus
Erlangen

Acknowledgements

This work was carried out between March 2002 and December 2005 at the Institute of Inorganic and Analytical Chemistry at the Justus-Liebig-University of Gießen under the supervision of Prof. Dr. S. Schindler.

I especially want to thank Prof. Dr. S. Schindler for his excellent guidance, the fruitful scientific discussions and for financial support.

Furthermore I wish to thank my colleagues Dr. M. Schatz, Dr. M. Leibold, Dr. J. Huber, S. Turba, C. Würtele, T. Neuwert, Dr. Jing-Yuan Xu, T. Nebe, L. Römmling, J. Müller, F. Mehlich, S. Kisslinger and I. Kerezsi for their interest in my work and for maintaining a pleasant atmosphere in the group. I want to mention especially Dr. M. Weitzer; Dr. D. Utz, Dr. S. P. Foxon, and Dr. H. Weiss for their advice and friendship in the starting phase of my work.

I would like to express my gratitude to Prof. Dr. R. Mukherjee, Dr. J. Mukherjee and Dr. V. Balamurugan and the whole group of R. Mukherjee for their help and friendship during my stay at the IIT Kanpur, India.

Last but not least I would like to thank the people of the Institute of Inorganic and Analytical Chemistry at the Justus-Liebig-University of Gießen and of the Institute of Inorganic and Analytical Chemistry at the Friedrich-Alexander-University of Erlangen-Nürnberg for their support of my work.

For my Parents

For Maike

Table of Contents

Ligands used

Chapter 2:

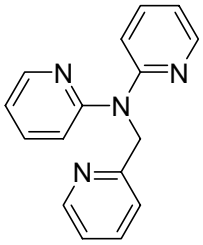

L1

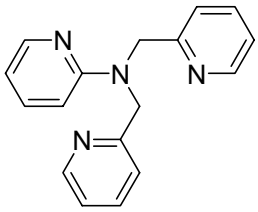

L2

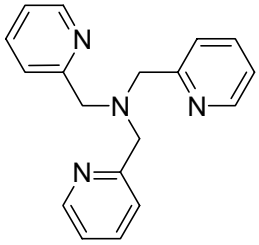

tmpa

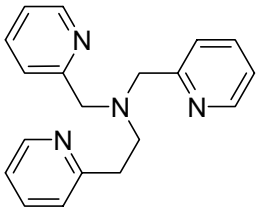

pmea

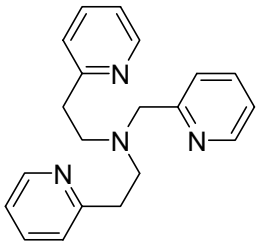

pmap

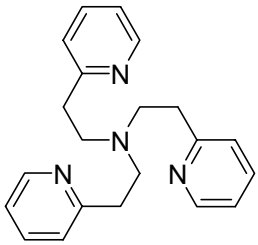

tepa

Chapter 3:

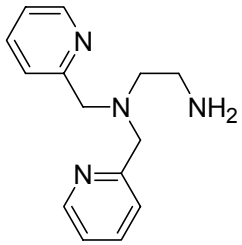

uns-penp

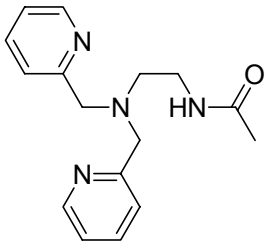

acetyl-uns-penp

Chapter 4:

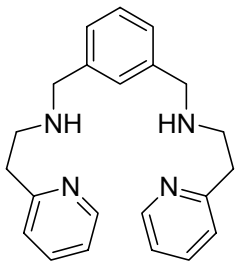

L^3

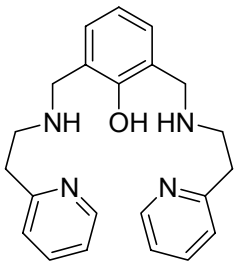

L^3-OH

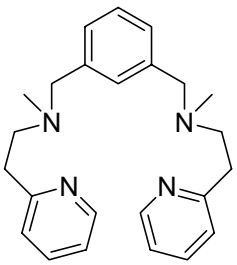

L^4

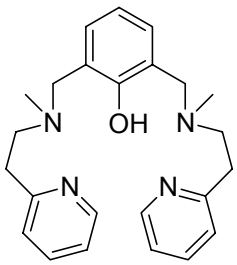

L^4-OH

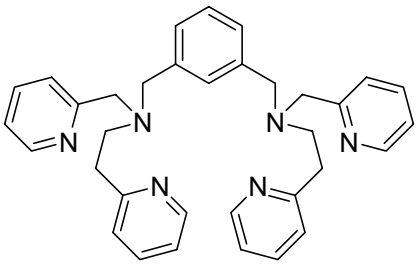

L^5

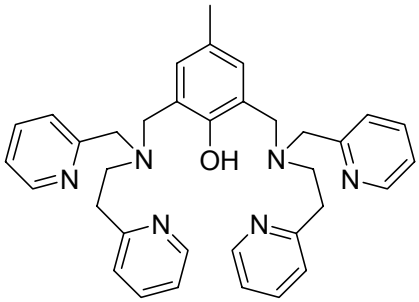

Me-L^5-OH

Chapter 5:

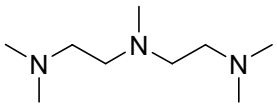

Me_5dien

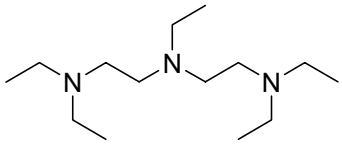

Et_5dien

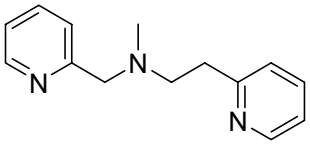

MeL

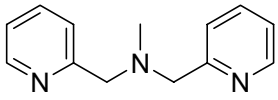

Me-bpa

Abbreviations

BPG	N,N-Bis(2-pyridylmethyl)glycinate
dbc	3,5-Di-*tert*-butyl-catecholate
e. g.	for example (Latin: exempli gratia)
EXAFS	Extended X-Ray absorption fine structure
Hc	Hemocyanin
Hg	Hemoglobin
His	Histidine
Hr	Hemerythrin
IR	Infrared spectroscopy
NTA	Nitrilotriacetate
3,4-PCD	Protocatechuat-3,4-dioxygenase
PDA	N-(2-Pyridylmethyl)iminodiacetate
rR	resonance Raman spectroscopy
SF	Stopped-flow
tcc	Tetrachlorocatecholate
tbc	Tetrabromocatecholate
Tyr	Tyrosine
UV-vis	Ultraviolet-visible spectroscopy
XAS	X-Ray absorption spectroscopy

Chapter 1 – Introduction

1.1 Motivation

In nature a diverse range of chemical reactions is catalysed by metalloenzymes. Metalloenzymes, a subclass of metalloproteins, bind and activate small molecules for specific catalytic reactions. Many metalloenzymes perform remarkable chemical transformations for which, under comparable conditions, no simple analogues in the laboratory exist (for e. g. catalytic reduction of N_2 to NH_3 (nitrogen fixation), the oxidation of water to O_2).

Bioinorganic chemistry constitutes the discipline at the interface of inorganic chemistry and biology. One area bioinorganic chemists are interested in is exploring the reactivity and trying to elucidate the reaction mechanisms of metalloproteins and metalloenzymes. These reactions take place at the so-called “active site” of the enzyme or protein. The active site is formed by metal ions coordinated by donor atoms of the amino acid chains. Parallel to investigations of these enzymes and proteins itself model complexes have been investigated to gain better insight into the biochemical reaction pathways and furthermore to use these compounds in selective catalytic oxidations of organic substrates under mild conditions.

Questions like “Why does an apple turn brown?” or “Why is our blood red, spider’s blood blue and Mr. Spock’s blood green?” lead to the biological transport and activation of dioxygen by metalloproteins and metalloenzymes. Many active sites of these compounds contain iron or copper ions.[1-4]

1.2 Iron and copper proteins

Iron proteins can be classified into two groups, the heme and the non-heme proteins. In heme proteins such as hemoglobin (Hg) or cytochrome P450 the iron centre is incorporated into a porphyrin ring. Hemoglobin is the oxygen transport protein of mammals and is responsible for the red colour of our blood.[3] Cytochrome P450 catalyzes the oxidation of organic substrates by dioxygen, performing key roles in the biosynthesis of essential substances (e.g. vitamin D3). In non-heme proteins like hemerythrin (Hr) or protocatechuat-3,4-dioxygenase

(3,4-PCD) iron is coordinated to amino acid side chains of the protein. Hemerythrin is the dioxygen transporting molecule of some marine worms like annelides and sipunculides.[5] Scheme 1-1 shows the binding of dioxygen to the active site of hemerythrin[3,5] and Figure 1-1 shows the active site of protocatechuat-3,4-dioxygenase.[3] In Chapters 2.1 and 3.1 reactions of model compounds for these iron proteins are described.

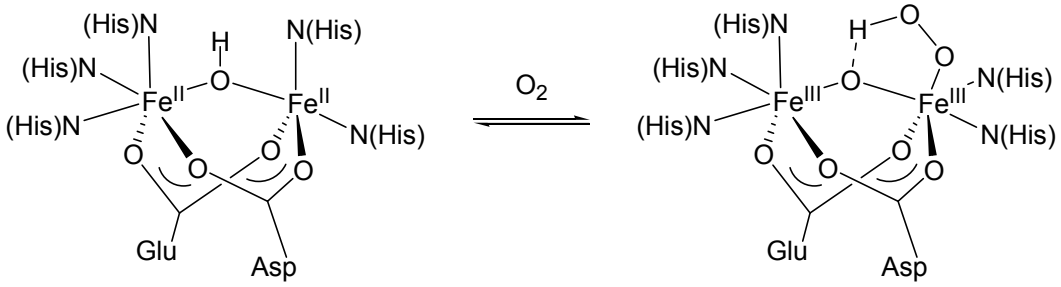

Scheme 1-1: Binding of dioxygen to the active site of hemerythrin

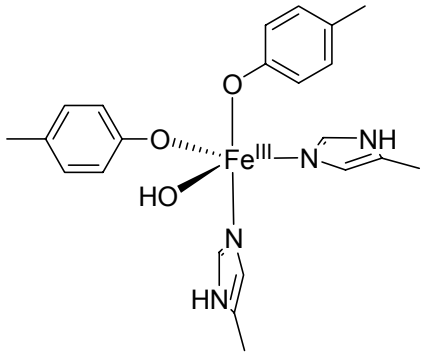

Figure 1-1: Active site of protocatechuat-3,4-dioxygenase[3]

In nature several important enzymes contain copper, ranging from active sites with one up to four copper centres. An overview of copper enzymes and the great variety of their reactions is presented in Figure 1-2.[6] The dioxygen transport protein hemocyanin (Hc, responsible for the blue blood of arthropods such as spiders and molluscs such as snails) is shown in Scheme 1-2.[3] The enzyme tyrosinase has a similar structure, however it acts as a monooxygenase and catalyses the *ortho*-hydroxylation of the amino acid tyrosine (and subsequent oxidation to a chinone). After the polymerisation is complete the pigment melanin is formed (Scheme 1-3), which is responsible for the colour of our skin and furthermore for the browning reaction of vegetables and fruit such as apples.[7] For further reactions and model compounds for these metalloproteins see introductions of Chapter 4 and Chapter 5.

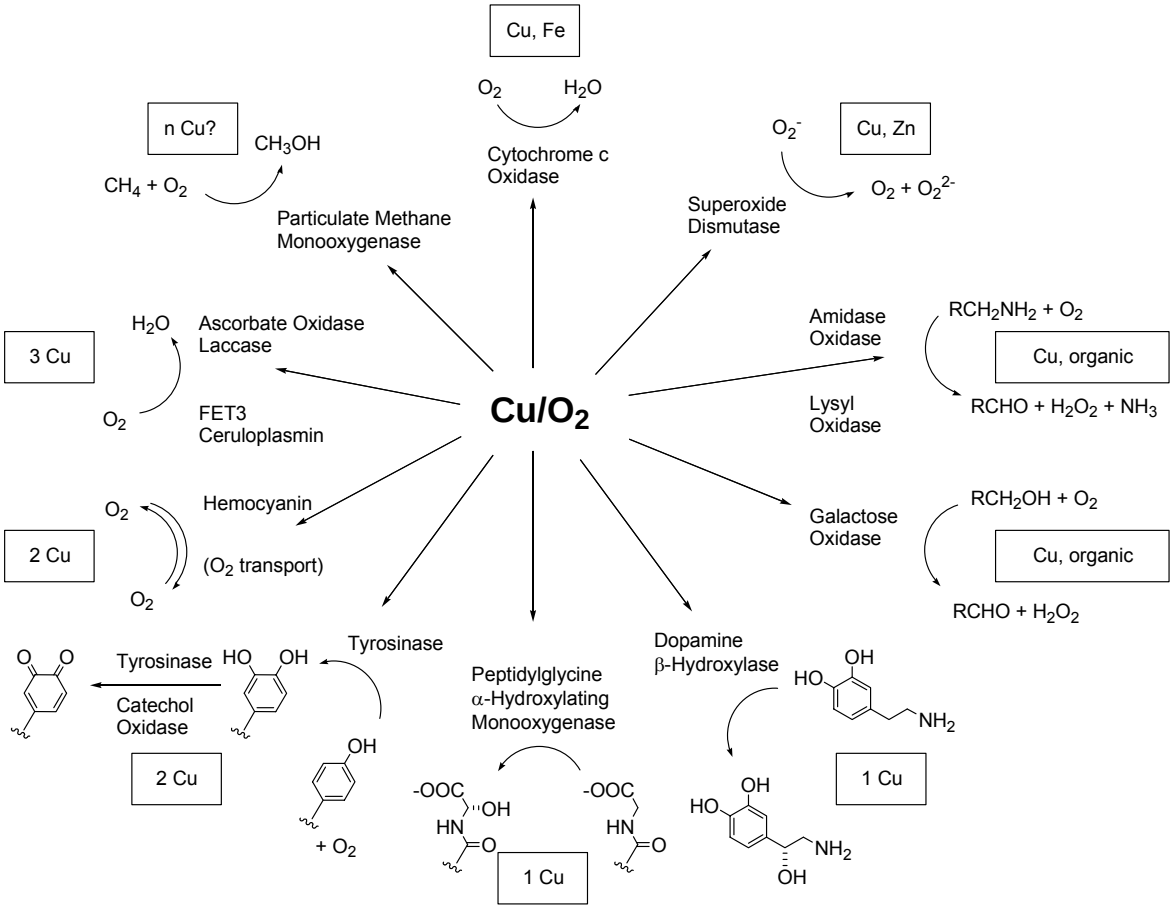

Figure 1-2: Selected copper enzymes

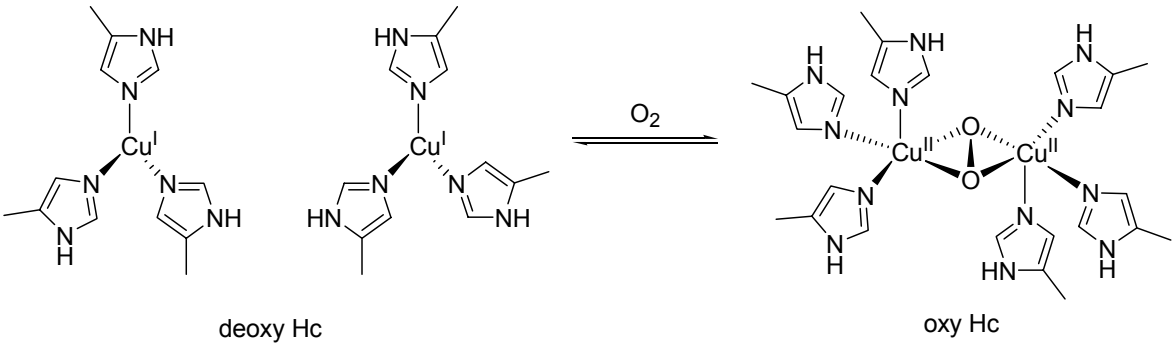

Scheme 1-2: Binding of dioxygen in hemocyanin

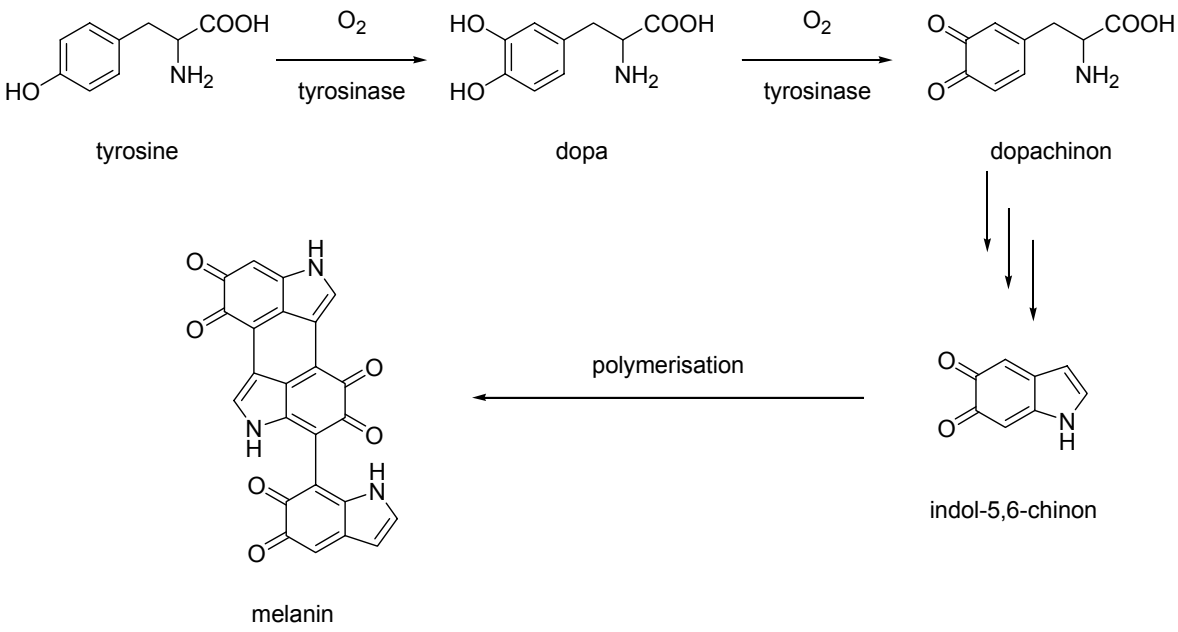

Scheme 1-3: Conversion of tyrosine to melanin catalysed by tyrosinase

1.3 Mechanisms of dioxygen binding

That metalloproteins can bind and activate dioxygen is a consequence of the protein structure. The nature of the protein structure modulates the electronic properties of the metal centres for the enzymatic reaction (e. g. oxidizing the metal centres is only possible if the associated change in geometry is stabilized by the protein). In model compounds for such proteins the ligand systems plays a crucial role in the stabilisation of metal-bound “dioxygen adduct” complexes and therefore the design and synthesis of suitable ligands plays an important role in bioinorganic chemistry. The geometry of the metal complexes is affected by the ligand and is therefore responsible for the stabilisation of the different geometries. These reactions are strongly dependent on solvent and temperature. In the past it was possible using different ligand systems to characterise structurally or spectroscopically copper dioxygen adduct complexes which are shown in Figure 1-3. Similar observations have been made for the according iron complexes, however so far less of these dioxygen adduct complexes have been characterised in detail.[8] The stability and the reactivity of the system can be influenced by changing the ligand system of the model. Accessible pathways for fine tuning are: the ligand donor atoms (e. g. aromatic or aliphatic amine ligand or change of HSAB-acidity), the steric demand, the denticity, the charge, the chelate ring size or introducing electron withdrawing or donating substituents into the ligand. The systematic

change of all these aspects lead to a great variety of copper complexes, which have their analogues in nature (see Figure 1-3).[4]

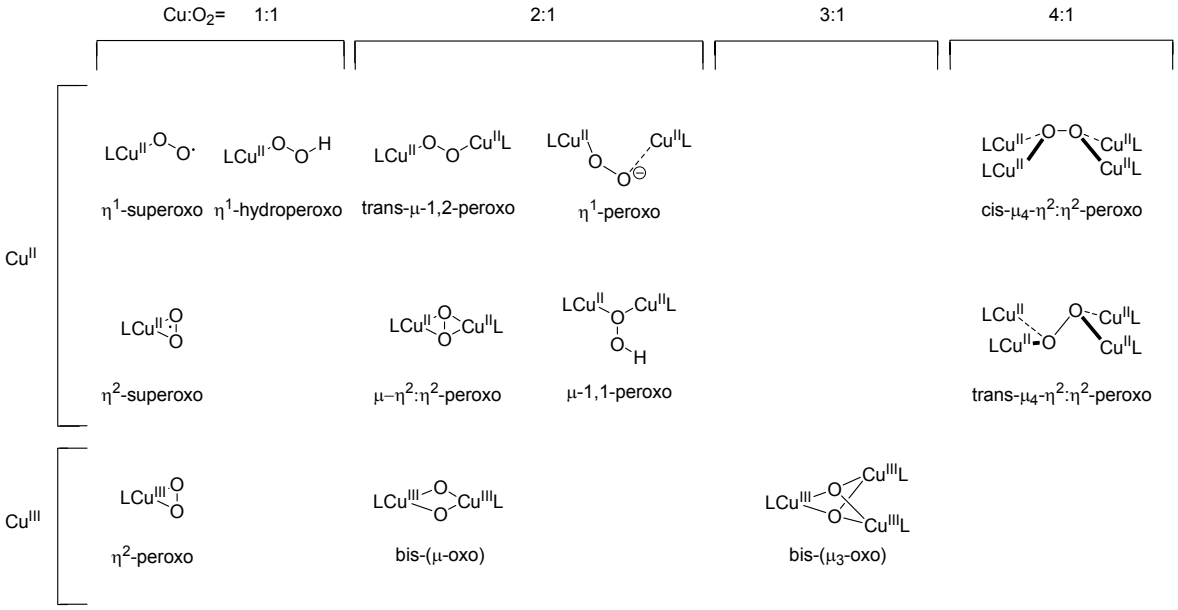

Figure 1-3: Cu/O_2 species

1.4 Characterisation

In order to characterise model complexes of metalloproteins the following physical methods can be employed:

- X-Ray-crystallography: Determination of molecular structure (bond lengths and angles).
- EXAFS (Extended X-Ray absorption fine structure): Information on metal-donor atom distances is obtained.
- XAS (X-Ray absorption spectroscopy): Information on oxidation state of the metal ions can be derived.
- IR/rR (Infrared/ resonance Raman spectroscopy): Information on vibrational modes is achieved.
- UV-vis (ultraviolet-visible spectroscopy): Information on charge transfer or d-d bands of the metal complexes is obtained.
- Kinetics (e. g. SF [Stopped-flow] experiments): Information on the reaction rate and the reaction mechanisms can be derived.

- NMR (nuclear magnetic resonance spectroscopy): Information of chemical environment of atomic cores (e. g. ^{1}H and ^{13}C)
- Electrochemistry: Determination of redox potentials of the metal centres
- Mössbauer spectroscopy: Determination of oxidation state of the metal centres

1.5 Projects

As discussed above it is important to study the reactions of model complexes of iron and copper proteins in detail. Investigations on the following projects were conducted and the results are presented in Chapters 2 – 5.

- The influence of chelate ring size on the reactivity of model complexes for the iron enzyme protocatechuate-3,4-dioxygenase (3,4-PCD) (Chapter 2).
- The effect on the reactivity of the model complexes of 3,4-PCD by systematically replacing the ligand's aromatic donor atoms with aliphatic donor atoms (Chapter 3).
- New model compounds for the enzyme tyrosinase were synthesised and structurally characterised. The magnetic coupling between the bridged copper ions has been determined (Chapter 4).
- The reactivity of another model for the enzyme tyrosinase has been studied by altering steric hindrance, the properties of the donor atoms and the chelate ring size of the ligand (Chapter 5).

Chapter 2 - Chelate Ring Size Variations and their Effects on Coordination Chemistry and Catechol Dioxygenase Reactivity of Iron(III) Complexes

This work has been published previously in *Inorganic Chemistry*.

Merkel, M., Pascaly, M., Krebs, B., Astner, J., Foxon, S., Schindler, S., *Inorg. Chem.*, 2005, 44, 21, 7582-7589.

2.1 Introduction

A large variety of mononuclear non heme iron enzymes are involved in redox processes with molecular oxygen.[8,9] For example, intradiol cleaving catechol dioxygenases catalyse the insertion of dioxygen into catechols[10] and during the oxidation reaction substrates are converted to acyclic *cis,cis*-muconic acid derivatives. Mimicking the structure and function of these enzymes has been an important goal in bioinorganic chemistry during the last decade.[8,11] The crystal structures of a number of complexes of protocatechuate 3,4-dioxygenase (3,4-PCD) from *Pseudomonas putida* reveal an endogenous His_2Tyr_2 donor set,[12-16] and model compounds have been prepared that contained phenolate donor groups. Although such complexes were good structural and spectroscopic models for the active site of 3,4-PCD, they exhibited only poor catechol oxidation abilities. One of the best structural and spectroscopic models to date of the 3,4-PCD-site is a model complex, based upon a modified salen ligand, prepared by Fujii and Funahashi.[17]

The first functional models for catechol dioxygenases were reported by Funabiki, who observed catechol cleavage in the presence of an iron salt, pyridine and bipyridine. However, the nature of the active species involved in the reactions is unknown.[18,19] At present, the most efficient biomimetic model compound for intradiol cleaving catechol dioxygenases is an iron(III) complex of the ligand tris[(2-pyridyl)methyl]amine (tmpa; also abbreviated as tpa in the literature; Scheme 2-1), reported by Que and coworkers in 1991.[20]

This result was derived by systematic variation of tetradentate tripodal ligands in which functional groups were changed from phenolate to carboxylate to pyridine in

order to alter electron-donating properties of the ligand.[8,21] The resulting change in Lewis acidity of the iron(III) centre was observed in the UV-vis-NIR spectra of the complexes. A correlation between the red shift in the LMCT bands of the catecholate complexes and higher catechol dioxygenase activity was observed.[22] In a previous study, we reported that besides electronic effects, the steric demand of the ligands clearly influenced the reactivity of the corresponding iron(III)-catecholate complexes towards dioxygen.[23] It has been reported previously that variations of the chelate ring size strongly affected the properties of manganese and copper compounds.[24-26] However, to date, no attempt has been made to investigate the properties of iron coordination compounds featuring ligands closely related to tmpa, in which the arms of the tripodal ligand have been lengthened or shortened by the insertion or removal of a methylene spacer group (see Scheme 2-1). Therefore, we describe herein the effect of chelate ring size variations on the coordination chemistry and catechol dioxygenase reactivity of the corresponding

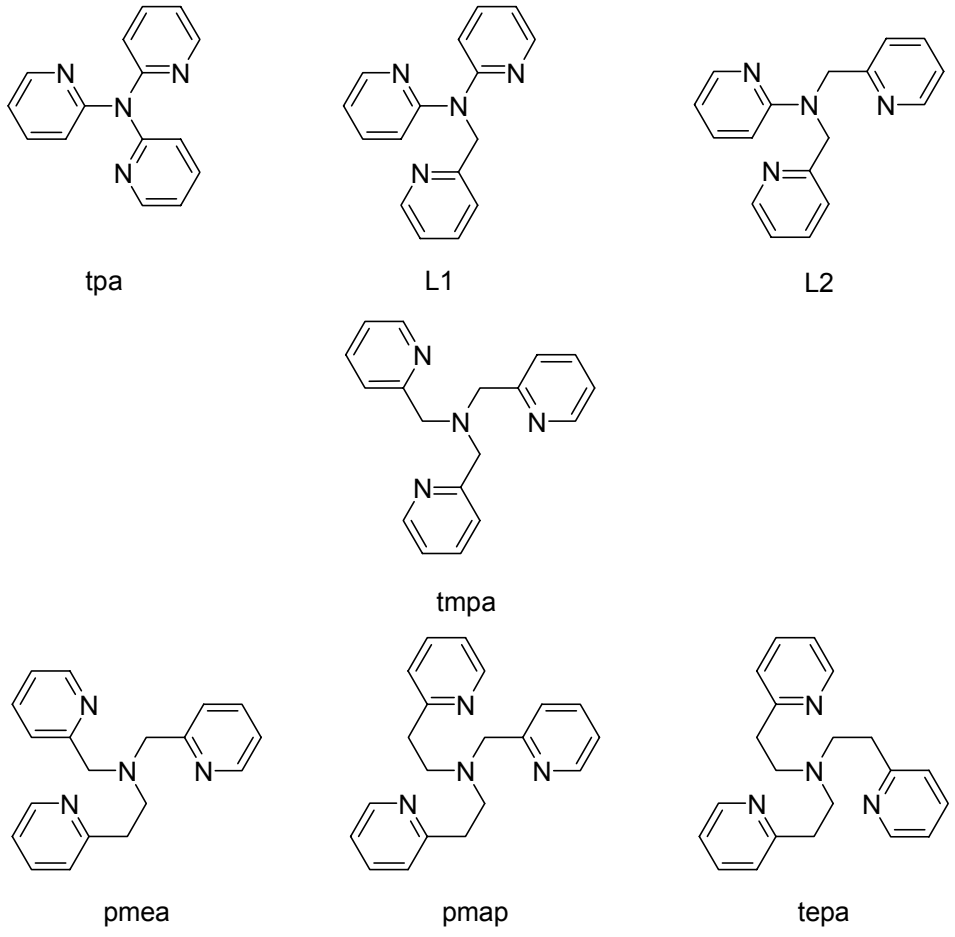

Scheme 2-1: Tmpa-based ligands with shortened and extended arms

iron(III) complexes of the ligands shown in Scheme 2-1 using the catecholates presented in Scheme 2-2.

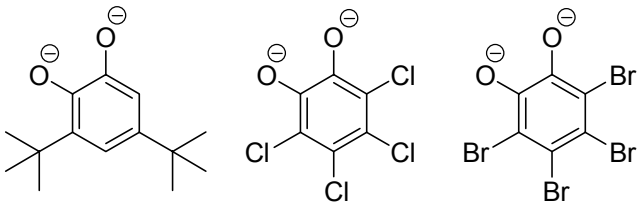

Scheme 2-2: Dianions of substrates and inhibitor substrates used in this study and their abbreviations

2.2 Experimental Section

2.2.1 General Remarks

All chemicals were purchased from commercial sources and used as received. **CAUTION!** *The perchlorate salts used in this study are potentially explosive and should be handled with care*.

2.2.2 Physical Measurements.

Elemental analyses were carried out on an Elementar vario EL III analyser. UV-vis spectra were measured at 25.0°C on a Hewlett-Packard 8453 diode array spectrometer using quarz cuvettes (1 cm).

2.2.3 Stopped-flow Measurements.

Spectroscopic grade methanol for the kinetic measurements was used without further purification. Preparation and handling of air-sensitive compounds was carried out in a glove box (M. Braun, Germany). Dioxygen saturated solutions for the kinetic measurements were prepared by bubbling dioxygen (Linde, Germany) through the solvent for 15 minutes in a glass syringe with a three-valve stopcock (solubility of dioxygen in methanol is 8.5 x 10^{-3} M at 760 Torr and 25°C).[27] Varying dioxygen concentrations were obtained by mixing, in appropriate amounts, an oxygen saturated solution with an argon saturated solution in syringes. Time resolved spectra of the reactions of dioxygen with the iron(III) complexes were recorded on a modified Hi-Tech SF-3 L low temperature stopped-flow unit (Hi-Tech,

Salisbury, UK) equipped with a J&M TIDAS 16-500 diode array spectrophotometer (J&M, Aalen, Germany). Data fitting was performed using the integrated J&M software Kinspec, Origin (OriginLab Corporation, Northampton, MA, USA) or Igor (WaveMetrics, Inc., Lake Oswego, OR, USA) for simple exponential functions.

2.2.4 Determination of the Catechol 1,2-Dioxygenase activity.

The catechol cleaving activities of the complexes prepared *in situ* in methanol were investigated by adding piperidine as an external base. The amount of base yielding the highest reaction rate possible for each individual complex was determined according to the following spectrophotometric titration. 0.02 mL of a 2 x 10^{-2} mol L^{-1} (one equivalent) solution of 3,5-H_2dbc (3,5-di-*tert*-butylcatechol) was added to 2 mL of a 2 x 10^{-4} mol L^{-1} methanolic solution consisting of $Fe(ClO_4)_3 \cdot H_2O$ and the ligand. The determined amount of base (piperidine) was added to the reaction mixture as a 2 x 10^{-2} mol L^{-1} solution (see Table 2-1). The decomposition of the complexes was followed at least three times by UV-vis spectroscopy.

Table 2-1: Results of the spectrophotometric titrations and catechol-1,2-dioxygenase activities.

Ligand	Base equivalents needed for optimal catecholate binding	Reaction rate constant [$M^{-1}s^{-1}$]
tpa	-[a]	-[b]
L1	-[a]	-[b]
L2	1.3	0.05
tmpa	2.25	Ref.[20]
pmea	2.25	0.022
pmap	2.5	0.004
tepa	2.5	-[b]

a: UV spectra did not show sufficient amounts of the desired $[Fe(L)dbc]^+$ complex during the titration

b: complex did not show a significant catechol dioxygenase activity

2.2.5 Spectrophotometric Titrations.

The spectrophotometric titrations were carried out with the same solutions as described above for the activity determination. To avoid cleavage of the substrate, all manipulations were carried out under an argon atmosphere. A 0.1 mL sample of

the 3,5-H_2dbc solution was added to 10 mL of the complex solution. The resulting solution was titrated with piperidine and the UV-vis spectra were monitored in a flow cell.

2.2.6 Ligand Syntheses.

The ligands tpa,[28] L1,[26] L2,[26] tmpa,[25] pmea,[25,29,30] pmap,[24,25] and tepa[24,25] (see Scheme 2-1) were synthesised according to methods reported previously.

2.2.7 Complex Syntheses.

[Fe(tmpa)(dbc)]B(C_6H_5)$_4$ (1) was prepared according to a method described previously.[20]

[Fe(L2)(tcc)Br] (2). Tetrachlorocatechol monohydrate (27 mg, 0.1 mmol) was added to a stirred solution of L2 (28 mg, 0.1 mmol) and anhydrous $FeBr_3$ (30 mg, 0.1 mmol) in methanol (8 mL). Triethylamine (28 μL, 20 mg, 0.2 mmol) was then added and the mixture was heated to reflux for a few seconds and filtered. Vapor diffusion of diethyl ether into the dark blue complex solution yielded needle-like crystals of compound **2** suitable for X-ray analysis. Yield: 32 mg (0.05 mmol, 50%). Anal. Calcd. for $C_{23}H_{16}BrCl_4FeN_4O_2$: C, 42.0; H, 2.5; N 8.5. Found: C, 42.2; H, 2.4; N, 8.7. M.p.: 203°C (decomposition).

[(Fe(L2)Br)$_2$O][(FeBr$_3$)$_2$O] x 2CH$_3$OH (3). Anhydrous $FeBr_3$ (30 mg, 0.1 mmol) was added to a stirred solution of L2 (28 mg, 0.1 mmol) in methanol (6 mL). The reaction mixture was heated for a few minutes and filtered. Vapor diffusion of diethyl ether into the complex solution yielded red crystals of compound **3** suitable for X-ray diffraction. Yield: 47 mg (0.03 mmol, 60%). Anal. Calcd. for $C_{36}H_{40}Br_8Fe_4N_8O_4$: C, 28.6; H, 2.7; N 7.4. Found: C, 28.9; H, 2.6; N, 7.7. M.p.: 204°C (decomposition).

[Fe(pmea)Cl$_2$]ClO$_4$ x (C_2H_5)$_2$O (4). Anhydrous $FeCl_3$ (16 mg, 0.1 mmol), $Fe(ClO_4)_3$ x $6H_2O$ (19 mg, 0.05 mmol), and pmea (46 mg, 0.15 mmol) were dissolved in acetone (7 mL). The reaction mixture was heated to reflux for a few seconds and filtered. Vapor diffusion of diethyl ether into the complex solution yielded crystalline yellow plates of compound **4** which were suitable for X-ray analysis. Yield: 56 mg (0.09 mmol, 62%). Anal. Calcd. for $C_{20.33}H_{23.33}Cl_3FeN_4O_{4.33}$ ([Fe(pmea)Cl_2]ClO_4 x

1/3($C_2H_5)_2O$): C, 44.0; H, 4.2; N 10.1. Found: C, 44.4; H, 3.9; N, 10.1. M.p.: 175°C (decomposition).

[Fe(pmea)(tbc)]ClO_4 x H_2O (5). $Fe(ClO_4)_3$ x $6H_2O$ (37 mg, 0.1 mmol) and pmea (30 mg, 0.1 mmol) were dissolved in acetone (7 mL). With stirring, tetrabromocatechol (42 mg, 0.1 mmol) and triethylamine (28 μL, 20 mg, 0.2 mmol) were added changing the colour of the solution to dark blue. The reaction mixture was heated and filtered. Vapor diffusion of diethyl ether into the complex solution yielded dark blue crystals of compound **5** that were suitable for X-ray analysis. Yield: 63 mg (0.07 mmol, 70%). Anal. Calcd. for $C_{25}H_{20}Br_4ClFeN_4O_7$: C, 34.0; H, 2.3; N 6.2. Found: C, 34.0; H, 2.3; N, 6.4. M.p.: 218°C (decomposition).

2.2.8 X-ray Crystallographic studies.

The intensity data of **2 - 5** were collected on a Bruker AXS SMART 6000 CCD diffractometer (Cu-Kα, λ = 1.54178 Å, Göbel mirror) using an ω-scan technique. The collected reflections were corrected for absorption effects.[18,31] All structures were solved by direct methods and refined by full-matrix least-squares methods on F^2.[32] Further data collection parameters are summarised in Table 2-2. Selected bond lengths and angles for the iron(III) complexes are reported in Table 2-3. Crystallographic data (excluding structure factors) for the structures reported in this paper have been deposited with the Cambridge Crystallographic Data Centre. Copies of the data can be obtained free of charge on application to the CCDC, 12 Union Road, Cambridge CB2 1EZ, UK, on full quoting the journal citation and deposition number CCDC 247601 (**2**), 247602 (**3**), 247603 (**4**) and 247604 (**5**).

2.3 Results and Discussion

In an early study, Cox and Que described the reaction of dioxygen with dbc iron(III) complexes using NTA (nitrilotriacetate) and the related ligands PDA (N-(2-pyridylmethyl)iminodiacetate) and BPG (N,N-bis(2-pyridylmethyl)glycinate).[21] While these oxidations proceeded very slowly they can be regarded as model reactions for the intradiol cleavage of dioxygenases, and from a kinetic study activation parameters were obtained. However, when the related tmpa ligand was used the reaction proceeded much faster and second order rate constants in DMF and methanol were obtained at 25°C (15 (DMF) and 10 (MeOH) M^{-1} s^{-1}). In contrast to

Table 2-2: Selected crystallographic data.

Compound	**2**	**3**	**4**	**5**
Empirical formula	$C_{23}H_{16}BrCl_4FeN_4O_2$	$C_{36}H_{40}Br_8Fe_4N_8O_4$	$C_{23}H_{30}Cl_3FeN_4O_5$	$C_{25}H_{20}Br_4ClFeN_4O_7$
M_r	657.96	1511.44	604.71	901.41
Temperature [K]	140(2)	130(2)	110(2)	110(2)
Radiation (λ[Å])	Cu-K_α (1.54178)	Cu-K_α (1.54178)	Cu-K_α (1.54178)	Cu-K_α (1.54178)
Crystal shape	rod	rod	Rod	rod
Crystal size [mm]	0.25 x 0.08 x 0.03	0.15 x 0.06 x 0.05	0.22 x 0.12 x 0.02	0.20 x 0.10 x 0.07
Crystal system	triclinic	monoclinic	Monoclinic	monoclinic
space group	*P*1bar (No. 2)	$P2_1/c$ (No. 14)	$P2_1/c$ (No. 14)	$P2_1/c$ (No. 14)
A [Å]	7.6179(2)	10.9771(2)	15.7539(4)	9.3253(2)
b [Å]	11.3109(2)	15.4213(2)	12.3338(3)	36.3832(7)
c [Å]	15.1385(3)	15.2598(2)	15.4396(4)	8.6778(2)
α [°]	83.574(1)			
β [°]	88.235(2)	99.740(1)	118.321(2)	92.141(2)
γ [°]	70.800(1)			
V [Å^3]	1224.09(5)	2545.96(7)	2640.9(2)	2942.2(2)
Z	2	2	4	4
$\rho_{calcd.}$ [g·cm^{-3}]	1.785	1.961	1.521	2.030
μ [mm^{-1}]	11.133	16.674	7.728	11.763
F(000)	654	1456	1252	1756
Scan range θ [°]	2.94 to 71.20	4.09 to 71.33	3.19 to 71.30	2.43 to 71.42
Index ranges	-8 ≤ h ≤ 8	-10 ≤ h ≤ 12	-19 ≤ h ≤ 16	-10 ≤ h ≤ 11
	-13 ≤ k ≤ 13	-17 ≤ k ≤ 18	-14 ≤ k ≤ 13	-44 ≤ k ≤ 41
	-16 ≤ l ≤ 18	-18 ≤ l ≤ 16	-16 ≤ l ≤ 18	-10 ≤ l ≤ 10
Reflections collected	7149	14507	14845	17053
Unique reflections	4066	4714	4872	5414
Reflections $I > 2\sigma(I)$	3564	3953	3451	4444
R_{int}	0.0364	0.0418	0.0930	0.0551
Data/restraints/parameters	4066/0/316	4714/0/292	4872/0/327	4486/0/334
Goodness-of-fit on F^2	0.997	1.084	0.943	1.031
Final *R* indices [$I > 2\sigma(I)$]	*R*1 = 0.0408	*R*1 = 0.0403	*R*1 = 0.0482	*R*1 = 0.0539
	*wR*2 = 0.1060	*wR*2 = 0.1114	*wR*2 = 0.1100	*wR*2 = 0.1326
R indices (all data)	*R*1 = 0.0446	*R*1 = 0.0478	*R*1 = 0.0716	*R*1 = 0.0646
	*wR*2 = 0.1081	*wR*2 = 0.1142	*wR*2 = 0.1176	*wR*2 = 0.1376
Largest diff. peak/hole [e·Å^{-3}]	0.929/-0.566	1.670/-0.823	0.482/-0.604	1.536/-1.043

the other investigated ligands no temperature dependence measurements of this system were performed and no activation parameters reported. As pointed out previously by Zuberbühler, for kinetic studies on the reaction of dioxygen with copper(I) complexes, it can be misleading to propose mechanistic arguments on the sole basis of a comparison of kinetic and equilibrium constants at a given temperature rather than on activation and thermodynamic parameters.[33]

A reaction mechanism was proposed for the intradiol cleavage of catechols (Scheme 2-3).[8] However, the proposed intermediates could not be detected spectroscopically.

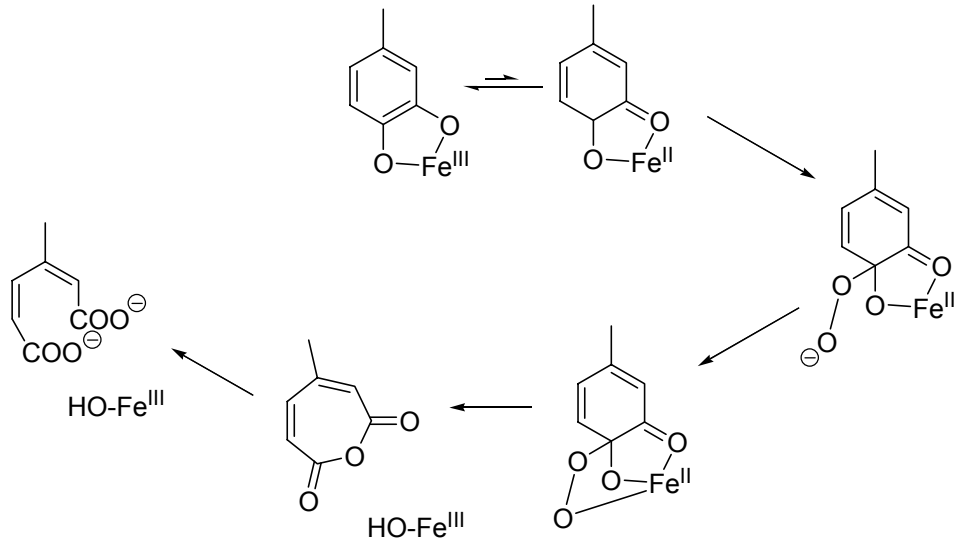

Scheme 2-3: Proposed mechanism for intradiol cleavage of catechols

Despite efforts to increase the rate of the intradiol cleavage reaction using other ligands, the iron(III) tmpa complex remains, at present, the most active catalyst (some examples are given in the references).[8,34,35] When BPIA[34] ([(1-methylimidazol-2-yl)methyl]bis[(2-pyridyl)methyl]amine, a ligand closely related to tmpa) or L-N_4H_2[36] (the non-methylated form of tetraazamacrocycle N,N'-dimethyl-2,11-diaza[3,3](2,6)pyridinophane, a ligand thoroughly investigated by Krüger and coworkers)[37] were used as ligands, reaction rates rather close to the tmpa system were observed.

The oxidative cleavage of [Fe(tmpa)(dbc)]$B(C_6H_5)_4$ (**1**) is accompanied by a dramatic change in the UV-vis spectrum. The reaction of dioxygen with **1** in methanol can be followed using low-temperature stopped-flow techniques and typical time-resolved spectra are presented in Figure 2-1. Measurements were performed using *pseudo*-first-order conditions ($[O_2]$ >> [**1**]) and absorbance vs. time traces were

obtained at different wavelengths that could be fitted to a one exponential function. Observed rate constants (k_{obs}) at different temperatures showed a linear dependence on the dioxygen concentration (Figure 2-2) with no intercept and herewith the second order rate law reported previously was confirmed (the published rate constant of 10 M^{-1} s^{-1} at 25°C[20] was very close, within error, to our determined rate constant).

From the temperature dependence studies the activation parameters were calculated using the Eyring equation as: $\Delta H^{\ddagger}$ = 23 $\pm$ 1 kJ mol^{-1} and $\Delta S^{\ddagger}$ = –199 $\pm$ 4 J mol^{-1} K^{-1}. Negative values for the activation entropy were reported for NTA and derivatives (for the NTA complex: $\Delta H^{\ddagger}$ = 12.8 kcal mol^{-1} and $\Delta S^{\ddagger}$ = –22 eu).[21] As discussed previously these data are in line with related reactions in copper chemistry[33,38-40] and indicate that the attack of dioxygen on the catecholate complexes is the rate determining step. However, it is not possible from these data to describe a detailed reaction pathway for this reaction because no intermediates were observed.

Unfortunately, our hope to spectroscopically observe one of the postulated intermediates (Scheme 2-3) using low-temperature stopped-flow kinetic methods (an approach used successfully in copper dioxygen chemistry) was not fulfilled. Only the UV-vis spectra of the starting complex and the final products were observed. Our kinetic results do not contradict the postulated reaction mechanism (Scheme 2-3); however, they also do not provide additional evidence for the occurrence of the described reaction steps. The kinetic data support a rate determining step of the reaction of the catecholate complex with dioxygen. However, at which site this attack takes place cannot be determined in a kinetic study without the observation of intermediates. Furthermore, for the same reason conclusions in regard to the mechanism of the enzyme should not be drawn from the results of this kinetic study.

Compared to the enzyme, the activity of the tmpa iron(III) complex is still low. Chelate ring size plays an important role in regard to the reactivity of coordination compounds and so far it has not been investigated for iron(III) complexes of the tmpa system. The ligands shown in Scheme 2-1 can be readily prepared in good yields by synthetic procedures described previously.

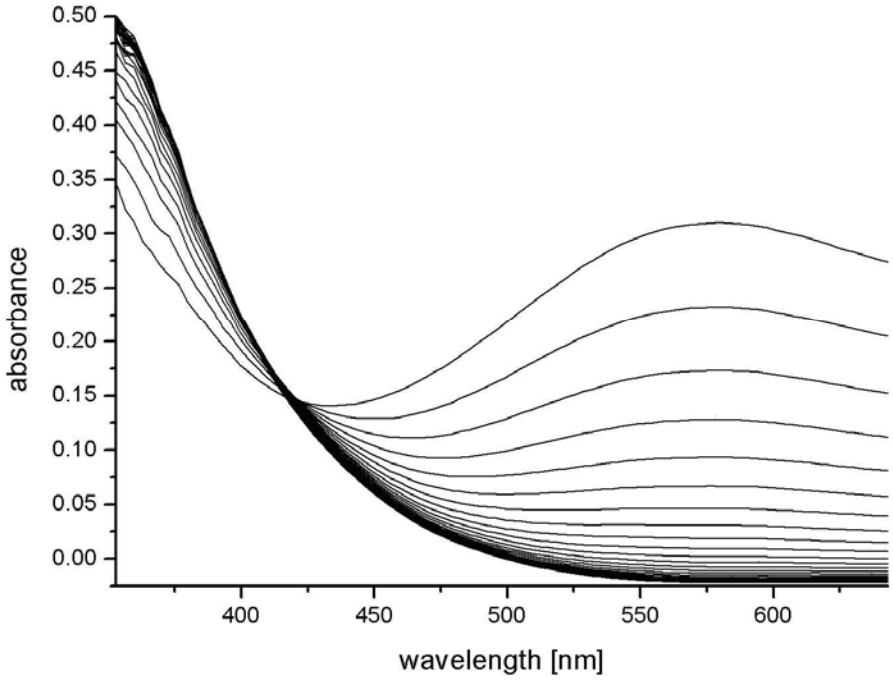

Figure 2-1: Time resolved spectra for the reaction of [Fe(tmpa)(dbc)]$B(C_6H_5)_4$ (1) (0.16 mmol L^{-1}) with dioxygen (4.25 mmol L^{-1} at 20°C, total time 153.9 s) in methanol.

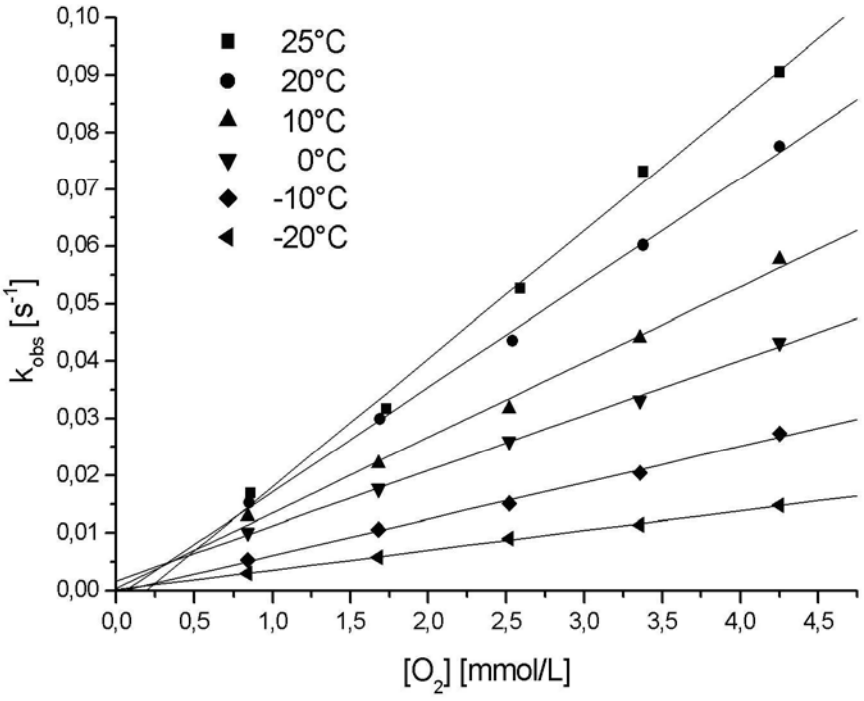

Figure 2-2: Plot of observed rate constants k_{obs} (obtained from measurements at 578.0 nm) vs. dioxygen concentration at different temperatures.

The reactivity of the iron(III) complexes of the ligands depicted in Scheme 2-1 was investigated (see Table 2-1). The iron(III) complexes were prepared *in situ* together with dbc and their catechol cleaving activity was determined according to the protocol described in the Experimental Section. Frustratingly, all of the complexes were found to react by orders of magnitude slower than the tmpa system and therefore were not further investigated. The more variations that were made on the original tmpa system, the lower the observed reaction rate constants were. For the ligands L1 and tpa the reason for the low reaction rates was a low concentration of the desired mononuclear $[Fe(L)dbc]^+$ complexes in solution. The geometric constraints of the ligands may lead to the formation of less reactive dinuclear species or even triscatecholato iron(III) complexes that are also favoured due to the high affinity of catecholates for iron(III) ions.

Similar to related studies on the reaction of dioxygen with copper(I) complexes of the same ligands,[25,26] increasing or decreasing chelate ring sizes in the iron(III) complexes (compared to the tmpa system) causes a dramatic decrease in the reactivity of these compounds (the larger the changes, the larger the decrease in reactivity).

Control experiments with just iron(III) perchlorate, 4.5 equivalents of piperidine and one equivalent of H_2dbc revealed only negligible decay of the formed catecholate complexes over a period of days. Furthermore, Funabiki et al. reported that in oxygenation reactions that utilised a mixture of bipyridine and pyridine as ligands, the main product was the simple oxidation product, 3,5-di-*tert*-butylquinone.[19] For the reason of comparison with other systems, piperidine was used as a base in all reactivity studies reported herein (no reactivity differences were observed with triethylamine instead of piperidine; triethylamine was used in the syntheses of the complexes reported below).

Iron(III) tmpa complexes[20,41,42] and an iron(II) complex of tpa[43] have been prepared and structurally characterised. However no crystal structures of the iron(III) complexes of the other ligands (depicted in Scheme 2-1) have been reported. Therefore Iron(III) complexes of the ligands (depicted in Scheme 2-1) were isolated as solids and crystals suitable for X-ray structural analysis were obtained for iron(III) complexes of the ligands L2 and pmea with and without catecholate as additional ligands.

[Fe(L2)(tcc)Br] (2). Compound **2** crystallizes in the triclinic space group P1bar with two molecules per unit cell. The structure of the neutral complex is depicted in Figure 2-3, while selected bond lengths and angles are given in Table 2-3. The iron(III) centre is surrounded by a distorted octahedral N_3O_2Br environment. As reported for copper(II) complexes of the ligand L2,[26] the shorter arm is not coordinated to the metal centre, avoiding the formation of a strained four membered chelate ring which leads to a facial coordination mode for L2 in complex **2**. The catecholate oxygens [O(1) and O(2)] and the bound pyridine nitrogen donors of L2 [N(2) and N(3)] occupy the equatorial plane of the coordination octahedron, whereas the apical sites are occupied by the bromide anion and nitrogen donor N(1) of the tripodal ligand. The iron(III) donor bond lengths reveal a stretching of the coordination octahedron along the N(1)–Fe(1)–Br(1) axis. The uncommon length of the Fe(1)–N(1) bond [2.398(3) Å] can be attributed to both the lack of π-donor abilities of the aliphatic amine nitrogen N(1) and to a *trans*-influence of the opposing bromo ligand. The distorted octahedral geometry is also reflected in the bond angles around the iron(III) centre; the bite angles involving the five membered chelate rings of L2 are significantly reduced from 90° [83.4(2)° for O(1)–Fe(1)–O(2), 72.3(2)° and 76.1(2)° for N(1)–Fe(1)–N(2/3)], whereas the *cis* angles

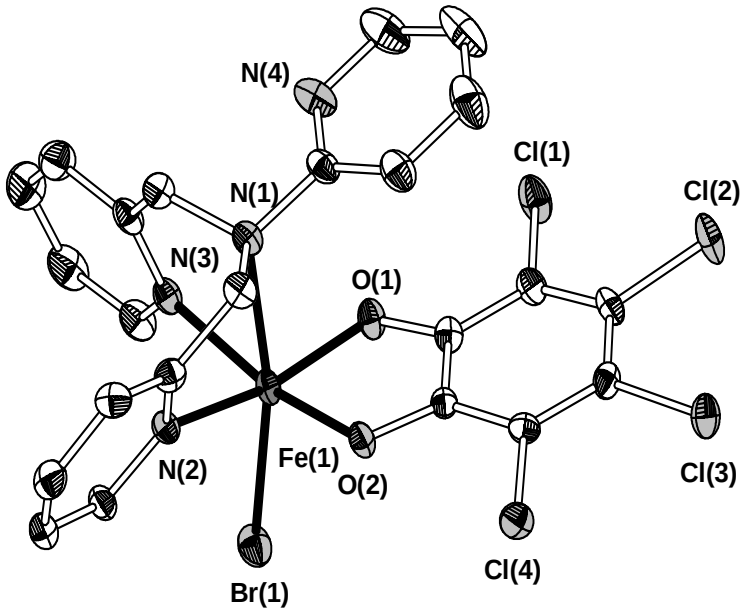

Figure 2-3: Ellipsoid plot of [Fe(L2)(tcc)Br] (50% probability ellipsoids); hydrogen atoms omitted for clarity.

incorporating the bromide anion are significantly larger than 90° because of its steric demand and electrostatic repulsions.

$[(Fe(L2)Br)_2O][(FeBr_3)_2O]$ x $2CH_3OH$ (3). Compound **3** crystallizes in the monoclinic space group $P2_1/c$ with two complex cations, two complex anions and four disordered methanol molecules per unit cell. The structure of the cationic metal complex is depicted in Figure 2-4, while selected bond lengths and angles are given in Table 2-3. The bridging μ-oxo group of the $[(Fe(L2)Br)_2O]^{2+}$ cation as well as that of the $[(FeBr_3)_2O]^{2-}$ anion are located on crystallographic centres of inversion so that one half of each complex is symmetry generated. The iron(III)···iron(III) distance in the cation is 3.550(2) Å. The remaining coordination sites of the iron(III) centre are occupied by the μ-oxo bridge and a bromide anion resulting in an N_4BrO donor set around each iron(III) centre. The most striking feature of the dinuclear complex **3** is that all three pyridyl groups of L2 are bound to the iron(III) centre, which is in stark contrast to all other known metal complexes of L2. As a consequence the very small bite angle of 61.6(2)° for N(1)–Fe(1)–N(2) is observed. The high tension of the four-membered chelate ring and the *trans*-influence of the opposing μ-oxo-bridge weaken the Fe(1)–N(2) bond [2.247(4) Å], which is, despite the possibility of π-bonding, even longer than the Fe(1)–N(1)

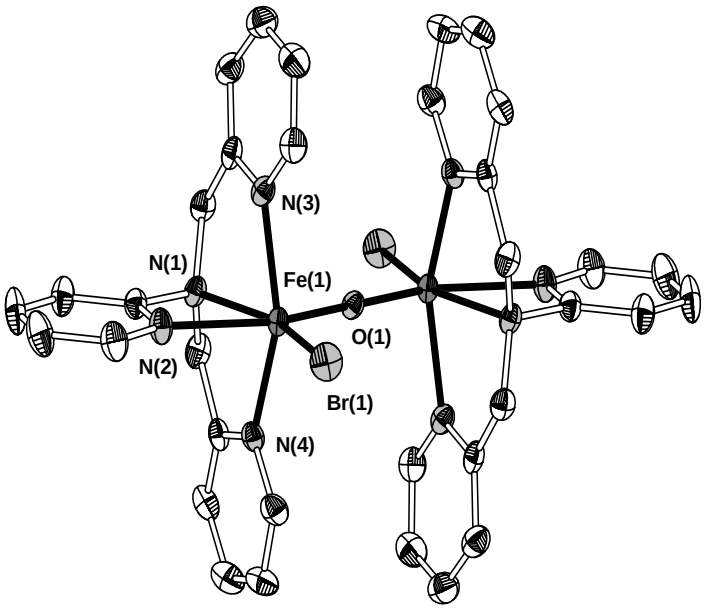

Figure 2-4: Ellipsoid plot of $[(Fe(L2)Br)_2O]^{2+}$ (50% probability ellipsoids); hydrogen atoms omitted for clarity.

bond [2.216(4) Å]. The other *cis* angles that are formed by the ligand and the iron(III) centre are also significantly distorted from 90°;[N(1)–Fe(1)–N(3) = 75.6(2)° and N(1)–Fe(1)–N(4) = 75.7(2)°]. The steric demand of the bromide anion in creases the Br–Fe–N/O angles. Due to the electrostatic repulsions between Br(1) and O(1), these donors form the largest *cis* angle found around the iron(III) centre [Br(1)–Fe(1)–O(1) = 106.83(3)°]. Such a large angle is enabled by the small opposing angle N(1)–Fe(1)–N(2) (*vide infra*).

$[Fe(pmea)Cl_2]ClO_4$ x $(C_2H_5)_2O$ (4). Compound **4** crystallizes in the monoclinic space group $P2_1/c$ with four complex cations, four perchlorate counter ions and four diethyl ether molecules per unit cell. An ellipsoid plot of the cation's structure is depicted in Figure 2-5, with selected bond lengths and angles in Table 2-3. The coordination geometry around the iron(III) centre Fe(1) is best described as distorted octahedral with an N_4Cl_2 donor set. The equatorial plane around Fe(1) consists of two chloride anions Cl(1) and Cl(2), the pyridyl donor atom N(3) and the amine donor atom N(1) of the ligand pmea. The apical sites are occupied by the pyridyl donors N(2) and N(4) with the two five-membered chelate rings located *cis* to each other. The largest *cis* angle within complex **4** is Cl(1)–Fe(1)–Cl(2) = 98.52(4)°. The rigid five membered chelate rings of pmea cause a strong distortion of the octahedral coordination sphere around the iron(III) centre, with the following

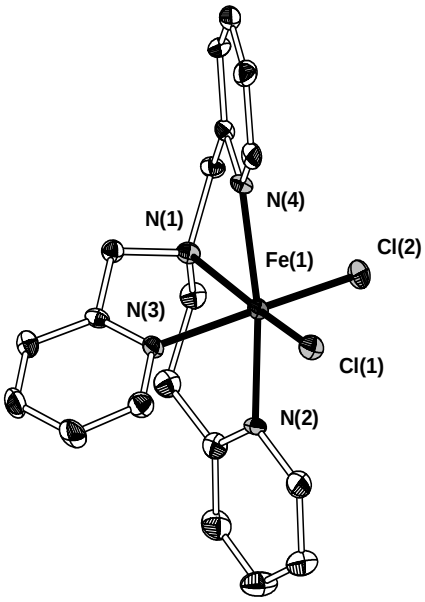

Figure 2-5: Ellipsoid plot of $[Fe(pmea)Cl_2]^+$ (50% probability ellipsoids); hydrogen atoms omitted for clarity.

angles deviating from 90°: [N(1)–Fe(1)–N(3) = 78.1° and N(1)–Fe(1)–N(4) = 74.5(2)°]. In contrast, the six membered chelate ring in complex **4** is more flexible and the angle N(1)–Fe(1)–N(2) has an almost ideal value of 91.9(2)°. The coordination of the two chloride anions leads to an expansion of the equatorial plane in their direction with the corresponding bond lengths being about 0.1 Å longer than the average Fe–N bond in complex **4**. Furthermore, the Fe–Cl bonds show a slight *trans* influence derived from the different nature of the opposing donors; the longer Fe(1)–Cl(2) bond is *trans* to the stronger Fe(1)–N(3) bond of a pyridine donor, while the shorter Fe(1)–Cl(1) bond is located *vis-à-vis* to the weaker Fe(1)–N(1) bond of the aliphatic amine.

[Fe(pmea)(tbc)]ClO_4 x H_2O (5). Compound **5** crystallizes in the monoclinic space group $P2_1/c$ with four complex cations, four perchlorate counter ions and four water molecules per unit cell. Each of the water molecules is hydrogen bonded to one perchlorate ion. The structure of the cation in **5** is depicted in Figure 2-6, selected bond lengths and angles are listed in Table 2-3. As observed for the iron complex **4**, the coordination geometry around the iron(III) centre is distorted octahedral. The nitrogen donor atoms of the N_4O_2 donor set are provided by the ligand pmea, while

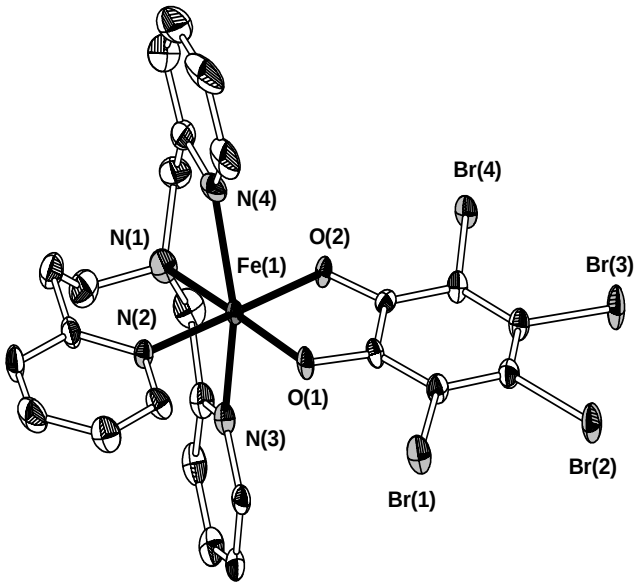

Figure 2-6: Ellipsoid plot of $[Fe(pmea)(tbc)]^+$ (50% probability ellipsoids); hydrogen atoms omitted for clarity.

Table 2-3: Selected bond lengths [Å] and angles [°] for compounds 2–5.

2					
Fe(1)–Br(1)	2.4525(7)	Br(1)–Fe(1)–O(1)	100.96(8)	O(1)–Fe(1)–N(3)	94.7(2)
Fe(1)–O(1)	1.946(2)	Br(1)–Fe(1)–O(2)	96.95(7)	O(2)–Fe(1)–N(1)	89.6(2)
Fe(1)–O(2)	1.958(2)	Br(1)–Fe(1)–N(1)	167.78(7)	O(2)–Fe(1)–N(2)	88.5(2)
Fe(1)–N(1)	2.398(3)	Br(1)–Fe(1)–N(2)	97.47(8)	O(2)–Fe(1)–N(3)	165.6(2)
Fe(1)–N(2)	2.169(3)	Br(1)–Fe(1)–N(3)	97.45(8)	N(1)–Fe(1)–N(2)	72.3(2)
Fe(1)–N(3)	2.136(3)	O(1)–Fe(1)–O(2)	83.4(2)	N(1)–Fe(1)–N(3)	76.1(2)
O(1)–C(18)	1.322(4)	O(1)–Fe(1)–N(1)	90.0(2)	N(2)–Fe(1)–N(3)	88.9(2)
O(2)–C(23)	1.323(4)	O(1)–Fe(1)–N(2)	160.6(2)		
3					
Fe(1)--Fe(1A)	3.550(2)	Br(1)–Fe(1)–O(1)	106.8(3)	O(1)–Fe(1)–N(4)	92.5(2)
Fe(1)–Br(1)	2.4046(8)	Br(1)–Fe(1)–N(1)	158.1(2)	N(1)–Fe(1)–N(2)	61.6(2)
Fe(1)–O(1)	1.7747(7)	Br(1)–Fe(1)–N(2)	96.5(2)	N(1)–Fe(1)–N(3)	75.6(2)
Fe(1)–N(1)	2.216(4)	Br(1)–Fe(1)–N(3)	103.9(2)	N(1)–Fe(1)–N(4)	75.7(2)
Fe(1)–N(2)	2.247(4)	Br(1)–Fe(1)–N(4)	102.8(2)	N(2)–Fe(1)–N(3)	83.5(2)
Fe(1)–N(3)	2.172(4)	O(1)–Fe(1)–N(1)	95.1(2)	N(2)–Fe(1)–N(4)	82.9(2)
Fe(1)–N(4)	2.152(4)	O(1)–Fe(1)–N(2)	156.7(2)	N(3)–Fe(1)–N(4)	151.2(2)
		O(1)–Fe(1)–N(3)	90.0(2)		
4					
Fe(1)–Cl(1)	2.274(2)	Cl(1)–Fe(1)–Cl(2)	98.52(4)	Cl(2)–Fe(1)–N(4)	92.4(8)
Fe(1)–Cl(2)	2.285(2)	Cl(1)–Fe(1)–N(1)	163.98(9)	N(1)–Fe(1)–N(2)	91.9(2)
Fe(1)–N(1)	2.180(3)	Cl(1)–Fe(1)–N(2)	100.01(8)	N(1)–Fe(1)–N(3)	78.1(2)
Fe(1)–N(2)	2.180(3)	Cl(1)–Fe(1)–N(3)	92.66(8)	N(1)–Fe(1)–N(4)	74.5(2)
Fe(1)–N(3)	2.164(3)	Cl(1)–Fe(1)–N(4)	93.07(8)	N(2)–Fe(1)–N(3)	82.8(2)
Fe(1)–N(4)	2.173(3)	Cl(2)–Fe(1)–N(1)	92.22(8)	N(2)–Fe(1)–N(4)	166.3(2)
		Cl(2)–Fe(1)–N(2)	89.72(8)	N(3)–Fe(1)–N(4)	92.6(2)
		Cl(2)–Fe(1)–N(3)	167.49(8)		
5					
Fe(1)–O(1)	1.927(4)	O(1)–Fe(1)–O(2)	83.4(2)	O(2)–Fe(1)–N(4)	89.1(2)
Fe(1)–O(2)	1.947(4)	O(1)–Fe(1)–N(1)	171.0(2)	N(1)–Fe(1)–N(2)	94.8(2)
Fe(1)–N(1)	2.172(5)	O(1)–Fe(1)–N(2)	90.8(2)	N(1)–Fe(1)–N(3)	76.6(2)
Fe(1)–N(2)	2.148(5)	O(1)–Fe(1)–N(3)	96.1(2)	N(1)–Fe(1)–N(4)	79.1(2)
Fe(1)–N(3)	2.134(5)	O(1)–Fe(1)–N(4)	108.1(2)	N(2)–Fe(1)–N(3)	92.7(2)
Fe(1)–N(4)	2.114(6)	O(2)–Fe(1)–N(1)	91.5(2)	N(2)–Fe(1)–N(4)	88.4(2)
O(1)–C(20)	1.319(7)	O(2)–Fe(1)–N(2)	172.7(2)	N(3)–Fe(1)–N(4)	155.7(2)
O(2)–C(25)	1.326(7)	O(2)–Fe(1)–N(3)	92.4(2)		

the oxygen donors derive from a tetrabromocatecholate dianion (tbc) that acts as an inhibitor substrate. The equatorial plane around Fe(1) is occupied by O(1) and O(2) of the tbc, the aliphatic nitrogen N(1) and the pyridyl donor N(2) of the extended ligand arm which forms the six membered chelate ring. This is in contrast to precursor complex **4**, where this arm was located in an apical position. Within this equatorial plane, the deviations from the ideal geometry are relatively small for a metal complex of a tmpa-type ligand. Large deviations can be found for the angles that span the apical positions: [N(1)–Fe(1)–N(3) = 76.6(2)° and N(1)–Fe(1)–N(4) = 79.1(2)° are narrowed, whereas O(1)–Fe(1)–N(3) = 96.1(2)° and O(1)–Fe(1)–N(4) = 108.1(2)° are widened significantly]. The Fe–N bond lengths are within the typical range for a high-spin iron(III) complex. As expected, the Fe(1)–N(1) bond is the longest Fe– N bond in **5** due to the lack of π-bonding abilities. The binding of the catecholate is slightly asymmetric, but the Fe–O bond lengths as well as those of the corresponding C–O bonds are still in good agreement with a dianionic binding of the inhibitor substrate.

2.4 Comparative Discussion.

In the following, the structures of the metal complexes **2** and **3** will be compared to the complexes $[Fe(tmpa)Cl_2]^+$ (**A**) and $[Fe_2OCl_2(tmpa)_2]^{2+}$ (**B**) that were crystallised by Que and coworkers.[42] Furthermore, structural aspects of the substrate-bound iron(III) complexes $[Fe(pmea)(tbc)]^+$ (cation of **5**) and $[Fe(tmpa)(dbc)]^+$ (**1**)[20] will be discussed.

Ligand L2 is a derivative of tmpa in which one ligand arm lacks a methylene spacer between the central amine group and the pyridyl group. This variation has dramatic effects on the coordination chemistry of L2. Not only have different bond lengths and angles been observed for the primary coordination sphere of the iron(III) centre, but also the coordination mode of the ligand was found to be tridentate in the mononuclear substrate complex **2** and tetradentate in the dinuclear compound **3**, whereas tmpa acts as a tetradentate ligand in both **A** and **B**. The very small N(1)–Fe(1)–N(2) angle of 61.6(2)° in **3** compared to 76.8° for the corresponding angle in **B** is indicative of the high ring tension that leads to the detachment of the pyridyl group of L2 upon substrate binding.

The complexes $[Fe(tmpa)(dbc)]^+$ (**1**) and $[Fe(pmea)(tbc)]^+$ (**5**) show a wide similarity, however there are differences that might explain the lower reactivity of the pmea complex towards dioxygen. A calculation of the angle between the least-squares planes of the catecholate unit and the equatorial pyridine group of the ligand in **1** and **5** was performed. In **5** this angle has a value of 1.5° and the corresponding groups are nearly coplanar, while in **1** the dihedral angle has a value of 35.0° due to the ligand's geometric constraints. The twist of the pyridyl group has an impact on the overlap of the ligand's π-orbital with the metal's *d*-orbitals and thus influences the electronic properties of the metal centre. Another difference can be observed for the $Fe–O_{cat}$ bond lengths which are both more than 0.03 Å longer in **5** than in **1** [1.917(3) Å and 1.898(2) Å, respectively]. Since this discrepancy might be a result of the different catechol substrates used in these complexes, we will not go into detail on this point. However, a higher covalency of these bonds that leads to shorter Fe–O distances would simplify charge transfer from the catecholate to the metal centre and thereby enhance reactivity towards dioxygen. The slight asymmetry in the substrate binding that was found in **1** (the Fe-O bonds differ by about 0.02 Å) can also be observed in the catecholate complexes in this work (ΔFe-O = 0.01 Å or 0.02 Å for **2** and **5**, respectively).

2.5 Summary

Activation parameters for the reaction of dioxygen with $[Fe(tmpa)(dbc)]B(C_6H_5)_4$ were determined by low-temperature stopped-flow kinetics. The large negative value of $\Delta S^{‡}$ ($–199 \pm 4$ J mol^{-1} K^{-1}) indicated an associative character of the reaction. However, no intermediates could be detected during the oxidation process to support the postulated mechanism outlined in Scheme 2-3. Furthermore, we could clearly demonstrate that chelate ring size modification in the iron tmpa catecholate system decreased the reaction rate dramatically. In our efforts to crystallize iron catecholate complexes of all ligands investigated we succeeded in structurally characterizing complexes with the ligands L2 and pmea. Single-crystal X-ray structure analyses of complexes **2** and **3** showed that either all pyridine nitrogen atoms of ligand L2 are coordinated (leading to one four-membered chelate ring in complex **3**), or as for complex **2** one arm of L2 is replaced by an additional ligand.

Chapter 3 - Iron(III) Complexes with the Ligands *N*',*N*'-bis[(2-pyridyl)methyl]ethylenediamine (uns-penp) and the Amide *N*-Acetyl-*N*'*N*'-bis[(2-pyridyl)methyl]ethylenediamine (acetyl-uns-penp)

This work has been accepted for publication in *European Journal of Inorganic Chemistry*.

Xu, J.-Y.; Astner, J.; Walter, O.; Heinemann, F. W.; Schindler, S.; Merkel, M.; Krebs, B.

3.1 Introduction

Tripodal ligands such as tris-((2-pyridyl)methyl)amine (= tmpa, also abbreviated as tpa in the literature) as well as derivates, e. g. N4py (Scheme 3-1), have been used successfully in experimental studies to model copper and iron enzymes. [4,8,40,44,45] Iron(II) complexes of the related ligand Rtpen (R = Me, Bz etc.) were shown to react with an excess of hydrogen peroxide to form an end-on hydroperoxo complex that can convert to a side-on peroxo complex at higher pH values.[46-50] More recently it was demonstrated that iron complexes with the ligand Bztpen as well as N4py can form an iron(IV) oxo species that is able to oxidize alkanes such as cyclohexane.[51]

Rtpen can be prepared in two different synthetic procedures. The first one described previously starts from a mono-substituted ethylendiamine that is reacted with picolyl-chloride.[48-50] The second one takes advantage of the amine *N*',*N*'-bis[(2-pyridyl)methyl]ethylenediamine (uns-penp; Scheme 3-1), a versatile tripodal ligand described previously, [52,53] as a starting material. Interestingly, so far only an iron(II) complex of uns-penp has been described in the literature that has been investigated in regard to its spin cross over properties. [54] Furthermore, very recently an iron(II) complex of a derivative of uns-penp was described. [55] However, so far no iron(III) complexes were described in the literature. Therefore, we decided to study the appropriate iron(III) complexes of this ligand as well as of its acetyl derivative (*N*-Acetyl-*N*',*N*'-bis[(2-pyridyl)methyl]ethylenediamine (acetyl-uns-penp; Scheme 3-1), an amide that was obtained during the synthesis of uns-penp.

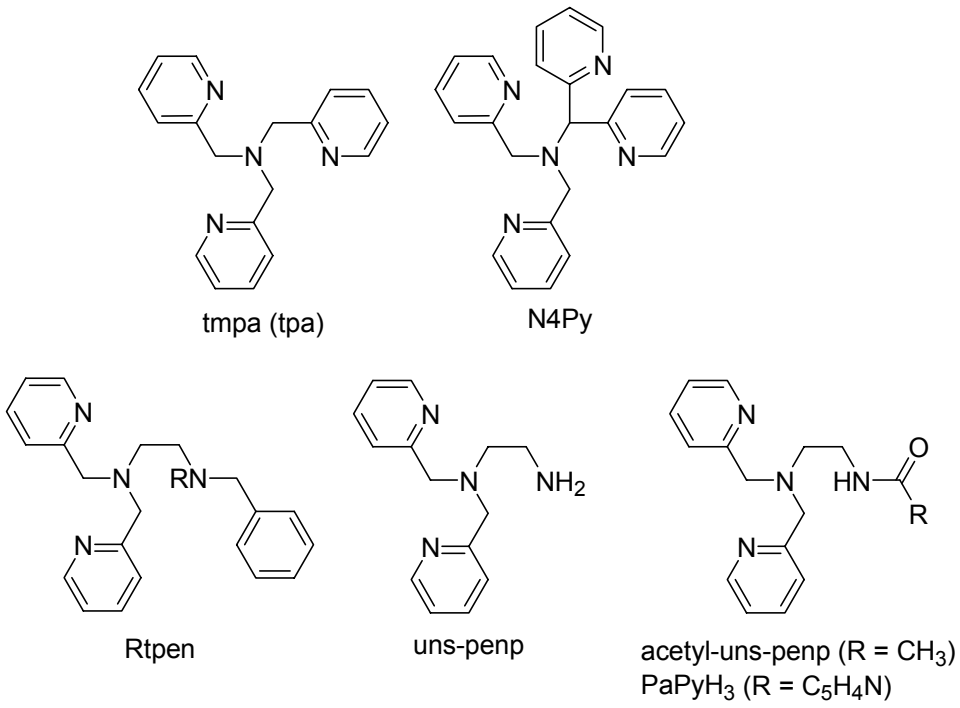

Scheme 3-1: Ligands discussed in the text

3.2 Results and Discussion

Only more recently different research groups have started to use uns-penp as a versatile ligand in different areas of coordination chemistry and different synthetic procedures were described.[52,53,55-59] However, most of the authors unfortunately do not refer to the original synthesis of this ligand by Mandel and coworkers[52] and in one case even describe it incorrectly a second time as a new compound (ten years later in the same journal).[54] Some of us have used this ligand previously in studies in copper chemistry and have improved its preparation.[53] During the two step synthesis of uns-penp its protected form, *N*-Acetyl-*N'*,*N'*-bis[(2-pyridyl)methyl]ethylenediamine (acetyl-uns-penp), was easily obtained in pure form in high yields. Recrystallisation from petroleum ethers afforded single crystals that were suitable for X-ray diffraction studies. Acetyl-uns-penp crystallises with two molecules per unit cell. Those are dimerised by hydrogen bonding between the carboxamido group and one of the pyridine groups. The molecular structure of one of these dimers is presented in Figure 3-1 (see Table 3-1 for a summary of the crystallographic data and refinement parameters). Besides the hydrogen bonding, the crystal structure shows no extraordinary features.

Furthermore, the synthesis of iron complexation with carboxamide ligands has raised the interest of inorganic chemists to gain better understanding of metal-peptide bond coordination chemistry in life sciences[60] and to use such complexes as model compounds for the anti-tumor drug bleomycin[61,62] or nitrile hydratase.[63-65] Important in that regard are the results reported by Mascharak and coworkers, who have investigated in detail the structures and properties of Fe(II)/Fe(III) complexes of a number of carboxamide ligands, several based on a pyridine-2-carboxamide framework, e. g. N,N-bis(2-pyridylmethyl)amine-*N*-ethyl-2-pyridine-2-carboxamide ($PaPy_3H$).[61,63,66-71] The ligand $PaPy_3H$ (Scheme 3-1) is related to acetyl-uns-penp; instead of the methyl group in acetyl-uns-penp it contains an additional coordinating pyridyl unit.

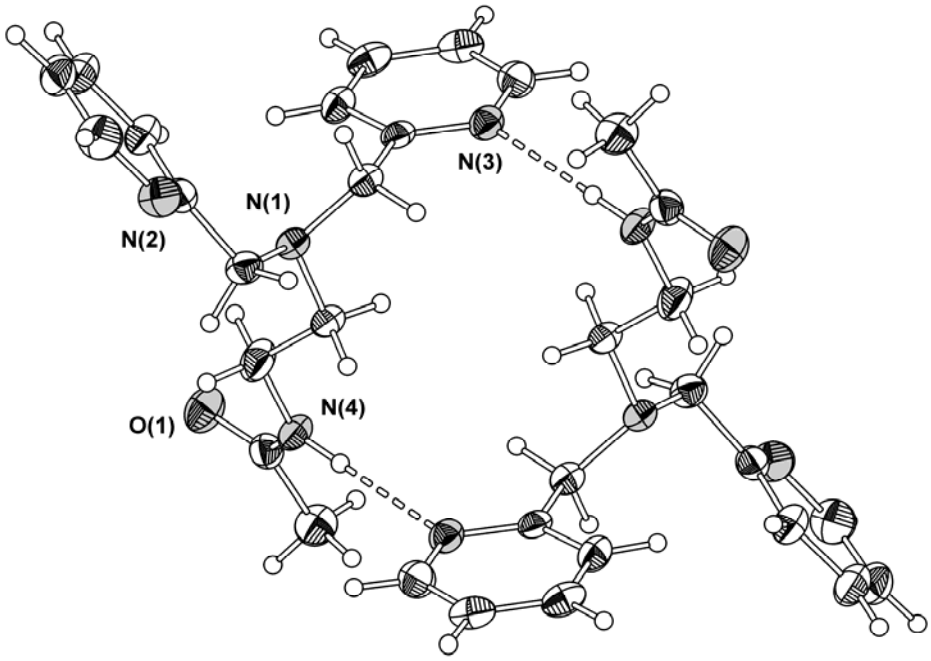

Figure 3-1: Ellipsoid representation of an acetyl-uns-penp dimer (50% probability).

3.2.1 $[Fe_2(acetyl\text{-}uns\text{-}penp)_2O](ClO_4)_2 \times H_2O$ (6).

Acetyl-uns-penp so far has only been used by some of us to synthesize and characterize a copper(II) complex with this ligand. Herein the amide is not deprotonated, however the carboxamido function of acetyl-uns-penp is no longer truly sp^2 hybridised and the nitrogen atom undergoes a weak interaction with the metal centre.[53] The copper complex of $PaPy_3H$ forms a dimer in which the oxygen atom of the amide is coordinated to the copper(II) ion.[72] In contrast the iron amide complexes of $PaPy_3H$ described by Mascharak and coworkers contained the deprotonated ligand

form.[67,70,72,73] However, our own efforts to synthesize the mononuclear deprotonated iron(III) complex [Fe(acetyl-uns-penp)]$(ClO_4)_2$ were only partially successful. Instead of the mononuclear species we obtained the dinuclear complex [Fe_2(acetyl-uns-penp)$_2$O]$(ClO_4)_2$ x H_2O (**6**). It is interesting to note at this point that the stoichiometrically identical compound [$Fe_2(PaPy_3H)_2O](ClO_4)_2$ (containing additional ethanol solvent molecules) derived through oxidation of the iron(II) complex is structurally completely different from **6**.[67] In this complex the oxo-bridge assembles two mononuclear amide complexes (with coordinated deprotonated amide nitrogen atoms while the oxygen atoms are not coordinated) to form the dimer (as one would expect). In contrast and as discussed below, in **6** the ligand acetyl-uns-penp is additionally bridging the two iron(III) ions and involves the amide nitrogen as well as the oxygen atom into the coordination.

Crystals of **6** at first were obtained from the reaction of $Fe(ClO_4)_3$, acetyl-uns-penp and NaN_3 in methanol followed by recrystallisation of the precipitate in acetonitrile. In contrast to our expectations no azide complex was formed but instead deprotonation of the amide occurred under these conditions and due to the presence of water the oxo-bridged dinuclear complex **6** was obtained. Taking this result into account it was furthermore possible to crystallise **6** successfully by replacing the NaN_3 by Et_3N or NaOH as deprotonating agent. The cation of **6**, as depicted in Figure 3-2, shows that the crystallographically equivalent iron(III) centres are triply bridged by one oxo and two carboxamido groups from two acetyl-uns-penp ligands, respectively, leading to an intramolecular Fe-Fe distance of 2.992 Å and an Fe-O-Fe angle of 113.1°. A summary of the crystallographic data and refinement parameters for the structures are presented in Table 3-1. Selected bond lengths and angles for the iron(III) complexes are reported in Table 3-2.

It is interesting to note that in **6**, the acetyl-uns-penp ligand shows an unusual pentadentate coordination mode displaying deprotonated carboxamido NCO bridging groups (η^2, μ_2) involving the delocalisation of π-bonding [d(C-O) = 1.283 Å, d(C-N) = 1.306 Å], which is in agreement with the values of a related (η^2, μ_2) NCO-bridged iron complex reported previously.[74] However, in contrast, structural properties of **6** are quite different to a related iron(III) complex with a bridging urea anion.[75] Compared to other diiron(III) complexes with three bridging ligands, of which at least one is a μ-oxo unit, **6** exhibits some unique structural features. The Fe-Fe separation is significantly

shorter than those of other μ-oxo-tribridged diiron(III) complexes (range 3.048-3.335 Å) and the Fe-O-Fe angle is among the smallest of them all (range 113.8-134.7°).[76] Each iron(III) ion adopts a distorted octahedron coordination geometry by a N_4O_2 donor set, in which two pyridine nitrogen atoms (N2 and N3), one carboxamido nitrogen atom (N4) and a carboxamide oxygen atom (O2A) from the second acetyl-uns-penp ligand reside in the equatorial plane while oxo-bridged O(1) and the tertiary amino N(1) atoms occupy the axial positions. The negative charge of the μ-oxo-bridge leads to a rather short Fe(1)-O(1) bond (1.7923 Å) and likewise due to the *trans* effect, the opposing Fe(1)-N(1) bond is weakened with a distance of 2.246(2) Å. All *cis* angles around O(1) are larger than the ideal 90°, with values of 98.35(5)° for O(1)-Fe(1)-O(2A), 102.11(6)° for O(1)-Fe(1)-N(2), 96.96(5)° for O(1)-Fe(1)-N(3) and 103.62(6)° for O(1)-Fe(1)-N(4). Obviously, deprotonation of the carboxamide groups faciliates the increase of bond lengths around the Fe(III) ions (Table 3-2).

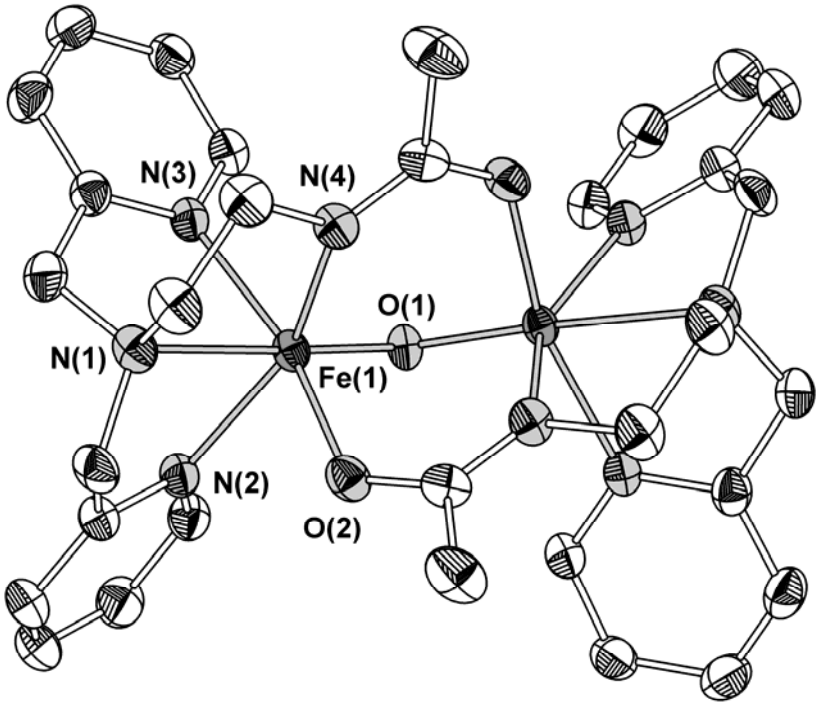

Figure 3-2: Ellipsoid representation of the dinuclear complex in 6

(50% probability; hydrogen atoms omitted for clarity)

Table 3-1: Crystallographic data and experimental details.

Compound	acetyl-uns-penp	**6**	**7**	**8**	**9**	**10**
Empirical formula	$C_{16}H_{20}N_4O$	$C_{32}H_{40}Cl_2Fe_2N_8O_{12}$	$C_{26}H_{30}BrCl_4FeN_4O_4$	$C_{53}H_{64}Cl_8Fe_2N_8O_{10}$	$C_{16}H_{21}Cl_3FeN_5O_4$	$C_{32}H_{42}Cl_4Fe_2N_{10}O_9$
M_r	284.36	455.66	740.10	1368.42	509.58	964.26
Temperature [K]	140(2)	200(2)	100(2) K	150(2)	100(2)	100(2)
Radiation (λ [Å])	Cu-K_α, 1.54178	Mo-K_α, 0.71073	Cu-K_α, 1.54178	Cu-K_α, 1.54178	Mo-K_α, 0.71073	Mo-K_α, 0.71073
Crystal colour and shape	colourless cuboid	brown prism	red plate	brown cuboid	yellow prism	brown, irregular
Crystal size [mm]	0.20 x 0.14 x 0.10	2.00 x 0.40 x 0.50	0.13 x 0.12 x 0.03	0.31 x 0.29 x 0.29	0.24 x 0.15 x 0.12	0.23 x 0.22 x 0.12
Crystal system	Triclinic	monoclinic	monoclinic	monoclinic	monoclinic	triclinic
Space group	*P 1* bar(No. 2)	*C*2/c (No. 15)	$P2_1$/c (No. 14)	$P2_1$/n (No. 14)	P2(1)/n (No 14)	P-1 bar (No 2)
a [Å]	9.3758(2)	16.2248(17)	12.4448(5)	10.4477(3)	11.241(1)	8.4308(5)
b [Å]	9.6178(2)	12.8536(13)	13.4022(6)	20.9973(7)	7.8366(6)	11.2769(6)
c [Å]	10.2342(3)	19.653(2)	18.1585(8)	13.9166(5)	24.330(2)	11.8246(8)
α [°]	82.807(2)					71.583(4)
β [°]	68.351(2)	112.910(1)	92.758(3)	94.824(2)	91.443(7)	76.621(5)
γ [°]	62.401(2)					80.422(4)
V [Å^3]	751.10(3)	3775.2(7)	3025.1(2)	3042.1(2)	2142.6(3)	1032.4(2)
Z	2	4	4	2	4	1
$\rho_{calcd.}$ [g·cm^{-3}]	1.257	1.603	1.625	1.494	1.580	1.551
μ [mm^{-1}]	0.652	0.983	9.127	7.570	1.111	1.024
F(000)	304	1880	1500	1412	1044	496
θ range [°]	4.66 to 71.30	2.09 to 28.28	3.56 to 71.35	3.82 to 71.44	3.14 to 27.88	3.30 to 27.87
Index ranges	$-10 \le h \le 11$	$-16 \le h \le 21$	$-14 \le h \le 14$	$-11 \le h \le 12$	$-14 \le h \le 14$	$-11 \le h \le 10$
	$-10 \le k \le 11$	$-17 \le k \le 16$	$-15 \le k \le 16$	$-22 \le k \le 24$	$-10 \le k \le 10$	$-14 \le k \le 14$
	$-11 \le l \le 12$	$-26 \le l \le 26$	$-20 \le l \le 22$	$-15 \le l \le 17$	$-32 \le l \le 32$	$-15 \le l \le 15$
Reflections collected	4369	13663	16266	17174	32406	27493
Unique reflections	2521	4476	5631	5614	5103	4910
R_{int}	0.0285	0.0263	0.0766	0.0650	0.0792	0.0272
Data/restraints/parameters	2521/0/195	4476/0/266	5631/0/368	5614/0/380	5103/0/263	4910/0/260
Goodness-of-fit on F^2	1.099	1.040	0.888	0.954	1.032	1.065
Final *R* indices [$I > 2\sigma(I)$]	*R*1 = 0.0490	*R*1 = 0.0365	*R*1 = 0.0492	*R*1 = 0.0463	*R*1 = 0.0330	*R*1 = 0.0240
	*wR*2 = 0.1381	*wR*2 = 0.0954	*wR*2 = 0.0981	*wR*2 = 0.1065	*wR*2 = 0.0671	*wR*2 = 0.0580
R indices (all data)	*R*1 = 0.0553	*R*1 = 0.0428	*R*1 = 0.0864	*R*1 = 0.0683	*R*1 = 0.0568	*R*1 = 0.0323
	*wR*2 = 0.1443	*wR*2 = 0.1000	*wR*2 = 0.1082	*wR*2 = 0.1118	*wR*2 = 0.0721	*wR*2 = 0.0606
Largest diff. peak/hole [e·Å^{-3}]	0.210/-0.325	0.937/-0.644	1.458/-0.501	0.400/-0.692	0.401/-0.525	0.434/-0.442

Table 3-2: Selected distances [Å] and angles [°] in 6 - 10.

atoms	**6**	atoms	**7**	**8**	atoms	**9**	atoms	**10**
Fe(1)-O(1)	1.792(2)	Fe(1)-X	2.4813(9)	1.7929(5)	Fe(1)–N(1)	2.127(2)	Fe(1)-O(1)	1.798(1)
Fe(1)-O(2A)	2.013(2)	Fe(1)-O(2)	1.961(3)	2.012(2)	Fe(1)–N(3)	2.136(2)	Fe(1)-N(3)	2.141(2)
Fe(1)-N(4)	2.100(2)	Fe(1)-O(3)	1.969(3)	2.008(2)	Fe(1)–N(4)	2.172(2)	Fe(1)-N(1)	2.147(2)
Fe(1)-N(2)	2.157(2)	Fe(1)-N(1)	2.266(4)	2.366(3)	Fe(1)–N(2)	2.214(2)	Fe(1)-N(2)	2.213(2)
Fe(1)-N(3)	2.162(2)	Fe(1)-N(2)	2.191(4)	2.170(3)	Fe(1)–Cl(1)	2.2622(5)	Fe(1)-N(4)	2.235(2)
Fe(1)-N(1)	2.245(2)	Fe(1)-N(3)	2.159(4)	2.175(2)	Fe(1)–Cl(2)	2.3081(6)	Fe(1)-Cl(1)	2.3166(4)
O(1)-Fe(1A)	1.792(2)	Fe(1)···Fe(1A)		3.586			O(1)-Fe(1A)	1.798(1)
O(2)-Fe(1A)	2.013(2)	Fe(1)···N(4)		3.692(3)			Fe(1)···Fe(1A)	3.596
Fe(1)···Fe(1A)	2.992	O(2)···N(4)		2.755(3)				
O(1)-Fe(1)-O(2A)	98.35(5)	X-Fe(1)-O(2)	96.2(2)	98.25(6)	N(1)-Fe(1)-N(3)	153.61(6)	O(1)-Fe(1)-N(3)	93.26(3)
O(1)-Fe(1)-N(4)	103.62(6)	X-Fe(1)-O(3)	99.8(2)	106.26(7)	N(1)-Fe(1)-N(4)	83.51(6)	O(1)-Fe(1)-N(1)	90.95(3)
O(2A)-Fe(1)-N(4)	93.13(7)	X-Fe(1)-N(1)	165.6(2)	161.78(7)	N(3)-Fe(1)-N(4)	90.55(6)	N(3)-Fe(1)-N(1)	153.72(5)
O(1)-Fe(1)-N(2)	102.11(6)	X-Fe(1)-N(2)	93.5(2)	95.87(7)	N(1)-Fe(1)-N(2)	78.07(6)	O(1)-Fe(1)-N(2)	93.08(3)
O(2A)-Fe(1)-N(2)	85.80(6)	X-Fe(1)-N(3)	95.4(2)	92.24(7)	N(3)-Fe(1)-N(2)	75.55(6)	N(3)-Fe(1)-N(2)	76.04(4)
N(4)-Fe(1)-N(2)	154.12(7)	O(2)-Fe(1)-O(3)	82.9(2)	81.31(8)	N(4)-Fe(1)-N(2)	79.08(6)	N(1)-Fe(1)-N(2)	77.84(4)
O(1)-Fe(1)-N(3)	96.96(5)	O(2)-Fe(1)-N(1)	95.4(2)	95.28(9)	N(1)-Fe(1)-Cl(1)	105.57(4)	O(1)-Fe(1)-N(4)	170.11(3)
O(2A)-Fe(1)-N(3)	164.53(6)	O(2)-Fe(1)-N(2)	168.1(2)	160.74(9)	N(3)-Fe(1)-Cl(1)	100.04(4)	N(3)-Fe(1)-N(4)	88.86(4)
N(4)-Fe(1)-N(3)	85.43(7)	O(2)-Fe(1)-N(3)	86.5(2)	96.38(9)	N(4)-Fe(1)-Cl(1)	89.42(4)	N(1)-Fe(1)-N(4)	82.98(4)
N(2)-Fe(1)-N(3)	88.81(6)	O(3)-Fe(1)-N(1)	90.1(2)	87.77(9)	N(2)-Fe(1)-Cl(1)	167.56(5)	N(2)-Fe(1)-N(4)	78.04(4)
O(1)-Fe(1)-N(1)	173.14(7)	O(3)-Fe(1)-N(2)	88.7(2)	82.20(9)	N(1)-Fe(1)-Cl(2)	89.33(5)	O(1)-Fe(1)-Cl(1)	102.82(2)
O(2A)-Fe(1)-N(1)	87.39(7)	O(3)-Fe(1)-N(3)	162.3(2)	161.50(9)	N(3)-Fe(1)-Cl(2)	92.30(5)	N(3)-Fe(1)-Cl(1)	100.45(3)
N(4)-Fe(1)-N(1)	79.68(7)	N(1)-Fe(1)-N(2)	76.2(2)	74.16(9)	N(4)-Fe(1)-Cl(2)	169.15(4)	N(1)-Fe(1)-Cl(1)	103.87(3)
N(2)-Fe(1)-N(1)	74.44(7)	N(1)-Fe(1)-N(3)	76.8(2)	74.12(9)	N(2)-Fe(1)-Cl(2)	91.49(4)	N(2)-Fe(1)-Cl(1)	163.93(3)
N(3)-Fe(1)-N(1)	77.19(7)	N(2)-Fe(1)-N(3)	99.5(2)	96.10(9)	Cl(1)-Fe(1)-Cl(2)	100.38(2)	N(4)-Fe(1)-Cl(1)	86.26(3)
Fe(1A)-O(1)-Fe(1)	113.1(2)						Fe(1A)-O(1)-Fe(1)	180.000(1)

X = Br(1) in **7** or O(4) in **8**

A**:** x,y,-z+1/2 (for **6**); -x+2,-y,-z+2 (for **10**)

Model complexes for intradiol catechol dioxygenases. One reason for our efforts to obtain the mononuclear iron(III) complex with the deprotonated acetyl-unspenp as ligand was our hope that this complex might be an excellent functional model for intradiol catechol dioxygenases. These mononuclear non-heme iron enzymes catalyse the oxidative cleavage of catechol derivatives by insertion of both atoms of dioxygen into the substrate - a key step in the degradation of aromatic compounds.[8-10]

Since Funabiki et al. reported the first functional models for catechol dioxygenases, increased efforts have been made by bioinorganic chemists to mimic the structure and function of these enzymes.[8-10,18,19,77,78] Besides macrocyclic ligands,[36,37,79] especially tetradentate tripodal ligands have shown considerable abilities to regulate the properties of model complexes, indicating that dioxygenase activity strongly depends on the nature of the ligand. The most effective biomimetic catalyst to date is the iron(III) tmpa (tpa) complex that was first reported by Que and coworkers[8,20]. Furthermore, several other systems with tripodal N_4 donor ligands showed considerable catechol dioxygenase activity.[23,34] Complexes with enzyme analogous N_2O_2 donor sets represent good structural and spectroscopic model compounds, however, they are poor functional models so far.[17,80-86] Our recent efforts to reach higher activities than the iron(III) tmpa complex by increasing or decreasing the chelate ring sizes in this system were unsuccessful.[87]

The substrate binding process in the reaction cycle of the catechol cleavage involves protonation of two ligands at the active site, Tyr447 and a hydroxide.[14,88] These two proton acceptors dissociate from the metal ion and herewith enable the proton donor molecule, the catechol, to coordinate in its dianionic form (see Scheme 3-2).

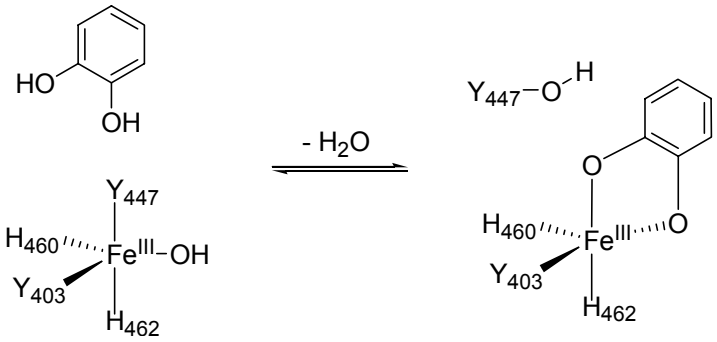

Scheme 3-2: Proposed substrate binding process in catechol-1,2-dioxygenases

The special electronic properties of the leaving Tyr447 group have been studied extensively using spectroscopic methods and seem to influence the reactivity of the enzyme to a large extent.[89] In previous work some of us used a tmpa derived ligand [(6-bromo-2-pyridyl)methyl]bis[(2-pyridyl)methyl]amine (brtpa) to mimic the weak bonding of one of the donor groups, however again it was observed that catechol dioxygenase reactivity decreased compared to the iron tmpa system, most likely due to steric hindrance.[35]

Replacing one pyridyl moiety of the tmpa ligand with a deprotonated carboxamide function we had hoped to finally increase reaction rates of the oxidation of catecholates compared to the tmpa system. However, as discussed below we did not reach this goal and furthermore, in contrast to the synthesis of complex **6**, we did not succeed in the preparation of deprotonated amide complexes when using acetyl-uns-penp, catecholates and base.

3.2.2 [Fe(acetyl-uns-penp)(tcc)Br] x $(C_2H_5)_2O$ (7).

When iron(III) bromide, acetyl-uns-penp, tetrachlorocatechol and triethylamine were mixed in acetone the complex [Fe(acetyl-uns-penp)(tcc)Br] x $(C_2H_5)_2O$ (**7**) was obtained. Slow diffusion of diethyl ether into the complex solutions allowed the precipitation of single crystals that were suitable for X-ray diffraction studies. Four complex molecules and four diethyl ether molecules form the unit cell of Compound **7**. The diethyl ether molecules are attached to the complex *via* hydrogen bonding to the non coordinating carboxamide function of the ligand. The structure of **7** is depicted in Figure 3-3 (the solvate molecule has been omitted for clarity; crystallographic data are presented in Table 3-1 and Table 3-2).

The iron(III) core is ligated by three nitrogen atoms, two catecholate oxygens and one bromide. The longest bonds formed by iron and its donor atoms are found for Fe(1)-Br(1) and Fe(1)-N(1) with 2.4813(9) and 2.266(4) Å, respectively. This causes stretching of the coordination octahedron along the Br(1)-Fe(1)-N(1) axis. The *cis* angles around the bromide ion are widened to an averaged angle of 96.2°. On the other hand, the formation of five membered chelate rings leads to small values for the N(1)-Fe(1)-N(2) and N(1)-Fe(1)-N(3) angles of 76.2(2) and 76.8(2)°, respectively.

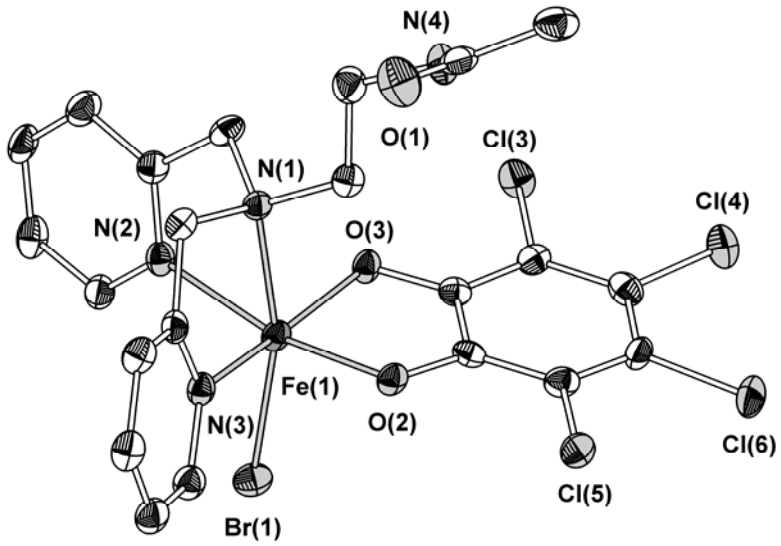

Figure 3-3: Ellipsoid representation of the iron(III) complex in 7 (50% probability; hydrogen atoms omitted for clarity).

3.2.3 [{Fe(acetyl-uns-penp)(tcc)}$_2$O] x $(C_2H_5)_2O$ x CH_3OH (8).

Interestingly, applying the same experimental conditions as for the synthesis of **7**, however using a slightly larger amount of base the dinuclear oxo bridged complex [{Fe(acetyl-uns-penp)(tcc)}$_2$O] x $(C_2H_5)_2O$ x CH_3OH (**8**) was obtained (the syntheses of **7** and **8** could be reproduced applying these conditions). The molecular structure of the cation of **8** is shown in Figure 3-4 (crystallographic data are presented in Table 3-1 and Table 3-2).

The unit cell contains two complexes as well as four diethyl ether and two disordered methanol molecules. Since the bridging oxygen atom O(4) is located on a symmetry centre, one half of the dinuclear complex is generated by inversion. The metal metal distance is 3.586 Å and both iron ions are surrounded by an N_3O_3 donor set. The nitrogen donor atoms are provided by the ligand acetyl-uns-penp, whereas the oxygen atoms belong to the dianionic tetrachlorocatecholate ligand and the μ-oxo-bridge. The coordination sphere of the iron centre has a distorted octahedral geometry. The negative charge of the μ-oxo-bridge leads to a rather short Fe(1)-O(4) bond (1.793 Å) and due to a *trans* effect, the opposing Fe(1)-N(1) bond is weakened. All *cis* angles around O(4) are larger than the ideal 90°. Especially those to the catecholate oxygens are widened, since this effect can be attributed to electrostatic repulsions. The negative charge of O(2) is reduced by the

intramolecular hydrogen bond and therefore the corresponding O(2)-Fe(1)-O(4) angle has a value of only 98.25(6)° compared to 106.74(9)° for O(3)-Fe(1)-O(4).

The most striking feature of **8** is the intramolecular hydrogen bond between the carboxamide nitrogen N(4) and O(2) of the catecholate. The donor acceptor distance has a typical value of 2.755(3) Å and the distance between Fe(1) and N(4) is 3.692 Å. This is in good agreement with similar intramolecular hydrogen bonding some of us reported recently.[35] In a way this hydrogen bonding indicates a possible pathway for the deprotonation of the catechol similar to the enzyme reaction shown in Scheme 3-2.

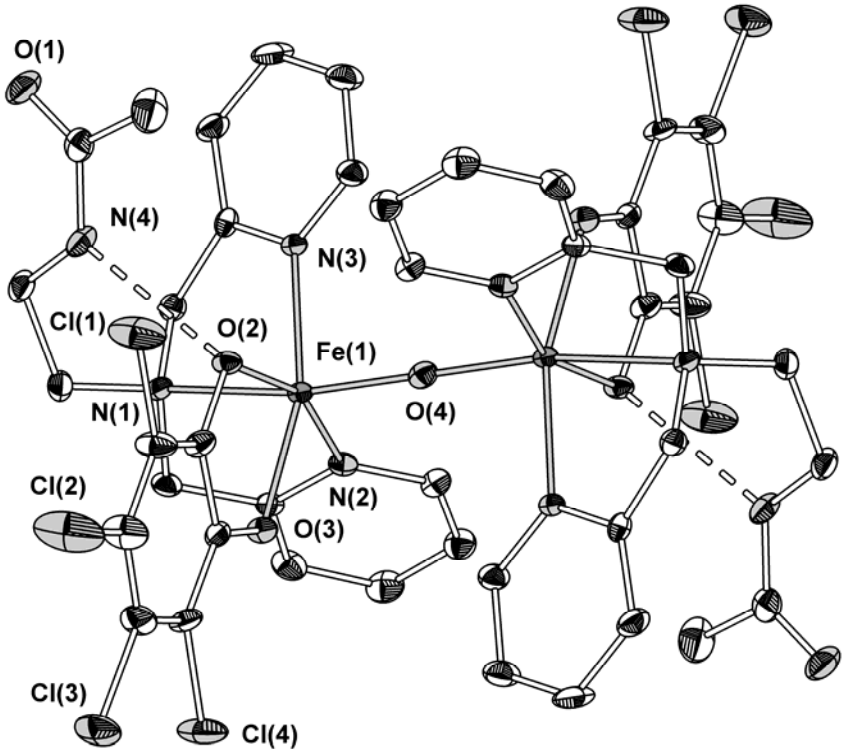

Figure 3-4: Ellipsoid representation of the dinuclear complex in 8 (50% probability; hydrogen atoms omitted for clarity).

Spectrophotometric titrations. To gain a better understanding of the influence of the base and furthermore to achieve optimised conditions for catechol cleavage by molecular dioxygen it is necessary to provide a high concentration of the mononuclear iron complex with one coordinated catecholate dianion ($[Fe(L)(3,5\text{-dbc})]^+$). To determine these ideal conditions for the catechol cleavage experiments, spectrophotometric titrations were performed (see Figure 3-5 and 3.4 Experimental) as described previously for related systems.[35]

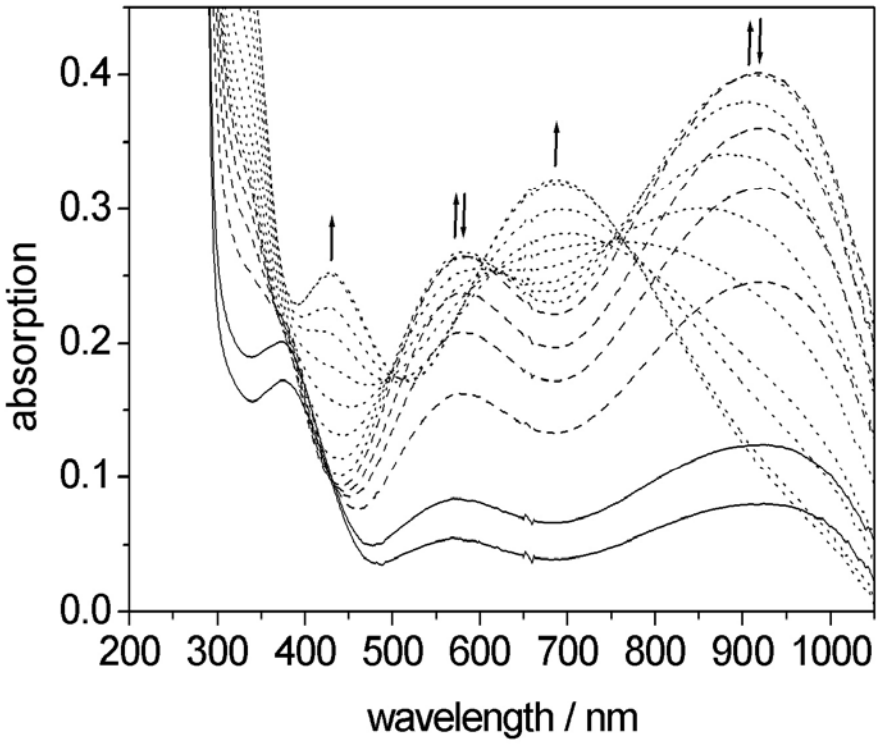

Figure 3-5: Spectrophotometric titration of a solution of iron(III) perchlorate hydrate, acetyl-uns-penp and 3,5-dbc against piperidine; solid lines: 0.0 and 0.5 equivalents; dashed lines: 1.0 - 1.6 equivalents; dotted lines: 1.8 – 4.0 equivalents.

This analysis allowed to gain insight into the species distribution in solution depending on the amount of external base that was added to a mixture of iron salt, the ligand and the substrate 3,5-dbc. At the beginning of the titration (0.0 – 0.5 equivalents of piperidine; piperidine was used for comparison with previous studies, however triethylamine works the same way) an absorption band at 375 nm can be observed that is assigned to an oxo-iron(III)-CT transition. We suggest that the main species in solution is a μ-oxo-bridged dinuclear compound without coordinated substrate. Such dinuclear complexes are thermodynamically favoured in presence of water and many examples have been reported in the literature.[42,90-99] With regard to the previous results of some of us it is possible that the carboxamido group of the ligand already undergoes a very weak interaction with the metal centre and is not truly sp^2 hybridised, however not yet deprotonated. [53] Furthermore, two weak transitions occur at 580 and 920 nm which are typical for catecholate-iron(III)-CT transitions and indicate the presence of a low concentration of the desired mononuclear substrate adduct. Upon further addition of base

(1.0 – 1.6 equivalents) these two absorption bands raise dramatically and so does the concentration of the mononuclear substrate adduct. In the last part of the titration (1.8 – 4.0 equivalents) the bands at 580 and 920 nm disappear and two new bands rise at 430 and 690 nm that are also assigned to catecholate-iron(III)-CT transitions. The shift to higher energies indicates a higher electron density on the iron(III) core that makes the charge transfer from the catecholate more difficult. In accordance to the crystal structure of **8** we suggest that a dinuclear μ-oxo-bridged substrate adduct is formed in which the large electron density of the oxo-group is partially transferred to the metal ions and one ligand arm is detached. Finally, the amount of base that is necessary to reach optimal reaction conditions for the catechol cleavage was determined from a plot of the absorption of the lower energy CT band versus the amount of base added (see Figure 3-6). The maximum of this plot is located at 1.7 equivalents.

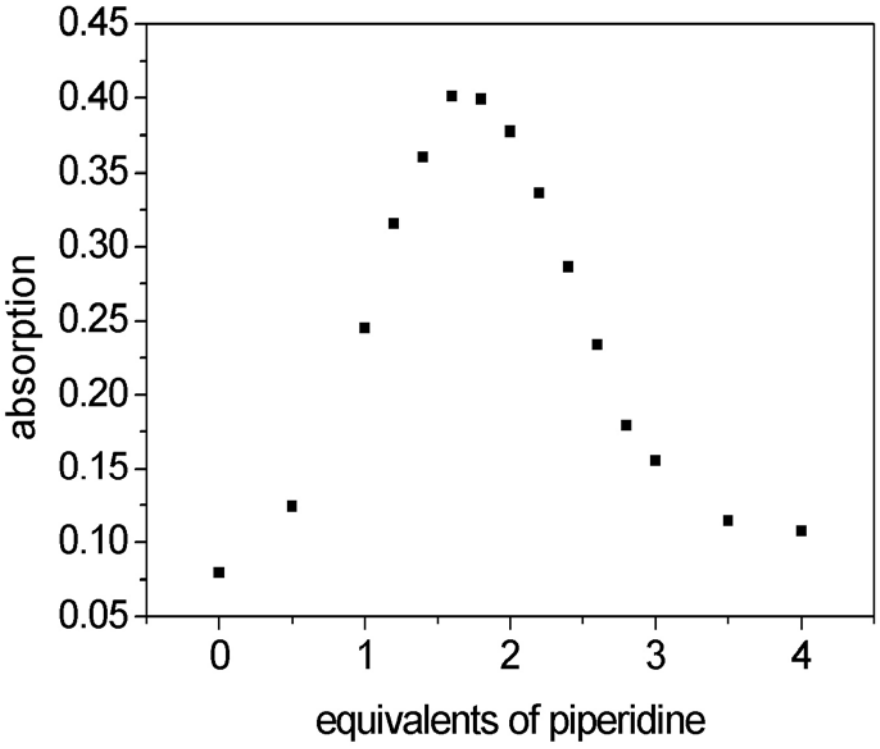

Figure 3-6: Absorbance vs. base equivalents-plot (λ = 980 nm).

Catechol 1,2-dioxygenase activity. An *in situ* prepared complex solution containing equimolar amounts of iron(III) perchlorate hydrate and acetyl-uns-penp was treated with 1 equivalent of 3,5-dbc and 1.7 equivalents of piperidine. The decrease in the lower energy LMCT band was monitored by UV-vis-spectroscopy.

The reaction was performed in air saturated methanol, resulting in a more than tenfold excess of dioxygen that ensures *pseudo*-first-order kinetics for the complete reaction. From the slope of the ln(absorbance) vs. time plot, the reaction rate was determined to be 0.05 $M^{-1}s^{-1}$, which is more than two orders of magnitude lower than that reported for the iron-tmpa system under similar reaction conditions.[20] Due to this low reactivity no further experiments were performed with this system.

3.2.4 $[Fe(uns\text{-}penp)Cl_2]ClO_4$ x CH_3CN (9).

The ligand uns-penp was obtained in good yields according to the procedures described in the literature. Mixing uns-penp together with iron(III) salts in methanol afforded a yellow material that could be recrystallised from acetonitrile by ether diffusion to yield crystals suitable for X-ray structural analysis. The ORTEP representation of $[Fe(uns\text{-}penp)Cl_2]^+$ is shown in Figure 3-7. The structure of the cation of **9** shows a distorted octahedral geometry coordinated with four N atoms of the uns-penp ligand and two chloride ions, as represented by the *trans* ligand angles of 153.61(6)° for N1-Fe1-N3, 167.56(5)° for N(2)-Fe(1)-Cl(1), and 169.15(4)° for

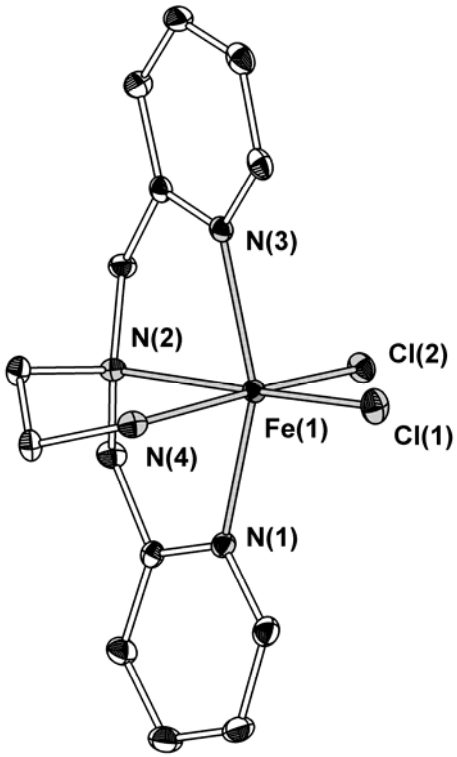

Figure 3-7: Thermal ellipsoids plot of the cation of 9 (50% probability; hydrogen atoms omitted for clarity).

N(4)-Fe(1)-Cl(2). Moreover, the angle for Cl(1)-Fe(1)-Cl(2) is 100.38(2)°, which is significantly larger than 90°. As is often the case with a tripodal ligand that forms 5-membered chelate rings, the coordination geometry is distorted toward the tertiary amino group (average N_{amine}-Fe-$N_{py/amine}$ = 77.55°). The Fe-N_{py} bonds (av 2.132 Å) are shorter than the Fe-N(amine) bond (av. 2.193 Å), which are comparable to the values of Fe(III) tmpa complexes. [20,100,101] Consequently the Fe(1)–Cl(1) bond which is *trans* to the tertiary amino group (2.2622(5) Å is shorter than the Fe(1)–Cl(2) bond *trans* to a primary amino nitrogen (2.3081(6) Å).

3.2.5 [{Fe(uns-penp)Cl}$_2$O](ClO$_4$)$_2$ x 2CH$_3$CN (10).

It is well known that a general problem in iron(III) chemistry is the formation of oxo-bridged dimers during the synthesis of the complexes such as for example the iron(III) tmpa complex or the acetyl-uns-penp ligand system described above. Addition of base can accelerate this reaction and therefore when base was added during the synthesis of **9** the dinuclear oxo bridged complex **10** was obtained instead. The thermal ellipsoids representation of the cation of **10** is shown in Figure 3-8. The molecular structure is composed of centrosymmetric dimeric cations with a linear Fe-O-Fe unit. Each iron centre is in a distorted octahedral environment ligated by the two pyridine nitrogen atoms, the primary and tertiary amine nitrogens, as well as the oxygen which is bound to the second iron centre. The Fe-O bond distance of 1.7981(2) Å is in keeping with the mean values of 1.79(6) (with a range of 1.73- 1.82 Å) for such bond lengths in oxo-bridged iron(III) complexes.[102] The Fe-N_{py} bonds of 2.141(2) Å and 2.147(2) Å are considerably shorter than the Fe-N_{amine} bond (2.213(2) and 2.235(2) Å). This is analogous to the structures of the respective (μ-oxo)diiron(III) complexes of tmpa. The chloride ligands coordinate *trans* to the tertiary amine nitrogen on each iron centre and *anti* to each other relative to the Fe-O-Fe axis. The Fe-Cl bond distances of 2.3166(4) Å are slightly longer than the values of **9** arising from steric hindrance in the dimer. The Fe-Fe distance of 3.596 Å is typical for complexes with singly bridged Fe-O-Fe cores, which are usually in the range 3.4 - 3.6 Å, whereby the longer distances are associated with Fe-O-Fe angles that are linear or close to linearity.

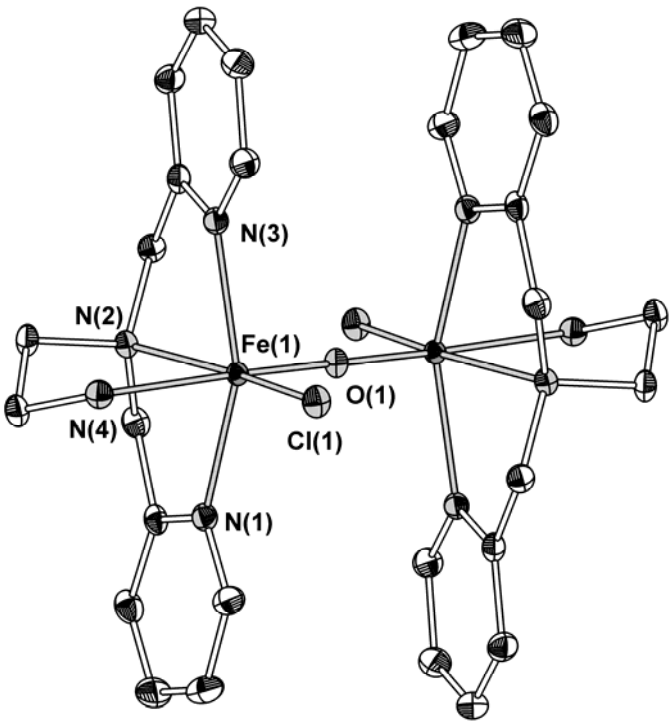

Figure 3-8: Thermal ellipsoids plot of the cation of 10 (50% probability; hydrogen atoms omitted for clarity).

Catechol 1,2-dioxygenase activity of the iron(III)-uns-penp system. The iron(III)-uns-penp complex was investigated under the same conditions used previously for the according iron(III) tmpa catecholate (3,5-dbc) system. [87] Stopped-Flow kinetic investigations revealed again that the rate of the reaction of the iron tmpa system is faster under these conditions, however, at least the iron-uns-penp complex was only slower by a factor of 20. No further detailed kinetic studies were performed on this system due to the fact that the rate could not be increased and that no reactive intermediates could be detected spectroscopically.

3.3 Conclusions

Acetyl-uns-penp has not been used in coordination chemistry so far despite its interesting ligand properties and in contrast to related ligands (in which additional pyridine or phenol donor groups are present) that attracted a lot of interest in amide chemistry recently.[57,66-70,72,73,103-105] Some of us recently reported a copper(II) complex, where the carboxamido function of acetyl-uns-penp is no longer truly sp^2 hybridised and the nitrogen atom undergoes a weak interaction with the metal centre.[53] In our present work, we demonstrated that acetyl-uns-penp is capable of

influencing coordination chemistry by building hydrogen bonds with hydrogen acceptors in the vicinity of the carboxamido function. The intramolecular hydrogen bond between one arm of the tripodal ligand and a coordinated substrate molecule in **8** suggests a pathway for the second substrate deprotonation step in the reaction cycle of intradiol cleaving catechol dioxygenases according to Scheme 3-2. Taken into account that the carboxamide also can undergo strong binding interactions with a metal centre upon deprotonation, as demonstrated in **6**, acetyl-uns-penp is a very versatile ligand. Furthermore, structural characterisation of two iron(III) complexes of the ligand uns-penp and its catechol dioxygenase reactivity provided additional information on the chemistry of this interesting ligand.

3.4 Experimental

3.4.1 Materials.

All chemicals were obtained from commercial sources and used without further purification.

CAUTION! *The syntheses and procedures described below involve compounds that contain perchlorate and azide ions, which can detonate explosively and without warning. Although we have not encountered any problems with the compounds used in this study, they should be handled with extreme caution.*

3.4.2 Physical Measurements.

UV-vis spectroscopy was performed on a Hewlett-Packard 8453 diode array spectrometer. Elemental analyses were carried out on an Elementar Vario EL III analyser at the University of Münster.

3.4.3 Syntheses

Ligand Syntheses. The ligand acetyl-uns-penp as well as uns-penp were prepared according to literature procedures.[53]

$[Fe_2(acetyl\text{-}uns\text{-}penp)_2O](ClO_4)_2 \times H_2O$ (6). Iron(III) perchlorate hexahydrate (177 mg, 0.5 mmol) and acetyl-uns-penp (142 mg, 0.5 mmol) were combined in 10 mL of methanol. After 10 min of stirring, to the resulting brown solution NaN_3 (49 mg, 0.75 mmol) was added, immediately leading to a very dark red suspension. After

2 h a brown precipitate was filtered off, washed with methanol and diethyl ether, and dried under vacuum. Dark brown prism crystals, air stable and suitable for X-ray diffraction analysis, were obtained by slow evaporation of an acetonitrile solution after one week (69 mg, 0.03 mmol, 30%). (Found: C, 42.6; H, 4.2; N, 12.7%. $C_{16}H_{20}ClFeN_4O_6$ (Mr = 455.66 g/mol) requires C, 42.2; H, 4.4; N, 12.3%).

6 could also be prepared analogously to the former synthesis except that Et_3N (101 mg, 1.0 mmol) or NaOH (40 mg, 1.0 mmol) were used instead of NaN_3.

[Fe(acetyl-uns-penp)(tcc)Br] x $(C_2H_5)_2O$ (7). Anhydrous iron(III) bromide (30 mg; 0.1 mmol) and acetyl-uns-penp (28 mg, 0.1 mmol) were dissolved in 7 mL of acetone. After addition of tetrachlorocatechol hydrate (27 mg, 0.1 mmol) and triethylamine (24 μL, 17 mg; 0.17 mmol) the reaction mixture was stirred for 10 minutes and filtered. Vapor diffusion of diethyl ether into the complex solution yielded single crystals of **7** (58 mg, 0.09 mmol, 90%), mp 181°C (decomposition) (Found: C, 39.0; H, 3.9; N, 7.9%. $C_{22}H_{20}N_4BrCl_4FeO_3$ (without solvent, Mr = 666.0 g/mol) requires C, 39.7; H, 3.0; N, 8.4%).

[{Fe(acetyl-uns-penp)(tcc)}$_2$O] x $(C_2H_5)_2O$ x CH_3OH (8). The synthetic procedure is identical the same as for the preparation of **7** with the only difference that a slightly larger amount of triethylamine (28 μL, 20 mg; 0.2 mmol) was used instead. Vapor diffusion of diethyl ether into the complex solution yielded single crystals of **8** (37 mg, 0.03 mmol, 60%), mp 223°C (decomposition) (Found: C, 43.8; H, 3.7; N, 9.1%. $C_{44}H_{40}N_8Cl_8Fe_2O_7$ (without solvent, Mr = 1188.2 g/mol) requires C, 44.5; H, 3.4; N, 9.4%).

[Fe(uns-penp)Cl_2]ClO_4 x CH_3CN (9). To a solution of uns-penp (219 mg; 0.9 mmol) in methanol (10 mL) was added a solution of $Fe(ClO_4)_3$ x $6H_2O$ (139 mg, 0.3 mmol) and $FeCl_3$ (109 mg, 0.6 mmol) in methanol (10 mL). The resulting brown solution was stirred for 1 h at room temperature during which time a greenish yellow solid precipitated and then filtered. The precipitate was washed with methanol and diethyl ether, and dried under vacuum. Yellow prism crystals for crystallographic studies were obtained by vapour diffusion of diethyl ether into the acetonitrile solution. Yield: 221 mg (ca. 50%). Anal. Calcd. for $C_{16}H_{21}Cl_3FeN_5O_4$: C, 37.71; H, 4.15; N 13.75%. Found: C, 37.59; H, 4.13; N, 13.68%.

[{Fe(uns-penp)Cl}$_2$O](ClO$_4$)$_2$ x 2CH$_3$CN (10) To a methanol suspension (15 mL) of Fe(ClO$_4$)$_3$ x 6H$_2$O (115 mg, 0.25 mmol), FeCl$_3$ (41 mg, 0.25 mmol) and uns-penp ligand (122 mg; 0.5 mmol) was added Et$_3$N (51 mg, 0.5 mmol) in 5 mL of methanol under stirring. After 1 h, the resulting greenish brown slurry was filtered and the precipitate was washed with methanol and diethyl ether. Dark brown cube crystals suitable for X-ray diffraction analysis were achieved by slow evaporation of an acetonitrile solution about one week. Yield: 200 mg (ca. 42%). Anal. Calcd. for $C_{32}H_{42}Cl_4Fe_2N_{10}O_9$: C, 39.86; H, 4.39; N 14.53%. Found: C, 39.62; H, 4.24; N, 14.41%.

3.4.4 X-ray Crystallographic Studies.

Intensity data of **6** was collected on a Siemens SMART CCD 1000 diffractometer using graphite monochromated Mo- K_α radiation (λ = 0.71073 Å) by the ω-scan technique. The collected reflections were corrected for absorption effects.[31] All structures were solved by direct methods and refined by least-squares techniques using the SHELX97 programme package.[32] Further data collection parameters are summarised in Table 3-1.

Intensity data of acetyl-uns-penp, **7**, and **8** were collected on a Bruker AXS SMART 6000 CCD diffractometer (Cu-K_α, λ = 1.54178 Å, Göbel mirror) using the ω-scan technique. The collected reflections were corrected for absorption effects.[31] All structures were solved by direct methods and refined by full-matrix least-squares methods on F^2.[32] Further data collection parameters are summarised in Table 3-1.

Intensity data of **9** and **10** were collected at a temperature of 100 K on a Bruker-Nonius KappaCCD diffractometer with graphite-monochromated Mo-K_α radiation (λ = 0.71073 Å). Data were corrected for Lorentz and polarisation effects. Absorption effects were corrected numerically[106] for **9** and by semi-empirical methods based on multiple scans[105] for **10**. The structures were solved by direct methods; full–matrix least–squares refinement was carried out on F^2 using SHELXTL NT 6.12.[107] All non–hydrogen atoms were refined anisotropically. All hydrogen atoms were geometrically positioned; their isotropic displacement parameters were tied to those of their corresponding carrier atoms by a factor of 1.2 or 1.5.

CCDC 266956 (acetyl-uns-penp), 263645 (**6**), 266957 (**7**), 266958 (**8**), 283894 (**9**), and 283895 (**10**) contain the supplementary crystallographic data for this paper. These data can be obtained free of charge at www.ccdc.cam.ac.uk/ conts/retrieving.html [or from the Cambridge Crystallographic Data Centre, 12, Union Road, Cambridge CB2 1EZ, UK; Fax: (internat.) +44-1223-336-033; E-mail: deposit@ccdc.cam.ac.uk].

3.4.5 Determination of the Catechol 1,2-Dioxygenase activity.

The catechol cleaving activity of an *in situ* prepared complex solution was tested using piperidine as an external base as described previously.[35] The amount of base afforded to reach the highest reaction rates was determined according to the spectrophotometric titration described below. To 2 mL of a 2 x 10^{-4} M methanolic solution of $Fe(ClO_4)_3$ x H_2O and the ligand were added 0.02 mL of a 2 x 10^{-2} M (1 equivalent) solution of 3,5-H_2dbc. The proper amount of base was added to the reaction mixture from a 2 x 10^{-2} M stock solution. To limit the occurrence of errors, the oxidation of the complex was followed three times by UV-vis spectroscopy.

3.4.6 Spectrophotometric Titrations.

The spectrophotometric titrations were carried out with the same solutions as described above for the activity determinations. To avoid cleavage of the substrate, all manipulations were carried out under an argon atmosphere. A 0.1 mL sample of the 3,5-H_2dbc solution was added to 10 mL of the complex solution. The resulting mixture was titrated with piperidine and the UV-vis-spectra were monitored using a flow cell (1 cm).

Chapter 4 - Reaction behavior of dinuclear copper(I) complexes with m-xylyl-based ligands towards dioxygen

This work has been published previously in *Journal of the Chemical Society, Dalton Transactions*.

Foxon, S. P.; Utz, D.; Astner, J.; Schindler, S.; Thaler, F.; Heinemann, F. W.; Liehr, G.; Mukherjee, J.; Balamurugan, V.; Ghosh, D.; Mukherjee, R., Reaction behavior of dinuclear copper(I) complexes with m-xylyl-based ligands towards dioxygen. *J. Chem. Soc., Dalton Trans.* **2004,** 15, 2321-2328.

4.1 Introduction

Modelling of the copper enzyme tyrosinase (a monooxygenase causing hydroxylation of monophenols and subsequent oxidation of catechols to quinones)[2,108-111] was first performed successfully by Karlin and coworkers who found that an intramolecular ligand hydroxylation of the complex $[Cu_2(R\text{-}XYL\text{-}H)]^{2+}$ during its reaction with dioxygen occurred (Scheme 4-1).[112,113]

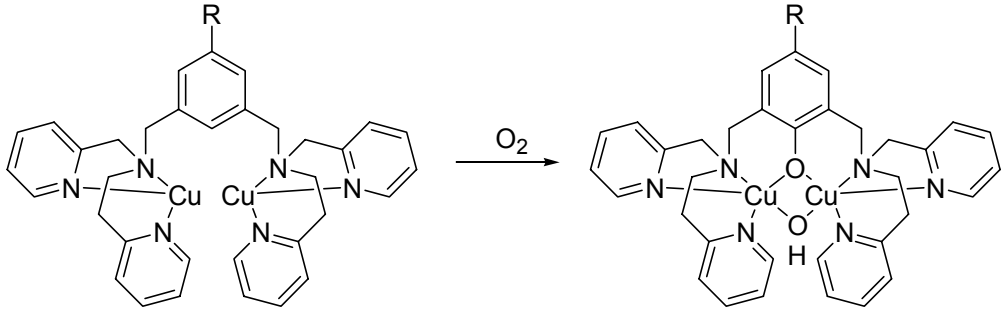

Scheme 4-1: Intramolecular ligand hydroxylation of $[Cu_2(R\text{-}XYL\text{-}H)]^{2+}$.

A detailed kinetic analysis performed at low temperature as well as a resonance Raman study revealed the formation of a $\mu\text{-}\eta^2\text{:}\eta^2$-peroxo complex as an intermediate.[39,114-116] However, it has been shown that bis-μ-oxo copper units are also capable of performing ligand hydroxylation reactions.[117]

At present it remains unclear why substitution of the pyridine groups in $[Cu_2(R\text{-}XYL\text{-}H)]^{2+}$ with pyrazole or benzimidazole donors completely suppresses the

above reaction, while with triazacyclononane units the intramolecular ligand hydroxylation reaction occurs.[40,117-125]

Furthermore, similar and structurally related binuclear copper(I) imine complexes also showed intramolecular ligand hydroxylation when reacted with dioxygen (Scheme 4-2), however, in these cases the intramolecular hydroxylation reaction was less sensitive towards ligand modifications.[123,126-136]

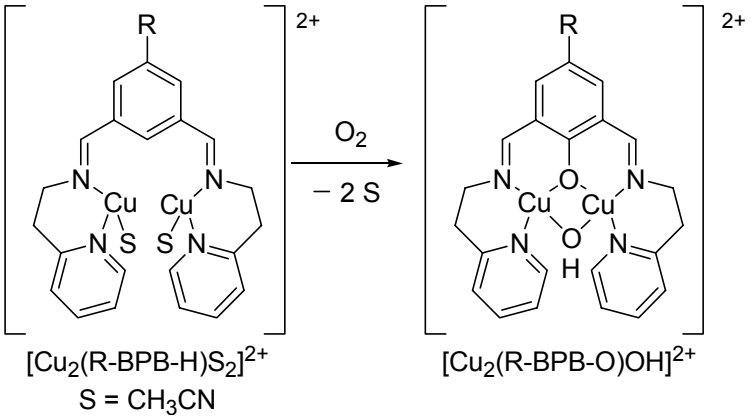

Scheme 4-2: Intramolecular ligand hydroxylation of $[Cu_2(H\text{-}BPB\text{-}H)S_2]^{2+}$

The reaction of dioxygen with complexes derived from reduction of the imine bonds of such complexes (e. g. $[Cu_2(H\text{-}BPB\text{-}H)S_2]^{2+}$ in Scheme 4-2) has not been studied so far in detail, although phenolate bridged binuclear copper(II) complexes with such amine ligands are well known (a few examples are given in the references).[137-141]

Therefore, in our efforts to gain a better understanding of the intramolecular ligand hydroxylation reactions of xylyl-bridged dicopper complexes, we investigated the reactivity of dioxygen towards the dinuclear copper(I) complex of the ligand α,α'-bis[(2-pyridylethyl)amino]-*m*-xylene (L^3, Scheme 4-3), the reduced form of the imine H-BPB-H (Scheme 4-2). Additionally we analysed the reaction of dioxygen with the copper(I) complex of the ligand α,α'-bis[*N*-(2-pyridylethyl)-*N*-(2-pyridylmethyl)-amino]-*m*-xylene (L^5) (Scheme 4-3) which differs from R-XYL-H (Scheme 4-1) by two shorter ligand "arms", leading to the formation of two smaller chelate rings in the metal complex.

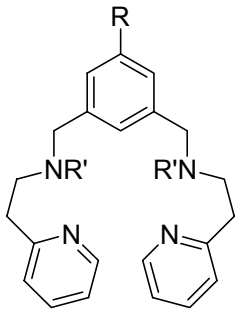

L^3: R' = H, R = H
L^4: R' = CH_3, R = H
L^5: R' = CH_2py, R = H

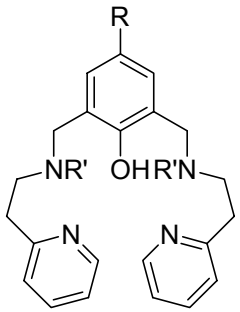

L^3-OH: R' = H, R = H
L^4-OH: R' = CH_3, R = H
Me-L^5-OH: R' = CH_2py, R = H

Scheme 4-3: Ligands used in this study

4.2 Results and Discussion

L^3, L^5 and Me-L^5-OH were readily prepared using standard synthetic procedures (see experimental section; however, alternative methods for the syntheses of L^5 and Me-L^5-OH have been used as well: e. g. L^5 can be prepared from L^3 using 2-picolyl chloride and base or by an *in situ* reductive alkylation[53,142] with 2-pyridinecarbaldehyde and $NaBH(OAc)_3$). The crude oils were purified by chromatography.

As described above it is well known that intramolecular ligand hydroxylation occurs when $[Cu_2(R\text{-}XYL\text{-}H)]^{2+}$ is reacted with dioxygen (Scheme 4-1). The different reaction pathways of related xylyl-bridged copper complexes during oxidation raised the question about the basic essential requirements for the occurrence of an intramolecular ligand hydroxylation. That intramolecular ligand hydroxylation was observed when the Schiff base complex $[Cu_2(H\text{-}BPB\text{-}H)S_2]^{2+}$ (Scheme 4-2) was reacted with dioxygen demonstrated that only two of the four "ethyl-pyridine arms" in $[Cu_2(R\text{-}XYL\text{-}H)]^{2+}$ are required for this kind of oxidation. However, it was not clear from the above finding if the imine donor atoms present in $[Cu_2(H\text{-}BPB\text{-}H)S_2]^{2+}$ are essential. It had been demonstrated by some of us earlier that imine donor atoms are not prerequisite by analysing the oxidation of the dinuclear copper(I) complex with L^4.[143,144] Once again intramolecular ligand hydroxylation was observed and therefore suggesting that only two nitrogen donor atoms of the ligand (per copper ion) are sufficient for intramolecular ligand hydroxylation reactions. Our findings were confirmed furthermore by the observations of Tolman and coworkers who observed ligand hydroxylations using bidentate ligands with nitro-

gen donor atoms.[117] However, the question remained and is addressed herein, as to whether the methyl group (or more general an alkyl group) needs to be attached to the secondary amine nitrogen donor atoms for intramolecular ligand hydroxylation to be observed.

Unfortunately we were unsuccessful in isolating the copper(I) complex of L^3 as a pure solid material. Therefore, solutions of this complex employed in the oxygenation experiments were prepared *in situ* by mixing $[Cu(CH_3CN)_4]ClO_4$ with L^3 in methanol (or dichloromethane) under an inert atmosphere. The yellow coloured complex $[Cu_2L^3(CH_3CN)_{2x}](ClO_4)_2$ (x = 1 or 2) is most likely formed, where one or two acetonitrile molecules are coordinated additionally as co-ligands to each copper(I) ion. After the reaction with dioxygen the green coloured phenolate-bridged product $[Cu_2(L^3\text{-}O)(OH)(ClO_4)]ClO_4$ (**11**) was isolated in good yield, clearly demonstrating again that intramolecular ligand hydroxylation had occurred. Crystals of complex **11** suitable for a single-crystal X-ray structure analysis were obtained by slow diffusion of Et_2O into a MeOH solution containing **11**. The quality of the crystals was poor and could not be improved by varying the crystallisation conditions. This seems to be a general problem when six-membered chelate rings are present in this type of ligands (see below) while in contrast it was much easier obtaining crystals of high quality for diffraction studies if only five-membered chelate rings are present.[137] This might be a consequence of the fact that copper(II) ions usually prefer five-membered chelate rings in their complexes. We obtained acceptable diffraction data for $[Cu_2(L^3\text{-}O)(OH)(ClO_4)]ClO_4$ (**11**) at 183(2) K. A summary of the crystallographic data, bond lengths and angles for **11** can be found in Table 4-1 and Table 4-2. An ORTEP[145] view of the cation of **11** is shown in Figure 4-1.

The two copper(II) centres (intramolecular separation Cu(1)…Cu(2) = 3.006(2) Å) in **11** are both penta-coordinate; Cu(1) is ligated by pyridyl nitrogen atom N(4), aliphatic amine N(3), phenolate oxygen O(1) and oxygen atoms O(2) and O(3) of the respective bridging hydroxo and perchlorate moieties. The bond angle between Cu(1), the μ-phenolate oxygen and Cu(2) [Cu(1)–O(1)–Cu(2)] = 101.1(3)°; the bond angle between Cu(1), the μ-hydroxo moiety and Cu(2) [Cu(1)–O(2)–Cu(2)] = 102.2(3)°. The coordination geometry about Cu(1) and Cu(2) is best described as close to square pyramidal with values of the trigonality index[146] (τ) equal to 0.12 for Cu(1) and 0.11 for Cu(2) (where $\tau = (\beta–\alpha)/60$, with α and β being

the two largest coordination angles around the metal centre: τ = 0 for square pyramidal geometry and τ = 1 for trigonal bipyramidal geometry). The basal plane of the square pyramid around Cu(1) contains O(1), O(2), N(3) and N(4) with O(3) occupying the axial coordination site. Metric parameters around Cu(2) are similar to Cu(1). A non-coordinating water solvent molecule and perchlorate anion (not shown in Figure 4-1) complete the structure of **11**.

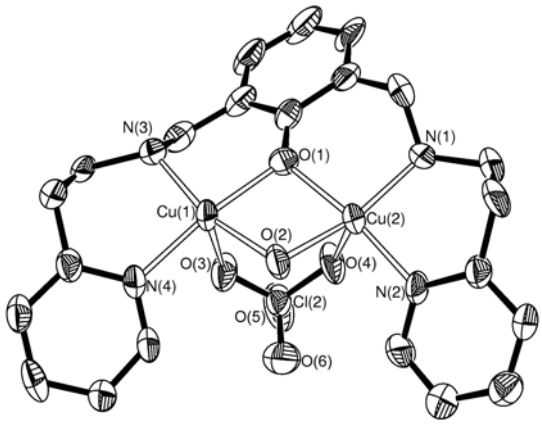

Figure 4-1: ORTEP[145] representation (50% probability displacement ellipsoids) of cation of 11. Hydrogen atoms omitted for clarity

Phenolate bridged complexes similar to **11** are well known and their properties have been studied extensively (a few examples are provided in the references).[120,121,137,139,141] A structurally related complex to **11** has been characterised by Grzybowski *et al*.[140] The ligand employed differed from L^3-OH in that a *para*-methyl group was present on the central aromatic ring (Scheme 4-3, L^3-OH, however with R = CH_3 instead of H). Although the authors presented detailed physicochemical studies no crystal structure of the complex was described probably due to the same difficulties we had with obtaining crystals of **11** suitable for X-ray crystal structure determination.

Comparison of the crystal structure of **11** with the complex $[Cu_2(L^4\text{-}O)(OH)](ClO_4)_2$ (**12**) described previously[144] shows that bond lengths and angles around the copper(II) centres are similar, with the distance between the two copper(II) ions being close to 3 Å. The situation is different if we compare the crystal structure of **11** with an analogous complex described earlier by some of us, where the chelate ring sizes are smaller.[137] There are significant differences in bond lengths and bond angles between the two complexes. The most striking effect of the smaller chelate

ring size is reflected in the bond angles N(1)–Cu(1)–N(2) and N(3)–Cu(2)–N(4): these values are 84.8(4)° and 84.1(4)° in the structure with the smaller chelate rings present and 96.3(3)° and 94.7(3)° for **11**.

Karlin and coworkers and some of us observed that reducing the chelate ring sizes in $[Cu_2(R\text{-}XYL\text{-}H)]^{2+}$ by substituting the "ethyl-pyridine arms" with "methyl-pyridine arms" completely suppressed intramolecular ligand hydroxylation.[143,147] Therefore, it was an obvious question to address as to whether partial substitution, i.e. the substitution of only two "arms", would support or suppress the intramolecular ligand hydroxylation reaction. Reaction of L^5 (Scheme 4-3) and $[Cu(CH_3CN)_4]ClO_4$ in acetone lead to the formation of $[Cu_2L^5](ClO_4)_2$ (**13**) that could be crystallographically characterised. A summary of the crystallographic data, bond lengths and angles for **13** is presented in Table 4-1 and Table 4-2. An ORTEP[145] view of the cation of **13** (including the weak interaction of an acetone molecule and a perchlorate anion) is shown in Figure 4-2:

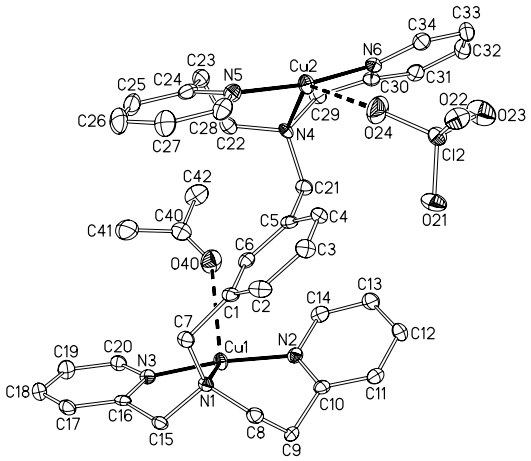

Figure 4-2: ORTEP[145] representation (50% probability displacement ellipsoids) of the cation of 13 (including the weakly coordinated acetone molecule and perchlorate anion). Hydrogen atoms omitted for clarity

Similar to the crystal structure of $[Cu_2(R\text{-}XYL\text{-}H)]^{2+}$ acetonitrile molecules are not coordinated to the copper(I) ions as additional ligands.[112] However, bond distances and angles are clearly different due to the "replacement" of a six membered chelate ring with a five membered chelate ring (e. g. Cu(1)–N(1) = 2.334(2) and Cu(2)–N(4) = 2.308(2) Å are longer in **13** compared with Cu(1)–N(1) = 2.121(8) and Cu(2)–N(4) = 2.196(7) Å in $[Cu_2(R\text{-}XYL\text{-}H)]^{2+}$).[112]

Oxidation of the solution-generated dicopper(I) complex of the *m*-xylyl-based dinucleating ligand L^5 and $[Cu(CH_3CN)_4]ClO_4$ in MeOH at 298 K with O_2 again lead to an intramolecular ligand hydroxylation. This was proved by isolation and characterisation of the hydroxylated ligand L^5-OH according to the published procedure for the hydroxylation of $[Cu_2(R\text{-}XYL\text{-}H)]^{2+}$.[112] No crystals of the product complex suitable for an X-ray crystal structure analysis were obtained (however, see below:

Table 4-1: Crystallographic data for 11, 13 and 17

	11	**13**	**17**
Molecular formula	$C_{22}H_{28}Cl_2Cu_2N_4O_{11}$	$C_{37}H_{42}Cl_2Cu_2N_6O_9$	$C_{24}H_{29}Cl_3Cu_2N_4O$
M_r	722.46	912.75	622.94
Temperature /K	183(2)	100(2)	293(2)
Radiation used (λ /Å)	Mo-$K\alpha$ (0.71073)	Mo-$K\alpha$ (0.71073)	Mo-$K\alpha$ (0.71073)
Crystal system	Triclinic	Triclinic	Triclinic
Space group	P–1 (P1 bar)	P–1 (P1 bar)	P–1 (P1 bar)
a /Å	10.570(5)	8.8457(5)	9.931(4)
b /Å	12.130(5)	12.839(2)	16.66(2)
c /Å	12.360(5)	18.430(2)	17.64(2)
α /°	68.590(5)	75.861(6)	61.26(5)
β /°	73.080(5)	78.533(5)	87.52(5)
γ /°	71.198(5)	85.776(6)	87.59(5)
V [Å^3]	1369(1)	1988.5(4)	2557(4)
Z	2	2	4
$D_{calc.}$ /g cm^{-3}	1.752	1.524	1.618
μ /mm^{-1}	1.814	1.265	2.002
Reflections measured	9128	51968	7019
Unique reflections, R_{int}	5370, 0.1048	8770, 0.0952	6583, 0.0987
Refined parameters	384	507	609
Goodness-of-fit on F^2	1.029	1.049	1.031
$R(F, F^2>2\sigma)$	0.0836	0.0447	0.0964
$R_w(F^2$, all data)	0.2358	0.0926	0.3169

Table 4-2: Selected bond lengths (Å) and interbond angles (°) for 11, 13 and 17

11					
Cu(1)–N(1)	2.026(8)	Cu(1)–N(2)	1.946(8)	Cu(1)–O(1)	1.973(7)
Cu(1)–O(2)	1.918(7)	Cu(1)–O(3)	2.528(8)	Cu(2)–N(3)	2.028(8)
Cu(2)–N(4)	1.941(8)	Cu(2)–O(1)	1.916(6)	Cu(2)–O(2)	1.943(7)
Cu(2)–O(4)	2.499(7)	Cu(1)…Cu(2)	3.006(2)		
N(1)–Cu(1)–N(2)	96.3(3)	N(1)–Cu(1)–O(1)	172.3(3)	N(1)–Cu(1)–O(2)	97.6(3)
N(2)–Cu(1)–O(1)	90.1(3)	N(2)–Cu(1)–O(2)	165.3(3)	O(1)–Cu(1)–O(2)	76.4(3)
N(3)–Cu(2)–N(4)	94.7(3)	N(3)–Cu(2)–O(1)	93.9(3)	N(3)–Cu(2)–O(2)	165.1(3)
N(4)–Cu(2)–O(1)	171.4(3)	N(4)–Cu(2)–O(2)	94.4(3)	O(1)–Cu(2)–O(2)	77.1(3)
13					
Cu(1)–N(1)	2.334(2)	Cu(1)–N(2)	1.909(2)	Cu(1)–N(3)	1.921(2)
Cu(1)–O(40)	2.835(2)	Cu(2)–N(4)	2.308(2)	Cu(2)–N(5)	1.902(2)
Cu(2)–N(6)	1.916(2)	Cu(2)–O(24)	3.087(2)		
N(1)–Cu(1)–N(2)	96.40(9)	N(1)–Cu(1)–N(3)	83.50(9)	N(2)–Cu(1)–N(3)	172.8(1)
N(1)–Cu(1)–O(40)	123.55(8)	N(2)–Cu(1)–O(40)	92.14(9)	N(3)–Cu(1)–O(40)	93.92(9)
N(4)–Cu(2)–N(5)	97.2(1)	N(4)–Cu(2)–N(6)	83.74(9)	N(5)–Cu(2)–N(6)	171.2(2)
N(4)–Cu(2)–O(24)	136.90(8)	N(5)–Cu(2)–O(24)	93.42(9)	N(6)–Cu(2)–O(24)	91.80(9)
17					
Cu(1)–N(1)	2.03(2)	Cu(1)–N(2)	2.06(2)	Cu(1)–O(1)	1.92(2)
Cu(1)–Cl(1)	2.339(5)	Cu(1)–Cl(2)	2.457(6)	Cu(2)–N(3)	2.03(2)
Cu(2)–N(4)	2.00(2)	Cu(2)–O(1)	1.95(2)	Cu(2)–Cl(2)	2.426(5)
Cu(2)–Cl(3)	2.421(5)	Cu(1)…Cu(2)	3.293(5)		
N(1)–Cu(1)–O(1)	168.2(5)	N(1)–Cu(1)–Cl(1)	94.5(5)	N(2)–Cu(1)–Cl(2)	126.9(4)
N(2)–Cu(1)–O(1)	91.2(6)	N(2)–Cu(1)–Cl(1)	118.5(4)	Cl(1)–Cu(1)–Cl(2)	114.0(2)
N(1)–Cu(1)–N(2)	93.6(6)	O(1)–Cu(1)–Cl(2)	79.1(4)	N(1)–Cu(1)–Cl(2)	89.3(4)
O(1)–Cu(1)–Cl(1)	92.7(4)	N(3)–Cu(2)–O(1)	90.3(6)	N(4)–Cu(2)–O(1)	167.6(5)
N(3)–Cu(2)–N(4)	93.1(6)	O(1)–Cu(2)–Cl(3)	94.6(4)	N(4)–Cu(2)–Cl(3)	95.5(4)
N(3)–Cu(2)–Cl(3)	110.0(4)	O(1)–Cu(2)–Cl(2)	79.4(4)	N(4)–Cu(2)–Cl(2)	90.7(4)
N(3)–Cu(2)–Cl(2)	142.8(4)	Cl(2)–Cu(2)–Cl(3)	106.4(2)		

independent synthesis of a phenolate bridged complex derived from Me-L^5-OH).

As described above, it was possible to observe a peroxo intermediate complex spectrophotometrically when $[Cu_2(R\text{-}XYL\text{-}H)]^{2+}$ was oxidised with dioxygen using low temperature stopped-flow techniques.[39,115,116] However, our efforts to detect such a transient "dioxygen adduct" with the dinuclear copper complexes of the ligands L^3, L^4 and L^5 using stopped-flow techniques were unsuccessful. Even at low temperatures only the formation of the final products was observed spectroscopically. This finding is in agreement with our earlier results on the related imine complex $[Cu_2(H\text{-}BPB\text{-}H)S_2]^{2+}$ described above (Scheme 4-2) and a dinuclear macrocyclic copper Schiff base compound; in both cases no "dioxygen adduct" was observed.[127-129] Furthermore, Murthy *et al*. could not detect spectroscopically such an intermediate during the analysis of the reaction of dioxygen with $[Cu_2(UN2\text{-}H)]^{2+}$ where the unsymmetric ligand UN2-H consists of one half of R-XYL-H and one half of L^4.[148] The probable reason in all these cases most likely is based on the kinetics of the reaction: the rate of formation of any "dioxygen adduct" is slower than its consecutive reactions and therefore cannot be detected.

4.3 Phenolate bridged complexes

As described above the phenolate-bridged complexes $[Cu_2(L^3\text{-}O)(OH)(ClO_4)]ClO_4$ (**11**) and $[Cu_2(L^4\text{-}O)(OH)](ClO_4)_2$ (**12**) could be readily prepared in good yields by oxidizing the copper(I) complexes of L^3 and L^4 with dioxygen while this was not possible with the ligand L^5. Therefore, we prepared three copper(II) complexes $[Cu_2(Me\text{-}L^5\text{-}O)X](ClO_4)_2 \bullet nH_2O$ (Me-L^5-OH = 2,6-bis[*N*-(2-pyridylethyl)-*N*-(2-pyridylmethyl)amino]-4-methylphenol) with X = $C_3H_3N_2^-$ (prz) (**14**), $MeCO_2^-$ (**15**) and N_3^- (**16**); *n* = 1 for **14** and *n* = 2 for **15** and **16**. Microanalytical data, IR spectra and solution electrical conductivity measurements are in conformity with our proposed formulations. The IR data demonstrates that in complex **16** the azide group most likely is present in a μ-1,1-bridging mode. So far we have been unsuccessful in determining the three-dimensional X-ray structures of the complexes **14–16** because of the poor quality of crystals obtained. In contrast we obtained crystals of $[Cu_2(Me\text{-}L^5\text{-}O)(H_2O)_2](ClO_4)_3$ by reacting the ligand Me-L^5-OH with $[Cu(H_2O)_6](ClO_4)_2$ in a mixture of water and methanol. A crystal structure determination supported the above formulation and showed that in the phenolate-bridged

complex an additional water molecule is coordinated to each copper(II) ion, in a similar manner to the structurally characterised complexes $[Cu_2(F\text{-}L^6\text{-}O)(H_2O)_2](ClO_4)_3$ and $[Cu_2(CF_3\text{-}L^6\text{-}O)(H_2O)_2](ClO_4)_3$ where L^6 = 2,6-bis[bis(2-pyridylmethyl)aminomethyl]-4-R-phenol.[149] The quality of the structural refinement of $[Cu_2(Me\text{-}L^5\text{-}O)(H_2O)_2](ClO_4)_3$ was not good enough for publication due to disorder problems encountered with the perchlorate anions. Efforts in obtaining better quality single-crystals have also been unsuccessful. However, we accurately determined a pK_a value of 4.76(2) for the deprotonation of $[Cu_2(Me\text{-}L^5\text{-}O)(H_2O)_2](ClO_4)_3$ leading to $[Cu_2(Me\text{-}L^5\text{-}O)(OH)](ClO_4)_2$. The pK_a value we determined is very close to the one obtained for the acid-base equilibrium between $[Cu_2(Me\text{-}L^6\text{-}O)(H_2O)_2](ClO_4)_3$ and $[Cu_2(Me\text{-}L^6\text{-}O)(OH)](ClO_4)_2$ (pK_a = 4.95).[149]

Treating complex **12** with an excess of chloride ions lead to the formation of $[Cu_2(L^4\text{-}O)Cl_3]$ (**17**). It was also possible to regenerate **12** from **17** by adding water to a solution of **17** in acetonitrile, with both exchange reactions being readily monitored by UV-vis spectroscopy. Confirmation of the composition of **17** was obtained from a single-crystal X-ray structure determination. The asymmetric unit contains two crystallographically independent molecules of complex **17**. Both molecules have essentially identical coordination geometries, but the corresponding bond lengths and bond angles are different. A summary of the crystallographic data, bond lengths and angles for **17** can be found in Table 4-1 and Table 4-2. An ORTEP[145] view of one of the crystallographically independent molecules of **17** is shown below in Figure 4-3.

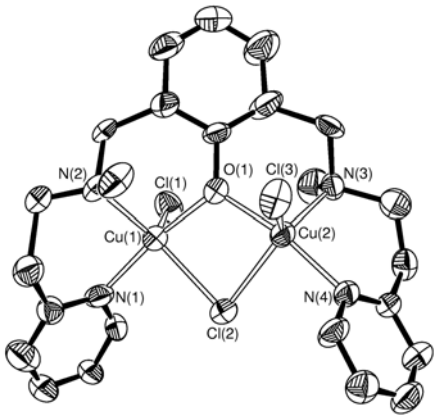

Figure 4-3: ORTEP[145] representation (50% probability displacement ellipsoids) of 17. Hydrogen atoms omitted for clarity.

Complex **17** is a dinuclear copper(II) complex of the same dinucleating ligand as in complex $[Cu_2(L^4\text{-}O)(OH)](ClO_4)_2$ (**12**).[144] The two copper(II) centres in complex **17** (Cu(1)…Cu(2) separation = 3.293(5) Å; for the other molecule 3.272(5) Å) are bridged by an endogenous phenolate and an exogenous chloride moiety, with additional chloride coordination at each copper(II) centre. Both Cu(1) and Cu(2) are penta-coordinate being ligated by one pyridyl nitrogen, one aliphatic amine nitrogen, a phenolate oxygen and two chloride ions. The phenolate oxygen and a chloride ion bridge the copper(II) centres. The geometry about each copper(II) centre is best described as distorted trigonal bipyramidal: τ[146] = 0.69 [Cu(1)] and τ = 0.41 [Cu(2)], the corresponding values for the other molecule are τ = 0.74 [Cu(1a)] and τ = 0.51 [Cu(2a)]. Cu(1) is displaced 0.09 Å and Cu(2) 0.11 Å out of the trigonal plane, towards the pyridyl nitrogen atom N(1) and N(4), respectively. The angles between the central phenolate ring and pyridyl rings are 18.4.1(8)^o and 42.1(7)^o for the molecule shown in Figure 4-3. The structural motif exhibited in complex **17** is rare; there are only three other structurally characterised copper(II) complexes of nitrogen donor-based ligands containing both a bridging phenolate anion and a chloride anion.[150-152]

4.4 Magnetic characteristics

Due to the presence of the phenoxo-/hydroxo-bridge in **12** significant antiferromagnetic exchange coupling is present (–440 cm^{-1}).[143] Variable-temperature (80–300 K) magnetic susceptibility analyses for **14–17** were performed. Their magnetic properties are of interest owing to the presence of an invariant phenoxide bridge and variable exogenous bridges. At 300 K the μ_{eff}/Cu values (in μ_B) for this set of compounds are: 1.73 (**14**), 1.76 (**15**), 1.77 (**16**) and 1.25 (**7**). The corresponding values at 80 K are: 1.28, 1.33, 1.34 and 0.34, respectively. Plots of χ_MT *vs*. T for two representative complexes **14** and **17** are shown in Figure 4-4.

The observed magnetic susceptibility data were fitted to the modified Bleaney-Bowers Equation (4.1)[153] by allowing for the presence of monomeric impurity, where ρ is the mole-fraction of the non-coupled copper(II) impurity.

$$\chi_M = \frac{2N\beta^2 g^2}{3kT}\left[1+\frac{1}{3}\exp\left(\frac{-2J}{kT}\right)\right]^{-1}(1-\rho)+\frac{N\beta^2 g^2 \rho}{2kT}+2N_\alpha \qquad (4.1)$$

In this expression, N, g and k have their usual meaning; 2*J* is the energy difference between the singlet and triplet states; χ_M is the molar susceptibility per dimer. The values of g and temperature-independent paramagnetic susceptibility (N_α) were kept fixed at g = 2.1 [typical value for a tetragonal Cu(II)] and 60 x 10^{-6} cm^3 mol^{-1}, respectively, during fitting procedure. To get a better control of g values the EPR spectra of **14–16** were recorded. In fact, in the polycrystalline state at 300 K each complex exhibits almost isotropic signal. The g values are: 2.08 for **14**, 2.07 for **15**, 2.11 (g_{av} value from a weak axial spectrum). The best-fit parameters of *J* and ρ using Eq. 4.1 were obtained by a non linear least-squares fitting procedure. The quality of fit was estimated by the *R* index defined as $R = \Sigma(\chi_M^{expt} - \chi_M^{calc})^2/\Sigma(\chi_M^{expt})^2$. The parameters that were obtained are collected in Table 4-3.

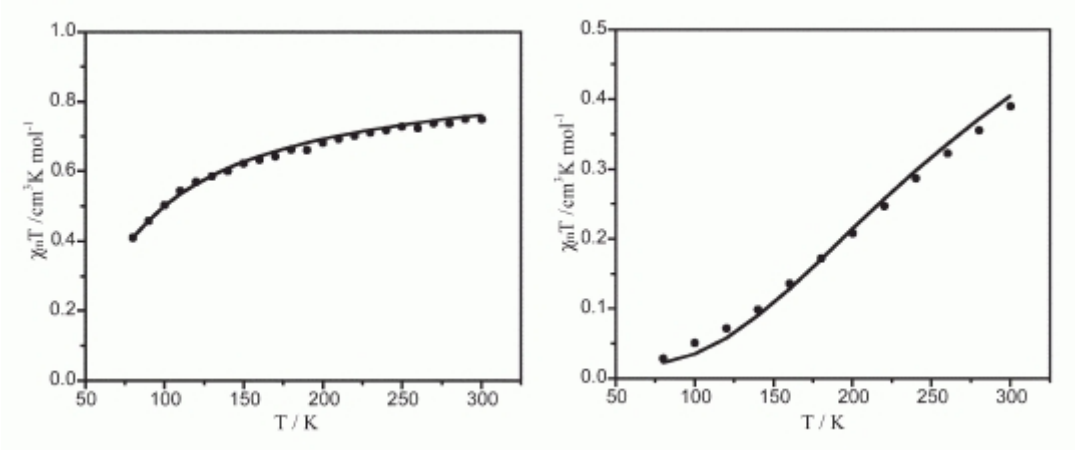

Figure 4-4: χ_mT *versus* temperature T plots for 14 and 17 (from left to right). Circles represent experimental data, the solid line represents the fit

There is an appreciable drop in the extent of antiferromagnetic coupling, comparing complexes **12** and **17** (Table 4-3). A similar trend was observed by Karlin and co-workers, for closely related systems (the geometry around the copper(II) centres, however, remained invariant).[151] Thus the extent of antiferromagnetic exchange coupling is much higher in **17** than that present in complexes **13** – **16**. Within the similar class of complexes **14**–**16**, temperature-dependent magnetic susceptibility studies reveal that (i) there is medium antiferromagnetic exchange coupling between pairs of copper(II) ions in each case and (ii) the magnitude of

the antiferromagnetic exchange depends on the identity of the exogenous bridge (prz > azide > acetate). It is worth noting that the present work complements the ones of several authors who investigated the effect of exogenous bridges in the transmission of magnetic exchange between two copper(II) centres.[154]

The effective magnetic moments for **14–16** in MeCN solution (300 K) were determined by using the NMR method to examine whether or not the solid state structures of the complexes are retained in solution. The μ_{eff}/Cu values for **14** and **15** are in reasonable agreement with solid-state values. However, for **16** the solution-state value (1.55 μ_B) is slightly less than the solid-state value (1.77 μ_B). This behaviour could be due to a relaxed geometry in the solution state, allowing a better pathway for magnetic coupling.

Table 4-3: Magnetic data for endogenously phenoxo-bridged dicopper(II) complexes

Complex	$-2J$ (cm^{-1})	ρ (%)	10^8R	Ref.
$[Cu_2(L^4\text{-}O)(OH)](ClO_4)_2$ (**12**)	–440			[155]
$[Cu_2(Me\text{-}L^5\text{-}O)(\mu\text{-}pyz)](ClO_4)_2 \times H_2O$ (**14**)	–92	0.44	5.67	this work
$[Cu_2(Me\text{-}L^5\text{-}O)(\mu\text{-}OAc)](ClO_4)_2 \times 2H_2O$ (**15**)	–86	0.40	11.60	this work
$[Cu_2(Me\text{-}L^5\text{-}O)(\mu\text{-}1,1\text{-}N_3)](ClO_4)_2 \times 2H_2O$ (**16**)	–88	0.53	20.20	this work
$[Cu_2(L^4\text{-}O)Cl_3]$ (**17**)	–374	0.91	7.05	this work
$[Cu_2(L\text{-}O)(OH)](PF_6)_2$	–600			[112,149]
$[Cu_2(L\text{-}O)Cl](BPh_4)_2 \times MeCOMe$	–335			[149]
$[Cu_2(L\text{-}O)(\mu\text{-}1,1\text{-}N_3)](PF_6)_2$	–440			[156]

L-OH = 2,6-bis[*N*-(2-pyridylethyl)aminomethyl]phenol.

4.5 Conclusions

Considering the large number of studies that have been performed on xylyl-bridged dicopper(I) complexes it is surprising that at present we do not have a detailed understanding of their reaction pathways when oxidised with dioxygen. Sorrell commented earlier that attempts to find a correlation between the physical

properties of the complexes and their ability to support intramolecular ligand hydroxylation reactions have been unsuccessful.[121] Chelate ring sizes in the complexes seem to play an important role; for imine complexes such as $[Cu_2(H\text{-}BPB\text{-}H)S_2]^{2+}$ (Scheme 4-2) or for the amine complex $[Cu_2(R\text{-}XYL\text{-}H)]^{2+}$ (Scheme 4-1) a decrease in the chelate ring size from six to five completely suppressed the intramolecular ligand hydroxylation. In our work presented herein we also observed intramolecular ligand hydroxylation when dioxygen was reacted with the copper(I) complex of L^3 with only six-membered chelate rings present. Furthermore, intramolecular ligand hydroxylation was observed with the copper(I) complex of L^5, where two five-membered chelate rings were introduced additionally. Several other copper(I) complexes containing only five-membered chelate rings are known, which also show ligand hydroxylation reactions. Therefore, the occurrence of intramolecular ligand hydroxylation cannot be a result of chelate ring size alone. Based on the results/observations available it is more probable that the overall geometry, which the ligand enforces on the copper centres, plays an important role in determining the fate of the metal-bound "activated dioxygen adduct". If the ligand backbone allows the approach of the "activated oxygen adduct" close to the aromatic C-H bond to be activated then intramolecular ligand hydroxylation is observed. However, if the steric demands of the ligand enforces a larger distance between the metal-bound "dioxygen adduct" and the aromatic ring then the hydroxylation reaction is suppressed and "normal" intermolecular oxidation reactions are observed.

4.6 Experimental

4.6.1 Reagents and materials

Reagents and solvents used, unless stated otherwise, were of commercially available reagent grade quality. $[Cu(CH_3CN)_4]PF_6$ and $[Cu(CH_3CN)_4]ClO_4$ were synthesised according to literature procedures.[157]

4.6.2 Physical measurements

Elemental analyses were obtained either from the University of Erlangen-Nürnberg or the Facility for Ecological and Analytical Testing (FEAT) laboratory, Indian Institute of Technology, Kanpur. Solution electrical conductivity measurements were

carried out with an Elico (Hyderabad, India) Type M-82 T conductivity bridge with a solute concentration of ≈1.0 x 10^{-3} M. Spectroscopic data were obtained by using the following instruments: infrared, Bruker Vector 22; ^{1}H NMR, Bruker DXP 300 AVANCE (300 MHz, University of Erlangen-Nürnberg); UV-vis, Agilent 8453 diode-array. Variable-temperature solid-state magnetic susceptibility measurements were performed either by the Faraday technique using a local built magnetometer (at a fixed main field strength of ≈ 10 kG)[153] or a Quantum Design (Model MPMSXL-5) SQUID magnetic susceptometer operating at a magnetic field of 0.5 T. Solution state magnetic susceptibility measurements were done by the NMR technique of Evans[158] in MeCN with a PMX-60 JEOL (60 MHz, IIT Kanpur) NMR spectrometer. Susceptibilities were corrected by using appropriate diamagnetic corrections.[159]

Stopped-flow measurements at ambient and at low temperatures were performed as described previously.[39,160] Solutions of copper(I) complexes were prepared by mixing stoichiometric amounts of copper(I) salts with the appropriate ligand under argon in a glove box (Braun, Germany; water and dioxygen less than 1 ppm) and then transferred with gas-tight syringes to the instrument. A dioxygen saturated solution was prepared by bubbling dioxygen through the solvent for 20 min.

4.6.3 Ligand Syntheses

α,α′-Bis[(2-pyridylethyl)aminomethyl]benzene (L^3). 2-(2-aminoethyl)pyridine 2.44 g (20 mmol) was added to a solution of isophthalaldehyde 1.34 g (10 mmol) in MeOH (110 cm^3) and the solution was stirred for 2 h at 60°C. $NaBH_4$ 1.00 g (26 mmol) was added slowly to the solution and the cloudy solution was stirred over-night. By careful addition of 10 M HCl the excess $NaBH_4$ was destroyed and the solution was brought to a pH value of 2. After concentration of the solution *in vacuo*, aqueous 5 M NaOH was added to the residue until a pH value of 12 was reached. The aqueous solution was extracted with CH_2Cl_2 (4 × 30 cm^3 portions) and the organic fractions were combined and dried over anhydrous Na_2SO_4. Removal of the solvent yielded the crude product as a yellow coloured oil which was chromatographed on silica gel (60 Å pore size, 70–230 mesh) with MeOH/Et_3N (50:1) as eluent (R_f = 0.37) yielding L^3 as a pale-yellow coloured oil (6.2 g, 90%). δ_H(300 MHz; solvent $CDCl_3$; standard $SiMe_4$) 8.42 [2 H, d, Ar–*H*], 7.49–6.93 [10 H,

m, Ar–*H*], 3.68 [4 H, s, ArC*H*$_2$NH–], 2.98 [8 H, m, –NHC*H*$_2$C*H*$_2$py]. δ_C(75 MHz; solvent $CDCl_3$; standard $SiMe_4$) 160.3, 149.5, 140.4, 128.9, 128.3, 127.5, 124.2, 121.4, 54.3, 49.1, 38.4.

α,α′-Bis[*N*-methyl-*N*-(2-pyridylethyl)amino]-*m*-xylene (L^4). L^4 was synthesised as described previously.[143]

α,α′-Bis[*N*-(2-pyridylethyl)-*N*-(2-pyridylmethyl)amino]-*m*-xylene (L^5). A solution of Et_3N (0.475 g, 4.69 mmol) in dry MeOH (20 cm^3) was added dropwise to a solution of 2-pyridylethyl-(2-pyridylmethyl)amine[161] (1.0 g, 4.69 mmol) in dry MeOH (40 cm^3) at 10°C with magnetic stirring. A solution of α-α′-dibromo-*m*-xylene (0.62 g, 2.35 mmol) in dry MeOH (40 cm^3), over a period of 10 min was then added. The reaction mixture was stirred for a further 2.5 h and then was kept at ~30°C overnight. The solvent was removed *in vacuo* to obtain the crude product as a brown-yellow coloured semi-solid. The desired ligand was obtained by exhaustive extraction of the aqueous phase with $CHCl_3$ (a little water was also added at this stage) until the aqueous layer was colourless. The organic fractions were combined and then dried over anhydrous Na_2SO_4. Filtration and removal of the solvent yielded the crude product as a red-brown coloured oil which was chromatographed on neutral aluminium oxide with ethyl acetate as eluent (R_f = 0.40) yielding L^3 as a yellow coloured oil (0.9 g, 60%). δ_H(300 MHz; solvent $CDCl_3$; standard $SiMe_4$) 8.46 [4 H, d, py–*H*], 7.60–7.04 [16 H, m, Ar–*H*], 3.79 [4 H, s, pyC*H*$_2$N–], 3.69 [4 H, s, ArC*H*$_2$N–], 2.98 [8 H, m, pyC*H*$_2$C*H*$_2$N–]. δ_C(75 MHz; solvent $CDCl_3$; standard $SiMe_4$) 160.6, 160.2, 149.1, 148.7, 139.2, 136.2, 136.0, 129.2, 128.1, 127.4, 123.4, 122.7, 121.7, 121.0, 60.1, 58.5, 54.1, 36.0.

2,6-Bis[*N*-(2-pyridylethyl)-*N*-(2-pyridylmethyl)amino]-4-methylphenol (Me-L^5-OH). A solution of 2,6-bis(chloromethyl)-4-methylphenol[152] in MeOH (20 cm^3) was added dropwise to a vigorously stirred solution of 2-pyridylmethyl-(2-pyridylethyl)methylamine (0.50 g, 2.44 mmol) and Et_3N (0.49 g, 4.88 mmol) in MeOH (40 cm^3) at 0°C. The solution was then stirred at ~10°C for 3 h and then stirred overnight at ~30°C. Solvent was removed *in vacuo* and the ligand was extracted with $CHCl_3$. The organic layer was washed first with a saturated brine solution and then with distilled water and dried over anhydrous Na_2SO_4. Removal of the solvent *in vacuo* afforded Me-L^5-OH as a brown coloured oil (0.67 g, 88%) that can be further purified by chromatography using basic alumina oxide with ethyl

acetate as eluent (R_f = 0.50). δ_H(300 MHz; solvent $CDCl_3$; standard $SiMe_4$) 8.54 [2 H, d, $^3J_{HH}$ = 4.4 Hz, py–*H*], 8.48 [2 H, d, $^3J_{HH}$ = 4.4 Hz, py–*H*], 7.54–7.44 [4 H, m, py–*H*], 7.25–7.01 [8 H, m, py–*H*], 6.84 [2 H, s, Ar–*H*], 3.86 [4 H, s, pyCH_2N–], 3.76 [4 H, s, ArCH_2N–], 3.00 [8 H, s, pyCH_2CH_2N–], 2.16 [3 H, s, –CH_3]. δ_C(75 MHz; solvent $CDCl_3$; standard $SiMe_4$) 160.3, 159.2, 153.5, 149.1, 148.8, 136.4, 136.2, 129.2, 127.5, 123.4, 121.9, 121.1, 59.9, 54.7, 53.9, 35.6, 20.6.

Preparation of $[Cu_2(L^3\text{-}O)(OH)(ClO_4)]ClO_4$ (11). L^3 (0.173 g, 0.50 mmol) in MeOH (5 cm^3) was added dropwise under nitrogen to a suspension of $[Cu(CH_3CN)_4]ClO_4$ (0.327 g, 1.00 mmol) in MeOH (15 cm^3). The solution turned yellow in colour and was very sensitive towards oxidation by air. Exposure to air lead to the formation of a deep green coloured solution. After removal of the solvent *in vacuo* a solid was obtained which was recrystallised by diffusion of Et_2O into a MeOH solution of complex **11** (0.26 g, 75%). Crystals of **11** suitable for a single-crystal X-ray structure determination were obtained in this manner. Found: C, 37.8; H, 3.7; N, 7.6. Calc. for $C_{22}H_{26}Cl_2Cu_2N_4O_{10}$: C, 37.5; H, 3.7; N, 7.9%.

Preparation of $[Cu_2(L^5)(C_3H_6O)(ClO_4)]ClO_4$ (13). Under inert conditions $[Cu(CH_3CN)_4]ClO_4$ (0.327 g, 1.00 mmol) was added in small portions to a stirred solution of 0.264 g (0.5 mmol) L^5 in acetone (15 cm^3). Diffusion of Et_2O into this solution lead to the formation of yellow coloured crystals suitable for a single-crystal X-ray structure determination.

Preparation of $[Cu_2(Me\text{-}L^5\text{-}O)(C_3H_3N_2)](ClO_4)_2 \times H_2O$ (14). A mixture of Me-L^5-OH (0.10 g, 0.179 mmol), NaOMe (0.0097 g, 0.358 mmol) and pyrazole (0.0012 g, 0.179 mmol) in MeCN (5 cm^3) was stirred at 0°C for 0.5 h. A solution of $[Cu(H_2O)_6](ClO_4)_2$ (0.133 g, 0.358 mmol) in MeCN (5 cm^3) was then added dropwise. After 12 h the resulting greenish brown coloured solution was filtered and allowed to evaporate slowly at room temperature. A deep brownish green coloured microcrystalline product that deposited was filtered off, washed with a MeCN-Et_2O (1:4) mixture (5 cm^3) and recrystallised from a 2:1 (v/v) mixture of Et_2O-MeCN (15 cm^3) (0.1 g, 49%). Found: C, 47.6; H, 4.3; N, 11.6. Calc. for $C_{38}H_{42}Cl_2Cu_2N_8O_{10}$: C, 47.1; H, 4.3; N, 11.6%. IR (KBr disc, selected peaks) $\tilde{\nu}_{max}$/cm^{-1}: 3440br (OH); 1090 and 630 (ClO_4^-). Molar conductance, Λ_M (MeCN, 298 K) = 245 Ω^{-1} cm^2 mol^{-1} (expected value for a 1:2 electrolyte[162]: 220–300 Ω^{-1} cm^2 mol^{-1}). UV-vis (MeCN)

λ_{max}/nm (ε/M^{-1} cm^{-1}): 660 (sh) (250), 470 (sh) (1000), 290 (sh) (9400) and 258 (19000). μ_{eff}/Cu (in MeCN, 298 K) 1.70 μ_B.

Preparation of $[Cu_2(Me\text{-}L^5\text{-}O)(O_2CMe)](ClO_4)_2 \times 2H_2O$ (15). A mixture of Me-L^5-OH (0.10 g, 0.179 mmol) and Et_3N (0.018 g, 0.178 mmol) in MeCN (5 cm^3) was stirred at 0°C for 20 min. $[Cu(H_2O)_6](ClO_4)_2$ (0.133 g, 0.358 mmol) was added and the mixture was stirred for 5 min resulting in a colour change from light brown to dark brown. A solution of $NaO_2CMe{\cdot}3H_2O$ (0.024 g, 0.179 mmol) in MeOH (2 cm^3) under magnetic stirring was then added. During the addition the colour changed from deep brown to deep greenish brown. After 4 h of stirring the reaction mixture was filtered through a celite pad and the filtrate kept for slow evaporation. The solid obtained was filtered off and recrystallised from a 1:2 (v/v) mixture (15 cm^3) of MeCN-Et_2O (0.112 g, 58%). Found: C, 45.4; H, 4.7; N, 8.8. Calc. for $C_{37}H_{44}Cl_2Cu_2N_6O_{13}$: C, 45.4; H, 4.5; N, 8.6%. IR (KBr disc, selected peaks) $\bar{\nu}_{max}$/cm^{-1}: 3436 (OH); 1570 and 1445 (OAc); 1084 and 626 (ClO_4^-). Molar conductance, Λ_M (MeCN, 298 K) = 260 Ω^{-1} cm^2 mol^{-1}. UV-vis (MeCN) λ_{max}/nm (ε/M^{-1} cm^{-1}): 680 (sh) (250), 450 (sh) (1250), 290 (sh) (9400) and 258 (sh) (19400). μ_{eff}/Cu (in MeCN, 298 K) 1.72 μ_B.

Preparation of $[Cu_2(Me\text{-}L^5\text{-}O)(N_3)](ClO_4)_2 \times 2H_2O$ (16). This compound was prepared in the same way as **14** using NaN_3 (0.012 g, 0.179 mmol) as the bridging ligand; microcrystals of **16** were obtained and recrystallised from a 1:2 (v/v) mixture (15 cm^3) of MeCN-Et_2O (0.121 g, 64%). Found: C, 44.0; H, 4.5; N, 13.3. Calc. for $C_{35}H_{41}Cl_2Cu_2N_9O_{11}$: C, 43.7; H, 4.3; N, 13.1%. IR (KBr disc, selected peaks) $\bar{\nu}_{max}$/cm^{-1}: 3440 (OH); 2076 (N_3^-); 1090 and 630 (ClO_4^-). Molar conductance, Λ_M (MeCN, 298 K) = 290 Ω^{-1} cm^2 mol^{-1}. UV-vis (MeCN) λ_{max}/nm (ε/M^{-1} cm^{-1}): 660 (sh) (300), 500 (sh) (800), 390 (sh) (1560), 290 (sh) (8580) and 258 (17870). μ_{eff}/Cu (in MeCN, 298 K) 1.55 μ_B.

Preparation of $[Cu_2(L^4\text{-}O)Cl_3]$ (17). A solution of $[Et_4N]Cl \times (H_2O)_x$ (0.075 g, 0.402 mmol) in MeCN (5 cm^3) was added dropwise to a magnetically stirred MeCN (5 cm^3) solution of $[Cu_2(L^4\text{-}O)(OH)](ClO_4)_2$[144] (0.060 g, 0.082 mmol). During the progress of the reaction the colour of the solution changed from deep green to reddish-brown. After an additional stirring for 4 h the solution was concentrated *in vacuo* and Et_2O was slowly allowed to diffuse into the solution. Shiny red-brown crystals of **17** were obtained within two days (0.020 g, 40%), which were suitable

for a single-crystal X-ray structure determination. Found: C, 45.8; H, 4.6; N, 8.7. Calc. for $C_{24}H_{29}Cl_3Cu_2N_4O$ (6): C, 46.3; H, 4.7; N, 9.0%. Molar conductance, Λ_M (DMF, 298 K) = 30 Ω^{-1} cm^2 mol^{-1} (expected value for a 1:1 electrolyte[162]: 65–90 Ω^{-1} cm^2 mol^{-1}). UV-vis (DMF) λ_{max}/nm (ε/M^{-1} cm^{-1}): 980 (sh) (100), 805 (140), 460 (730) and 284 (sh) (2000).

4.6.4 Crystallography

Data collection and refinement details for 11, 13 and 17. Intensity data for **11** and **17** were collected on a Enraf Nonius CAD-4-Mach four-circle diffractometer (ω-2θ scan technique) (University of Erlangen-Nürnberg and IIT Kanpur) and for **13** on a Nonius Kappa CCD instrument using graphite-monochromated Mo-K_α radiation (λ = 0.71073 Å). Intensity data for **11**, **13** and **17** were corrected for Lorentz-polarisation effects. The structures were solved by direct methods for **11** and **13** and Patterson heavy-atom method for **17**. **11** and **17** were refined by full-matrix least-squares methods on F^2 using SHELXL-97[32] which was incorporated in the WINGX 1.61 collective crystallographic package.[163] All non-hydrogen atoms were refined with anisotropic thermal parameters. Problems during the refinement procedure for **17** were encountered; the problem was due to the poor diffracting nature of the crystals. All carbon atoms of the methylene groups of the *m*-xylyl spacers, *N*-methyl groups and one of the carbon atoms of the ethylene spacer on each arm of the ligand in one of the molecules of **17** (the molecule shown in Figure 4-2 did not show any disorder) were disordered over two positions and were refined with isotropic displacement parameters. The positions of hydrogen atoms in **17** were calculated assuming ideal geometries of the atoms concerned, and their positions and thermal parameters were not refined. **13** was refined by full-matrix least-squares methods on F^2 using SHELXTL NT 6.12.[107] Absorption effects have been corrected on the basis of multiple scans using SADABS (T_{min} = 0.791, T_{max} = 1.000).[164] All non-hydrogen atoms were refined with anisotropic displacement parameters and are geometrically positioned with isotropic displacement parameters being 1.2 or 1.5 times U(eq) of the preceding C atom.

CCDC reference numbers 211842 (**11**) 238967 (**13**) and 211448 (**17**).

See http://www.rsc.org/suppdata/dt/b4/b406329p/ for crystallographic data in CIF or other electronic format.

Chapter 5 - Copper(I) Complexes with Tridentate Ligands and their Reactivity towards Dioxygen

This work has been submitted for publication in *Inorganic Chemistry.*

Astner, J.; Weitzer, M.; Foxon, S. F.; Schindler, S.; Heinemann, F. W.; Mukherjee, J.; Gupta, R.; Mahadevan, V.; Mukherjee, R.; Copper(I) Complexes with Tridentate Ligands and their Reactivity towards Dioxygen. *Submitted for publication to Inorg. Chem.*

5.1 Introduction

The activation of molecular oxygen by copper complexes plays a central role in synthetically useful stoichiometric and catalytic oxidative conversions of organic molecules and in biological systems.[4,40,45,154,165] Copper superoxo and peroxo intermediates are very important species in the process of activating the O-O bond in dioxygen for further reactions.[4,45,166,167] One of the major goals in the research of metal/dioxygen interactions is to gain a real understanding of the mechanism of the activation and the cleavage of the O-O bond and its consecutive attack of the substrate.

Tetradentate tripodal ligands proved to be useful in stabilizing *trans*-peroxo copper complexes and with tris(2-pyridylmethyl)amine (tmpa, Figure 5-1) the first dinuclear copper peroxo complex was crystallographically characterised.[168] Furthermore, in addition to the roles played by well-known triazacyclononane (TACN) and tris-pyrazolylborate derivatives,[4,45,169,170] simple bidentate and tridentate open-chain ligands[4,45,171-176] have been used to investigate reactivity between copper(I) complexes and dioxygen. Such studies have clearly demonstrated stabilisation of both $[Cu^{II}_2(\mu\text{-}\eta^2\text{:}\eta^2\text{-}O_2)]^{2+}$ [side-on peroxodicopper(II)] and $[Cu^{III}_2(\mu\text{-}O)_2]^{2+}$ [bis(μ-oxo)dicopper(III)] species with these ligands.[4,45]

Bis(μ-oxo)dimetal "diamond" cores are of great interest in copper as well as in iron chemistry because they seem to play an important role in the oxidation of substrates.[4,8,45,177] An important finding was the observation that copper dioxygen adducts with TACN derivatives can undergo reversible interconversion of a $\mu\text{-}\eta^2\text{:}\eta^2$-

peroxo to a bis(μ-oxo) core depending on solvent, ligand substituents and concentration.[45,122,178]

For studying the factors which govern the binding mode and the interconversion properties of these copper/O_2 adducts some of us performed preliminary investigations with the copper(I) complex of the tridentate ligand 1,1,4,7,7-pentamethyldiethylethylenetriamine (Me_5dien, Figure 5-1).[40] Me_5dien can be regarded as an open-chain analogue of a substituted triazacyclononane (R_3-TACN)[179,180] and using this ligand we observed spectroscopically the formation of a bis(μ-oxo) copper complex at low temperatures in acetone, dichloromethane and propionitrile.[40]

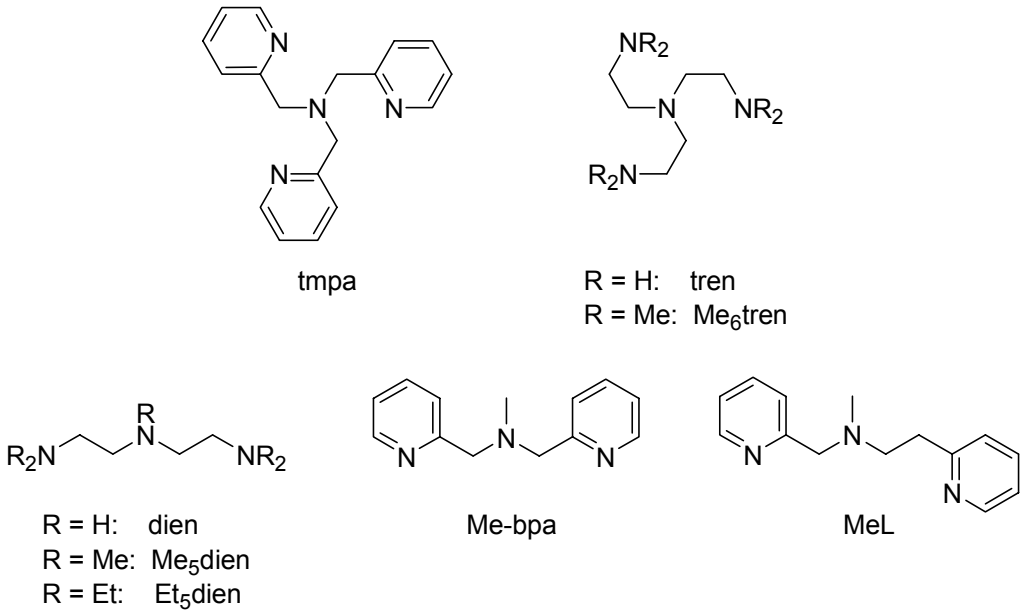

Figure 5-1: Ligand abbreviations.

Furthermore, Me_5dien is closely related to the tetradentate tripodal aliphatic amine tris(2-dimethylaminoethyl)amine (Me_6tren, Figure 5-1). Me_5dien is structurally related to Me_6tren by the replacement of one ethyleneamine "arm" in Me_6tren by a methyl group on the bridgehead nitrogen atom. As a consequence only 3 donor atoms coordinate to the copper(I) ion with an additional acetonitrile molecule as ligand as observed in the previously reported crystal structure.[181] In the past some of us demonstrated in a detailed kinetic study that the reaction of dioxygen with the copper(I) complexes of Me_6tren and tmpa as ligands follows the same mechanism with some differences in the kinetic parameters and the stabilities of the formed "dioxygen adduct" intermediates.[179] Therefore, we assumed that this parallelism would hold in a similar way if Me_5dien, *N*-methyl-[bis(2-pyridyl)methyl]amine (Me-bpa), and *N*-methyl-[(2-pyridyl)ethyl(2-pyridyl)methyl]amine (MeL) are used as

ligands (Figure 5-1). Herein we report a detailed study on the reactivity of the copper(I) complexes towards dioxygen using these tridentate ligands.

5.2 Experimental Section

5.2.1 Materials and Reagents.

Commercial reagents were used as obtained without further purification. Solvents were dried according to standard procedures. Absolute (dry) acetone for kinetic measurements was either obtained commercially (Acros) or by distillation of analytical grade acetone from dry B_2O_3. All handling (as well as storage) of oxygen sensitive compounds and materials used in the kinetic studies was carried out in a glovebox (Braun, Germany, O_2 < 0.1 ppm, H_2O < 0.1 ppm) within an argon atmosphere.

5.2.2 Physical Measurements.

Elemental analyses were obtained from the Department of Inorganic Chemistry, Indian Association for the Cultivation of Science, Kolkata, India or from the Institute of Organic Chemistry, Justus-Liebig-Universität Gießen, Germany. Infrared spectra (KBr pressed discs) were recorded on a Bruker Vector 22 spectrophotometer (4000-600 cm^{-1}) or on a Bruker IFS 25 (7000-400 cm^{-1}). Electronic spectra were recorded either using a Perkin Elmer Lambda 2 or Agilent 8453 diode-array spectrophotometer.

5.2.3 Kinetic Measurements.

Instrumentation setup and protocols for kinetic measurements have been described previously.[160,179] The copper(I) complex of Me_5dien and the other ligands were formed *in situ* during the mixing time in the mixing cell. Dioxygen saturated solutions of the ligand were prepared in the following way: 5 mL of a stock solution of the ligand was added to dioxygen saturated acetone (the acetone was bubbled with dry dioxygen gas (grade 4.8, Messer Griesheim, Germany) in a Schlenk tube – closed with a septum – to avoid moisture for at least 20 min. The solubility of dioxygen in acetone is 8.0 mM at 20°C.[44] Four series of different dioxygen concentrations were used to carry out a total of 244 measurements with the copper(I) complex of Me_5dien. The concentrations of the copper(I) complex solutions used

were 1.0 x 10^{-4} M and the concentrations of the dioxygen solutions were (1.0 - 4.0) x 10^{-3} M. The temperature was varied between -90.0 and -35.0°C and the data collection time ranged from 2.82 to 0.12 s. Complete spectra were collected with the integrated J&M software Kinspec 2.30 and analysed by the program Specfit (BioLogic Science Instruments, Claix, France).[182]

5.2.4 X-ray Crystallography.

X-ray data were collected either on a Siemens P4 four-circle diffractometer for [(Me-bpa)Cu(Cl)$_2$] (**18**), a Bruker-Nonius KappaCCD diffractometer for [{(Me-bpa)Cu(Cl)(ClO$_4$)}$_2$] (**19**) or on an Enraf Nonius CAD-4-Mach3 four-circle diffractometer for complexes [{(MeL)CuCl(ClO$_4$)}$_2$] (**20**) and [(MeL)Cu(NCS)$_2$] (**21**) with graphite-monochromated Mo-K$_\alpha$ radiation (λ = 0.71073 Å). For **18** and **19** data were corrected for Lorentz and polarisation effects. Absorption effects were corrected by semi-empirical methods based on Psi-scans[183] for **18** or numerically[184] for **19**. The structures were solved by direct methods; full-matrix least-squares refinement was carried out on F^2 using SHELXTL NT 6.12.[107] All non-hydrogen atoms were refined anisotropically. All hydrogen atoms were geometrically positioned; their isotropic displacement parameters were tied to those of their corresponding carrier atoms by a factor of 1.2 or 1.5. The ClO_4^- anion in **19** is subjected to rotational disorder; two sites for the oxygen atoms were refined that are occupied by 53.4(5) and 46.6(5)%, respectively.

For **20** and **21** data were corrected for Lorentz-polarisation effects; anomalous dispersion was applied for all non-hydrogen atoms and analytical absorption corrections were also applied. The structures were solved with SIR97 and refined isotropically with the SHELXL package incorporated in the WINGX 1.61 crystallographic collective package.[185] Anisotropic refinements were performed by full-matrix least-squares procedure on F^2, where the function minimised was $\Sigma w(F_o - F_c)^2$ with w = 1. The positions of the hydrogen atoms were calculated assuming ideal geometries, but not refined.

Crystallographic data (excluding structure factors) for the structures reported in this paper have been deposited with the Cambridge Crystallographic Data Centre. Copies of the data can be obtained free of charge on application to the CCDC, 12 Union Road, Cambridge CB2 1EZ, UK, on full quoting the journal citation and

deposition number CCDC 279865 (**18**), 279866 (**19**), 253089 (**20**) and 287248 (**21**).

5.2.5 Syntheses of ligands.

Commercially available Et_5dien was distilled over KOH prior to use. Commercially available Me_5dien (Aldrich) was purified in the following way. The hydrochloride salt of Me_5dien was prepared by reacting conc. HCl with the amine, followed by recrystallisation of the crude product from water. Concentrated KOH solution was added to the hydrochloride salt and the free amine was extracted with CH_2Cl_2. After evaporation of CH_2Cl_2 the amine was distilled from solid KOH and stored under an argon atmosphere.

***N*-methyl-[bis(2-pyridyl)methyl]amine (Me-bpa).** 33% Aqueous formaldehyde solution (1.70 g, 20.9 mmol) was added to a solution of bis[2-(2-pyridyl)methyl]amine (2.08 g, 10.45 mmol) in 1,2-dichloroethane (50 mL). After 15 min, $NaBH(OAc)_3$ (4.42 g, 21.00 mmol) was added portionwise to the stirred solution and the reaction mixture was left to stir for a further 24 h at room temperature. The reaction was quenched by the addition of an aqueous solution of 2 M NaOH (100 mL), the organic layer was separated and the aqueous layer was extracted with CH_2Cl_2 (3 $\times$ 100 mL portions). The organic fractions were combined and dried over $MgSO_4$. Filtration and removal of the solvent *in vacuo* yielded an oily semi-solid which was taken up in diethyl ether (100 mL), filtered and the diethyl ether removed *in vacuo* to yield Me-bpa as a translucent golden coloured oil (yield: 2.09 g, 9.8 mmol, 94%). ^{1}H NMR (300 MHz, $CDCl_3$) δ: 2.31 (s, 3H, –NC*H*$_3$), 3.77 (s, 4H, –NC*H*$_2$py), 7.15 (m, 2H, py–*H*), 7.52 (d, $^3J_{HH}$ = 8 Hz, py–*H*), 7.66 (dt, 2H, $^3J_{HH}$ = 8 Hz, 2 Hz, py–*H*), 8.54 (d, 2H, $^3J_{HH}$ = 5 Hz, py–*H*). ^{13}C NMR (75 MHz, $CDCl_3$) δ: 42.7, 63.6, 122.0, 123.1, 136.4, 149.0, 159.2.

***N*-methyl-[(2-pyridyl)ethyl(2-pyridyl)methyl]amine (MeL).** This ligand was prepared as reported previously[186] or according to the following procedure.

33% Aqueous formaldehyde solution (1.79 g, 21.00 mmol) was added to a solution of 2-pyridylmethyl-(2-pyridylethyl)amine[187] (2.13 g, 10.00 mmol) in 1,2-dichloroethane (50 mL). After 15 min, $NaBH(OAc)_3$ (4.42 g, 21.00 mmol) was added portionwise to the stirred solution and the reaction mixture was left to stir for a further 24 h at room temperature. The reaction was quenched by the addition of an aque-

ous solution of 2 M NaOH (100 mL), the organic layer was separated and the aqueous layer was extracted with CH_2Cl_2 (4 × 80 mL portions). The organic fractions were combined and dried over $MgSO_4$. Filtration and removal of the solvent *in vacuo* yielded an orange brown oil which was extracted with diethyl ether (30 mL), filtered and the diethyl ether removed *in vacuo* to yield the ligand as a golden yellow oil (yield: 1.90 g, 84%). ^{1}H NMR (300 MHz, $CDCl_3$) δ: 2.31 (s, 3H, –NC*H*$_3$), 2.81 (t, 2H, $^3J_{HH}$ = 5 Hz, 10 Hz, -NC*H*$_2$CH$_2$py), 3.05 (t, 2H, $^3J_{HH}$ = 7 Hz, 6 Hz, -NCH$_2$C*H*$_2$py), 3.77 (s, 4H, –NC*H*$_2$py), 7.15 (m, 2H, py–*H*), 7.30 (d, $^3J_{HH}$ = 8 Hz, py–*H*), 7.66 (dt, 2H, $^3J_{HH}$ = 8 Hz, 2 Hz, py–*H*), 8.53 (d, 2H, $^3J_{HH}$ = 5 Hz, py–*H*). ^{13}C NMR (75 MHz, $CDCl_3$) δ: 36.2, 42.4, 57.7, 63.8, 121.0, 121.8, 122.9, 123.2, 136.2, 136.3, 149.0, 149.2, 159.6, 160.6.

5.2.6 Synthesis of Copper(II) Complexes.

CAUTION! *Transition metal perchlorates are hazardous and may explode. Only small quantities should be prepared, and they should be used with great care.*

[(Me-bpa)Cu(Cl)$_2$] (18). $CuCl_2 \cdot 2H_2O$ (0.08 g, 0.47 mmol) in MeOH (1 mL) was added dropwise to Me-bpa (0.10 g, 0.47 mmol) in MeOH (2 mL). On addition of the metal salt the pale yellow solution turned deep royal blue. Diethyl ether (10 mL) was added with stirring causing the immediate precipitation of a green solid. The solid was collected, washed with a little diethyl ether and dried to give **18** as a green solid (yield: 0.138 g, 79%). Blue block crystals of **18** suitable for a single-crystal X-ray structure analysis were grown within 48 h from the slow diffusion of diethyl ether into a methanol solution of **18**. Anal. calc. for $C_{13}H_{15}Cl_2CuN_3$: C, 44.90; H, 4.35; N, 12.08%. Found C, 44.58; H, 4.27; N, 11.91. Absorption spectrum [λ_{max} /nm (ε /M^{-1} cm^{-1})]: (MeOH) 680 (128); (CH_2Cl_2) 758 (211); (MeCN) 752 (214).

[{(Me-bpa)Cu(Cl)(ClO$_4$)}$_2$] (19). A mixture of $Cu(ClO_4)_2$ x 6 H_2O (0.09 g, 0.24 mmol) and $CuCl_2$ x 2 H_2O (0.04 g, 0.24 mmol) in 1:1 MeCN:H_2O mixture (1 mL) was added dropwise to Me-bpa (0.10 g, 0.47 mmol) in the same solvent mixture (2 mL). On addition of the metal salt the pale yellow solution turned a deep blue colour. The mixture was stirred for 1 h and the blue coloured precipitate was collected by filtration and dried *in vacuo*. Dissolution of the complex in MeCN:H_2O (1:1)

mixture and slow evaporation resulted in the formation of blue crystalline material of **19** suitable for X-ray structural analysis (yield: 0.159 g, 79%). Anal. calc. for $C_{26}H_{30}Cl_4Cu_2N_6O_8$: C, 37.92; H, 3.67; N, 10.21%. Found C, 37.88; H, 3.35; N, 10.08. IR (KBr disc, selected peaks) /cm^{-1}: 1109, 1086, 1030, 625 $\nu(ClO_4^-)$. Absorption spectrum [λ_{max} /nm (ε /$M^{-1}cm^{-1}$)]: (MeCN) 258 (24 300), 290 sh (6660), 650 (220).

[{(MeL)Cu(Cl)(ClO_4)}$_2$] (20). MeL in EtOH (10 mL) was added dropwise to a stirred solution of $CuCl_2$ x 2 H_2O (0.226 g, 1.32 mmol) in EtOH (10 mL). The mixture was heated on a water bath (~ 50^{o}C) for 5 min. A saturated solution (2 mL) of $NaClO_4$ x H_2O was added to the cooled solution and left to evaporate slowly at room temperature. After 24 h, dark blue crystals of **20** formed and were filtered off, washed with cold EtOH, and dried *in vacuo* (yield: 0.46 g, ~82%). Dark blue coloured crystals of **20** suitable for a single-crystal X-ray structural analysis were obtained by slow evaporation at room temperature of an EtOH solution of **20**. Anal. calc. for $C_{28}H_{34}Cl_4Cu_2N_6O_8$: C, 43.00; H, 3.10; N, 23.40%. Found: C, 43.30; H, 3.30; N, 23.20%. IR (KBr disc, selected peaks) /cm^{-1}: 1110, 1080, 1050, 630 ν (ClO_4^-). Absorption spectrum [λ_{max} /nm (ε /$M^{-1}cm^{-1}$)]: (MeCN) 259 (20 320), 290 sh (4620), 650 (200).

[(MeL)Cu($NCS)_2$] (21). Solid KSCN (0.024 g, 0.24 mmol) was added to a stirred solution of **20** (0.05 g, 0.12 mmol) in MeCN (5 mL). The resulting dark green coloured solution was stirred for a further 2 h and then filtered through a pad of celite. The filtrate was left to evaporate slowly at room temperature. Within 24 h well-formed dark green crystals of **21** suitable for a single-crystal X-ray structure determination were collected by filtration, washed with water, and air-dried (yield: 0.04 g, ~80%). Anal. calc. for $C_{16}H_{17}CuN_5S_2$: C, 47.22; H, 4.18; N, 17.21%. Found: C, 47.25; H, 4.21; N, 17.30%. IR (KBr disc, selected peak) /cm^{-1}: 2090 $\nu(NCS^-)$. Absorption spectrum [λ_{max} /nm (ε /M^{-1} cm^{-1})]: (MeCN) 256 (13640), 290 (2600), 392 (1030), 680 (200), 950 sh (70).

5.3 Results and Discussion

5.3.1 Syntheses of ligands and copper complexes.

The aliphatic amines dien, Me_5dien and Et_5dien were commercially available and only needed to be purified by distillation prior to use. The extensive purification of Me_5dien was necessary for the kinetic investigations described below. The modified synthesis of *N*-methyl-[bis(2-pyridyl)methyl]amine (Me-bpa) and *N*-methyl-[(2-pyridyl)ethyl(2-pyridyl) methyl]amine (MeL) reported herein presents a significant improvement in comparison with currently known literature procedures.[186,188-190] In contrast to the classical Eschweiler Clark reaction (Leuckart reaction),[191-194] the reductive amination with $NaBH(OAc)_3$ in 1,2-dichloroethane[195] and 37% aqueous formaldehyde afforded pure Me-bpa and MeL in excellent yields.

5.3.2 Copper complexes.

Copper(I) complexes of the ligands used herein were only prepared *in situ* for the kinetic measurements due to the known problems of decomposition (disproportionation) if higher concentrations of copper(I) complexes were used.[196] However, a copper(I) complex of Me_5dien has been described previously by Holm and coworkers and structural characterisation of this compound was reported.[181] Furthermore, the copper(I) complex of MeL was obtained by Karlin and coworkers, however, no structural characterisation was reported.[197] So far our efforts to obtain crystals of copper(I) complexes of Me-bpa and MeL suitable for X-ray structural characterisation were unsuccessful. In contrast when related ligands were used that enforce six-membered chelate rings upon metal coordination, the according copper(I) complexes can be prepared quite easily and show much larger stabilities.[196,198,199]

Copper(II) complexes were readily obtained by reaction of the copper(II) salt with the appropriate ligands in a stoichiometric ratio. Crystal structure characterisations of copper(II) complexes of Me_5dien, Me-bpa and MeL were reported previously (only a selection of references for Me_5dien is given).[181,200-208] Herein we report four new crystal structures of copper(II) complexes with the ligands Me-bpa and MeL.

To understand the different reaction pathways of the copper(I) complexes of Me_5dien and Me_6tren with dioxygen it is useful to compare the X-ray structures of

both complexes even though the geometries in solution could be completely different from the crystal structures. $[Cu(Me_5dien)CH_3CN]^+$ has an irregular structure around the copper(I) centre that has been described as distorted tetrahedral.[181] The Cu-N bond in the centre is significantly shorter than the other two Cu-N bonds and one molecule of acetonitrile is additionally coordinated. For $[Cu(Me_6tren)]ClO_4$ the geometry is best described as trigonal-pyramidal, or including the weak interaction with the perchlorate anion in the axial position, the structure can be regarded as trigonal-bipyramidal.[180] The copper(I) ion is situated slightly below the plane of the three equatorial nitrogen atoms. There is no acetonitrile molecule coordinated to the copper(I) centre even though the complex was recrystallised from acetonitrile. The strong coordination of the axial nitrogen atom in $[Cu(Me_6tren)]ClO_4$ may prohibit coordination of an acetonitrile ligand. From previous experiments it is known that in solution nitrile solvent molecules strongly interact with the copper(I) Me_6tren complex.[180] As a consequence of the "missing coordinating arm" in Me_5dien compared to Me_6tren the reaction of dioxygen with the copper(I) complex of Me_6tren leads to a *trans*-μ-peroxo species while with Me_5dien as ligand a bis(μ-oxo) intermediate complex is obtained (see below).[40,180]

So far only one copper(II) complex of Me-bpa has been characterised structurally by some of us.[202] However, the crystal structure of the copper(II) complex of a derivative of Me-bpa has been described previously.[209] Similarly, for MeL only two crystal structures of copper(II) complexes have been reported by some of us.[200,201] However, a copper(II) complex of a derivative of MeL was described.[210] To gain better information on the geometry of these complexes in the solid state we therefore prepared copper(II) complexes of Me-bpa and MeL ligands and structurally characterised them.

5.3.3 Description of the molecular structure of 18.

Blue crystals of **18** suitable for X-ray structure determination were grown by slow diffusion of diethyl ether into a methanol solution of the complex. An ORTEP representation of **18** is shown in Figure 5-2. Table 5-1 and Table 5-2 contain the data collection and structure refinement parameters and the essential bond distances and bond angles.

Complex **18** is a discrete monomer. Each copper(II) centre is penta-coordinated by two pyridyl nitrogen atoms N(26) and N(36) and one tertiary amine nitrogen N(10) of the ligand Me-bpa and two chloride ligands Cl(1) and Cl(2). The ligand Me-bpa coordinates the copper(II) ion in a meridional mode and the coordination environment around the copper(II) ion is best described as distorted square pyramidal. The Addison structural distortion index parameter τ is 0.38 ($\tau = (\beta-\alpha)/60$, with α and β being the two largest coordination angles)[146] with N(10), N(26), N(36) and Cl(1) forming the basal plane and chloride ion Cl(2) occupying the axial position [Cu(1)–Cl(2) = 2.419(2) Å]. In a perfect square-pyramidal geometry, τ equals 0, while it is 1 in a perfect trigonal-bipyramidal geometry.[146] The Cu(II)–N(aliphatic amine) bond length [2.087(3) Å] is longer than the Cu(II)–N(pyridine) bond distances [2.003(3) and 2.009(3) Å] as expected.

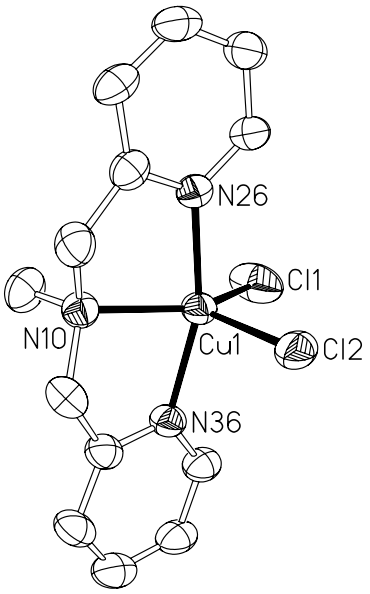

Figure 5-2: Molecular structure of [(Me-bpa)Cu(Cl)$_2$] (18).

5.3.4 Description of the structure of complex 19.

An ORTEP representation of **19** is shown in Figure 5-3. Table 5-1 contains the data collection and structure refinement parameters, and Table 5-2 summarizes the essential bond distances and bond angles. The X-ray structure analysis establishes that the complex has a *pseudo*-dimeric arrangement of two copper(II) ions surrounded by a Me-bpa ligand coordinated to each copper(II) ion in a meridional

mode, the two halves of the dimer being related by a crystallographic inversion centre. The geometry at each copper centre is best described as distorted square pyramidal, with two pyridine nitrogen atoms N(26) and N(36) and one aliphatic nitrogen atom N(10) from Me-bpa and one chloride ion Cl(1) coordinated in the equatorial plane. An additional bonding interaction exists at 2.8283(6) Å, provided by a chloride ion Cl(1A) of a neighbouring molecule. The Addison structural distortion index parameter τ is 0.21. From the equatorial plane the copper(II) ion is displaced towards Cl(1A) by 0.015(1) Å. The Cu---Cu separation between the two mononuclear units [Cu(1)---Cu(1A)] is 3.6540(6) Å and the angles Cu(1)–Cl(1)–Cu(1A) and Cl(1)–Cu(1)–Cl(1A) are 91.12(2)° and 88.88(2)° respectively. Due to its inherent inversion symmetry the four-membered Cu_2Cl_2 ring [Cu(1)–Cl(1)–Cu(1A)–Cl(1A)] is exactly planar. The coordination sphere of each of the copper(II) centres is completed by a distant oxygen atom of ClO_4^- at a distance of 2.73(2) Å. Taking this interaction into account the structure would correspond to a CuN_3Cl_2O coordination, giving rise to a *pseudo*-tetragonally elongated octahedral geometry around each copper(II) ion. The copper(II)–$N_{pyridyl}$, copper(II)–N_{amine}, and copper(II)–Cl distances are in line with the metric parameters of closely related complexes.[211,212]

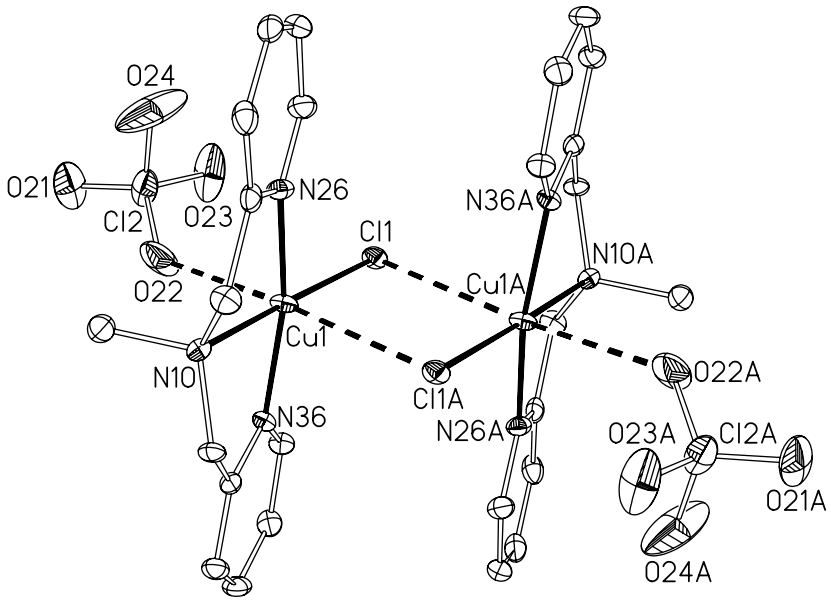

Figure 5-3: Molecular structure of [{(Me-bpa)Cu(Cl)(ClO_4)}$_2$] (19).

5.3.5 Description of the structure of complex 20.

The IR spectra of [{(MeL)Cu(Cl)(ClO_4)}$_2$] clearly demonstrated the presence of coordinated perchlorate ions; however, in MeCN solution they are dissociated (solution electrical conductivity data, 1:2 electrolyte).[162] An ORTEP representation of the crystal structure of this compound is shown in Figure 5-4.

As for **19** (Figure 5-3), structural analysis of **20** also shows a *pseudo*-dimeric arrangement of two copper(II) ions. The MeL ligand binds each copper(II) ion in a meridional mode. Each copper(II) ion is coordinated in the equatorial plane by two pyridine nitrogen atoms N(1) and N(3) and one aliphatic nitrogen atom N(2) from MeL and one chloride ion Cl(1). An additional bonding interaction exists at 2.891(2) Å, provided by a chloride ion of a neighbouring molecule Cl(1A). From the equatorial plane the copper(II) ion is displaced towards Cl(1A) by 0.035 Å. The coordination environment for each copper(II) ion is best described as distorted square-pyramidal (τ = 0.12). The Cu---Cu separation between the two mononuclear units [Cu(1)---Cu(1A)] is 3.820(3) Å and the angles Cu(1)–Cl(1)–Cu(1A) and Cl(1)–Cu(1)–Cl(1A) are 94.77(5)° and 85.23(5)°. It reveals that the four-membered Cu_2Cl_2 ring [Cu(1)–Cl(1)–Cu(1A)–Cl(1A)] is planar. A weak interaction between each copper(II) ion with the O(1) atom of a perchlorate ion [Cu(1)–O(1) = 2.840(6) Å] in the axial position is also clearly observable (*cf.* 2.73(2) Å in **19**).

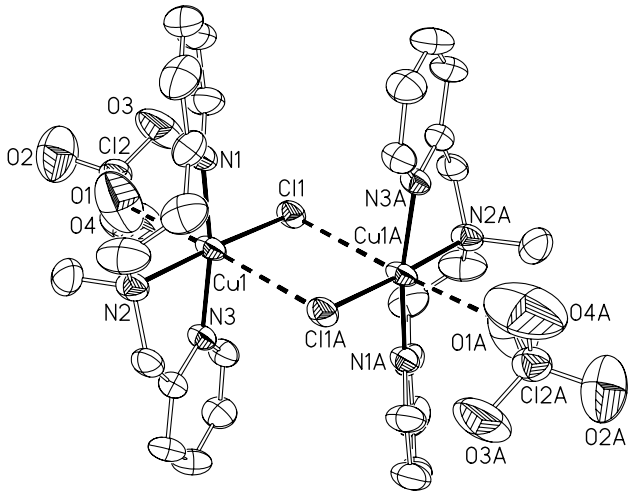

Figure 5-4: Molecular structure of [{(MeL)Cu(Cl)(ClO_4)}$_2$] (20).

Table 5-1: Data collection and structure refinement parameters for 18 - 21.

Complex	18	19	20	21
Molecular formula	$C_{13}H_{15}Cl_2CuN_3$	$C_{26}H_{30}Cl_4Cu_2N_6O_8$	$C_{28}H_{34}Cl_4Cu_2N_6O_8$	$C_{16}H_{17}CuN_5S_2$
M_r	347.72	823.5	851.5	407.01
Temperature/K	298(2)	100(2)	293(2)	293(2)
Radiation used (λ/Å)	Mo-Kα (0.71073)	Mo-Kα (0.71073)	Mo-Kα (0.71073)	Mo-Kα (0.71073)
Crystal system	Monoclinic	Triclinic	Triclinic	Triclinic
Space group	$P2_1/n$	$P\bar{1}$	$P\bar{1}$	$P\bar{1}$
a/Å	8.445(1)	8.1433(4)	8.236(2)	8.408(5)
b/Å	12.759(1)	10.0878(5)	10.156(2)	8.536(2)
c/Å	13.322(1)	10.8258(4)	11.270(8)	14.320(1)
α/deg	90	102.119(3)	102.85(5)	101.90(8)
β/deg	94.95(1)	101.160(3)	100.74(5)	105.98(6)
γ/deg	90	107.751(4)	107.81(5)	104.05(8)
V/Å^3	1430.1(2)	795.79(6)	841.5(8)	916(7)
Z	4	2	1	2
D_c/*g cm*$^{-3}$	1.615	1.718	1.680	1.475
μ/*mm*$^{-1}$	1.889	1.730	1.639	1.426
crystal size/mm	0.48 × 0.38 × 0.30	0.28 × 0.21 × 0.14	0.60 × 0.50 × 0.20	0.50 × 0.40 × 0.20
Complex	**18**	**19**	**20**	**21**
Reflections measured	4496	15533	3170	3447
Unique reflections, R_{int}	3452, 0.0315	4274, 0.0516	2943, 0.0078	3206, 0.0329
goodness-of-fit on F^2	1.013	1.052	1.063	0.968
$R1$, $wR2$ [$I > 2\sigma(I)$]	0.0481, 0.0883	0.0392, 0.0779	0.0508, 0.1420	0.0676, 0.1835
$R1$, $wR2$ (all data)	0.0913, 0.1019	0.0717, 0.0844	0.0597, 0.1484	0.1330, 0.2135
Max./min. el. density/e Å^{-3}	+0.448, −0.351	+0.615, –0.769	+0.762, –0.778	+0.770, –0.899

Table 5-2: Selected bond lengths (/Å) and bond angles (/°) for compounds 18 - 21.

		18			
Cu(1)–N(36)	2.009(3)	Cu(1)–N(10)	2.087(3)	Cu(1)–N(26)	2.003(3)
Cu(1)–Cl(1)	2.287(2)	Cu(1)–Cl(2)	2.419(2)		
N(36)–Cu(1)–N(10)	80.7(2)	N(36)–Cu(1)–N(26)	161.8(2)	N(10)–Cu(1)–N(26)	81.2(2)
N(36)–Cu(1)–Cl(1)	95.85(9)	N(10)–Cu(1)–Cl(1)	139.10(9)	N(26)–Cu(1)–Cl(1)	96.76(9)
N(36)–Cu(1)–Cl(2)	94.45(8)	N(10)–Cu(1)–Cl(2)	105.99(8)	N(26)–Cu(1)–Cl(2)	92.08(9)
Cl(1)–Cu(1)–Cl(2)	114.91(5)				
		19			
Cu(1)–N(36)	1.983(2)	Cu(1)–N(10)	2.036(2)	Cu(1)–N(26)	1.989(2)
Cu(1)–Cl(1)	2.2587(6)	Cu(1)–Cl(1A)*	2.8283(6)	Cu(1)–O(22)$^{\#}$	2.728(9)
Cu(1)···Cu(1)*	3.6540(6)				
N(36)–Cu(1)–N(10)	82.70(7)	N(36)–Cu(1)–N(26)	164.54(8)	N(10)–Cu(1)–N(26)	81.92(8)
N(36)–Cu(1)–Cl(1)	97.96(6)	N(10)–Cu(1)–Cl(1)	177.26(6)	N(26)–Cu(1)–Cl(1)	97.48(6)
N(36)–Cu(1)–Cl(1A)*	89.23(6)	N(10)–Cu(1)–Cl(1A)*	88.47(5)	N(26)–Cu(1)–Cl(1A)*	91.90(6)
Cl(1)–Cu(1)–Cl(1A)*	88.88(2)	Cu(1)–Cl(1)–Cu(1A)*	91.12(2)		
* -x, -y+1, -z; $^{\#}$ -x+1, -y+2, -z					
		20			
Cu(1)–N(1)	1.982(3)	Cu(1)–N(2)	2.065(3)	Cu(1)–N(3)	1.996(3)
Cu(1)–Cl(1)	2.269(2)	Cu(1)–Cl(1)*	2.891(2)	Cu(1)–O(1)	2.840(6)
Cu(1)···Cu(1)*	3.820(2)				
N(1)–Cu(1)–N(2)	89.1(2)	N(1)–Cu(1)–N(3)	169.8(2)	N(2)–Cu(1)–N(3)	81.8(2)
N(1)–Cu(1)–Cl(1)	93.9(2)	N(2)–Cu(1)–Cl(1)	177.0(2)	N(3)–Cu(1)–Cl(1)	95.3(2)
N(1)–Cu(1)–Cl(1)*	100.8(2)	N(2)–Cu(1)–Cl(1)*	93.8(2)	N(3)–Cu(1)–Cl(1)*	84.6(2)
Cl(1)–Cu(1)–Cl(1)*	85.23(4)	Cu(1)–Cl(1)–Cu(1)*	94.77(4)		
* 1-x, -y, 1-z					

Table 5-2 (cont'd): Selected bond lengths (/Å) and bond angles (/°) for compounds 18 - 21.

			21		
Cu(1)–N(1)	2.002(6)	Cu(1)–N(2)	2.125(8)	Cu(1)–N(3)	1.994(6)
Cu(1)–N(4)	1.97(2)	Cu(1)–N(5)	2.098(9)		
N(1)–Cu(1)–N(2)	91.5(3)	N(1)–Cu(1)–N(3)	171.4(2)	N(1)–Cu(1)–N(4)	91.4(4)
N(1)–Cu(1)–N(5)	94.7(3)	N(2)–Cu(1)–N(3)	82.0(3)	N(2)–Cu(1)–N(4)	141.1(4)
N(2)–Cu(1)–N(5)	108.8(5)	N(3)–Cu(1)–N(4)	90.1(4)	N(3)–Cu(1)–N(5)	92.8(3)

5.3.6 Description of the structure of complex 21.

Complex **21** was synthesised following a controlled nucleophilic substitution reaction of the perchlorate and chloride ligands in complex **20** in MeCN. The *N*-coordinated NCS group in **21** is clearly observable in the IR spectrum and as expected the complex is non-conducting in MeCN solution. An ORTEP representation of the molecular structure of **21** is shown in Figure 5-5. The copper(II) ion is five-coordinate with a coordination environment clearly in between square pyramidal and

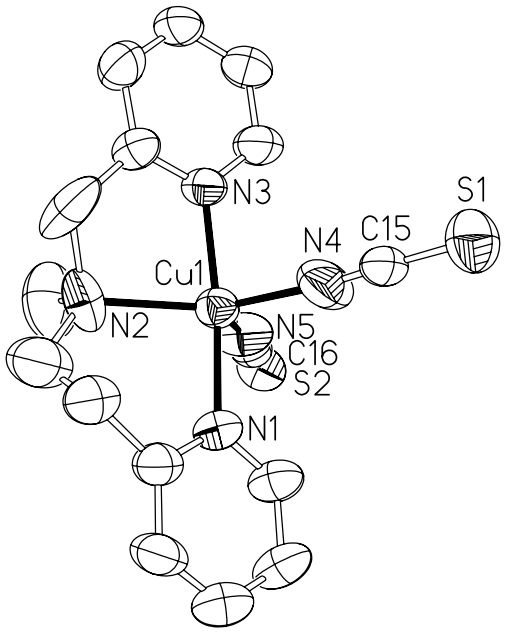

Figure 5-5: Molecular structure of [(MeL)Cu(NCS)$_2$] (21).

trigonal-bipyramidal and τ = 0.485. The copper(II)–N_{amine} and copper(II)–$N_{pyridyl}$ distances are comparable to those in compound **20**, [{MeL}CuCl(ClO_4)}$_3$(μ-OCO_2)] ClO_4,[201] and [(MeL)Cu($Cl)_2$].[200]

5.3.7 Kinetic investigations of the reactions of [Cu(Me_5dien)RCN] ClO_4 with dioxygen.

Although the crystal structure of [Cu(Me_5dien)(CH_3CN)]ClO_4 was solved previously, handling of this complex is difficult as disproportionation of the complex hinders kinetic studies. To overcome this problem we reacted the copper(I) salt (ClO_4^- as anion) with Me_5dien *in situ* (as described previously for the copper(I) Me_6tren complex)[179] directly during the mixing time of the stopped-flow experiment. This was possible because the complex formation reaction is almost diffusion controlled and hence much faster than the reaction of the copper(I) complex with dioxygen. A detailed kinetic analysis was performed in that way.

Time-resolved spectra were recorded using low-temperature stopped-flow techniques. During rapid mixing of acetone solutions of Me_5dien/O_2 and [Cu($CH_3CN)_4$]ClO_4 respectively, fast temperature-dependent UV-vis spectral changes are detectable. An example for time-resolved spectra for the oxygenation reaction at -90.0°C is shown in Figure 5-6. Absorbance maxima are observed at 403 nm and below 320 nm. Unfortunately in acetone, the second absorption is not fully visible due to the absorbance of the solvent itself. However, previous measurements with a different diode array setup allowed furthermore the detection of both absorption bands with maxima at 314 and 407 nm in propionitrile. Carrying out the reaction of [Cu(Me_5dien)CH_3CN]$^+$ with dioxygen in CH_2Cl_2 or propionitrile (see Figure 5-7) caused nearly identical spectra changes, however no kinetic studies were performed in these solvents (reaction rates were different). According to the UV-vis data we assign the formed complex as an bis(μ-oxo)dicopper(III) species (resonance Raman measurements to further support this assignment so far were unsuccessful).

Compared to the triazacyclononane complex [Cu(i-Pr_3TACN)(CH_3CN)]$^+$ (in THF) with absorbances at λ_{max} = 324 nm (ε = 11 000 $M^{-1}cm^{-1}$) and 448 nm (ε = 13 000 $M^{-1}cm^{-1}$)[178,213], for the present species a strong hypsochromic shift of the second band is observed. However, very similar results (λ_{max} = 410 nm in CH_2Cl_2) were

obtained for the oxo-bridged form of the copper complex of related open chain ligands (Figure 5-8) described previously by Karlin and coworkers.[171,198,199]

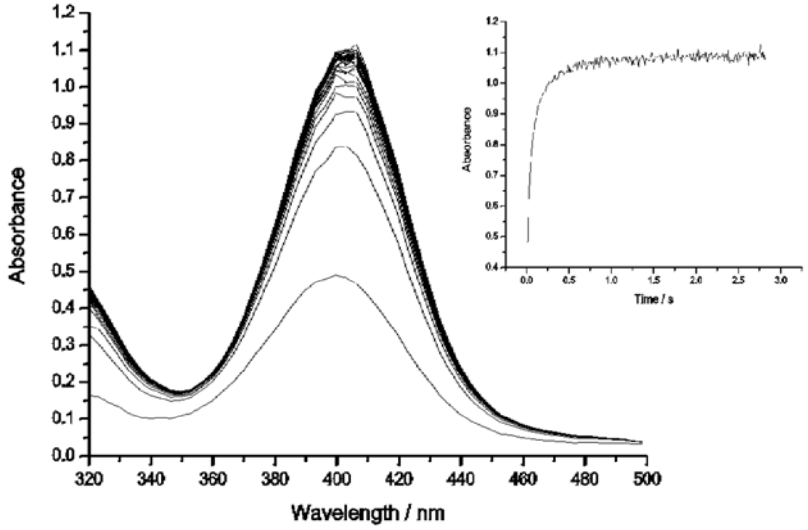

Figure 5-6: Time-resolved, low-temperature UV-vis spectra for the reaction of $[Cu(Me_5dien)(CH_3CN)]ClO_4$ with dioxygen in acetone solution. [Complex] = 1.0 x 10^{-4} M, $[O_2]$ = 3.0 x 10^{-3} M, T = -90.0°C, total time = 2.82 s. Insert: absorbance *vs.* time trace at 404 nm.

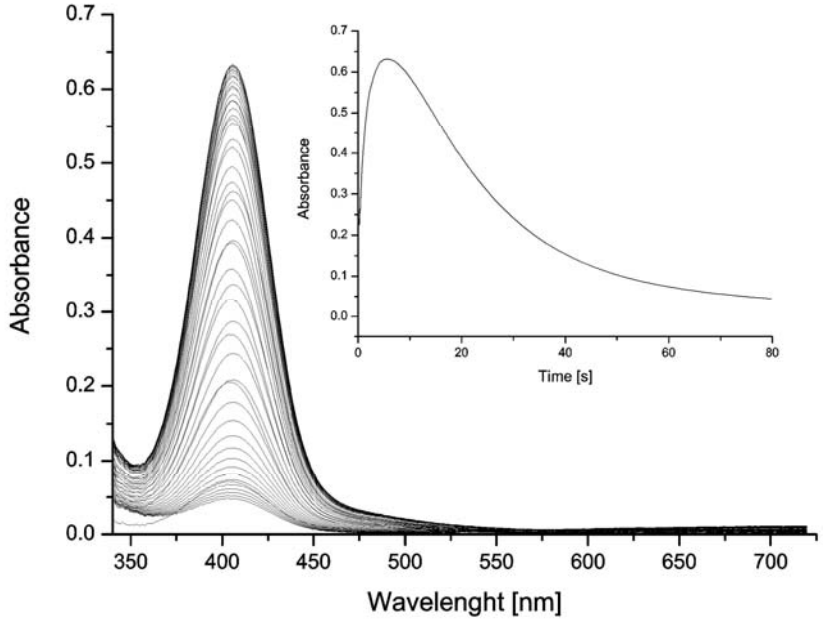

Figure 5-7: Time-resolved, low-temperature UV-vis spectra for the reaction of $[Cu(Me_5dien)(CH_3CN)]ClO_4$ with dioxygen in propionitrile solution. [Complex] = 4.4 x 10^{-4} M, $[O_2]$ = 1.47 x 10^{-3} M, T = -90.0°C, total time = 80 s. Insert: absorbance *vs.* time trace at 407 nm.

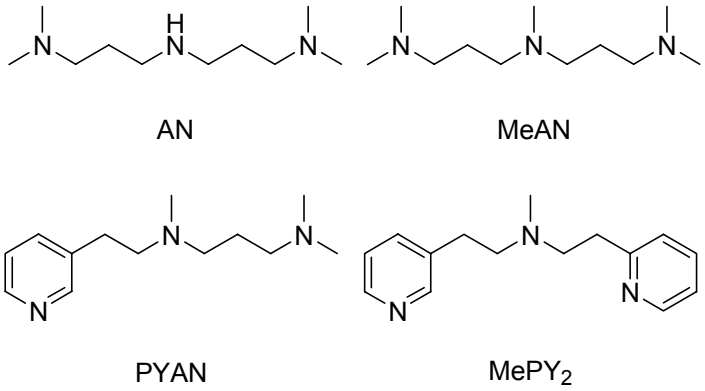

Figure 5-8: Ligands used in kinetic studies by Karlin and coworkers[214]

For the final calculation the formation of the copper bis(μ-oxo) complex and the back reaction was analysed. As a consequence of a slow but significant decay and a fast back reaction the bis(μ-oxo) copper complex is not fully formed for the whole temperature range. Despite the fact that no spectroscopic evidence for the formation of a superoxo species was obtained, such intermediates must occur, at least as extremely short-lived species according to the following reaction Scheme 5-1:

$$[Cu(Me_5dien)(CH_3CN)]^+ + O_2 \rightleftharpoons [Cu(Me_5dien)(O_2)]^+ + CH_3CN$$

$$[Cu(Me_5dien)(CH_3CN)]^+ + [Cu(Me_5dien)(O_2)]^+ \rightleftharpoons [Cu(Me_5dien)_2(\mu\text{-}O)_2]^{2+} + CH_3CN$$

$$[Cu(Me_5dien)_2(\mu\text{-}O)_2]^{2+} + CH_3CN \longrightarrow \text{decomposition}$$

Scheme 5-1: Proposed mechanism for reaction of $[Cu(Me_5dien)(CH_3CN)]^+$ with O_2

As the reaction scheme above indicates, the adduct formation must be stepwise *via* a mononuclear superoxo complex. However, its supposed steady state behaviour and the actual rate law allows to use a simpler kinetic description for data fitting without including such a reactive intermediate. Similar kinetic data fitting procedures have been described previously.[122,198,199] For the numerical analysis with the program *Specfit* the following model (Scheme 5-2) was used, in which A and C were set as coloured species.

$$\underset{A}{2\,[Cu(Me_5dien)(CH_3CN)]^+} + \underset{B}{O_2} \underset{k_{-1}}{\overset{k_1}{\rightleftharpoons}} \underset{C}{[Cu(Me_5dien)_2(\mu\text{-}O)_2]^{2+}} + 2\,CH_3CN$$

$$\underset{C}{[Cu(Me_5dien)_2(\mu\text{-}O)_2]^{2+}} \xrightarrow{k_2} \underset{D}{\text{decomposition}}$$

Scheme 5-2: Simplified reaction of $[Cu(Me_5dien)(CH_3CN)]^+$ with O_2 for data fitting

From the *Specfit* calculations Eyring plots for k_1, k_{-1} and k_2 were obtained and are presented in Figure 5-9 to Figure 5-11. Discrepancies in the Eyring plots (especially for k_{-1} and k_2 in the lowest temperature area) are presumably a consequence of well known photochemical effects that are quite common with such compounds under irradiation of an intensive UV lamp.[199] Nevertheless, a good determination of the activation parameters was possible and the results are summarised in Table 5-3.

The features in the UV-vis spectra and the successful fitting with the model shown above suggest the formation of a pure bis(μ-oxo) complex with neither evidence of the formation nor an equilibrium of a copper peroxo species, as in the work of Tolman or Karlin.

The kinetic results of the reaction of $[Cu(Me_5dien)(CH_3CN)]^+$ with dioxygen in acetone compared to previous work from Karlin, Zuberbühler and co-workers, who - in this case - used related open-chain ligands (Figure 5-8), are summarised in Table 5-3.[171,198,199,215] However, in contrast to $[Cu(Me_5dien)(CH_3CN)]^+$ all copper(I) complexes of the other shown ligands either only form μ-η^2:η^2-peroxo complexes, mixtures of μ-η^2:η^2-peroxo complexes and bis(μ-oxo) dioxygen species (depending on the solvent).[171,198,199,215,216] Only for the copper(I) complex of AN does the formation of the bis(μ-oxo) copper complex takes place explicitly if the oxidation reaction is performed in CH_2Cl_2.[198]

It is remarkable that the binding of dioxygen to the $[Cu(Me_5dien)(CH_3CN)]^+$ complex is much faster than the other complexes, which is most likely a consequence of their larger chelate ring size (6-membered chelate rings in general stabilize copper(I) complexes,[25] however this does not explain all results; see below) compared to $[Cu(Me_5dien)(CH_3CN)]^+$. In all cases the $\Delta S^{\#}$ value is strongly negative, which indicates an associative mechanism. The back reaction (k_{-1}) can be compared to AN and MeAN whereas the complexes with the aromatic donors show a slower rate constant. The decomposition reaction of the dioxygen adducts of the copper complexes with pure aliphatic ligands is faster (as would be expected) compared with the complexes with the aromatic PYAN and MePY2 ligands.

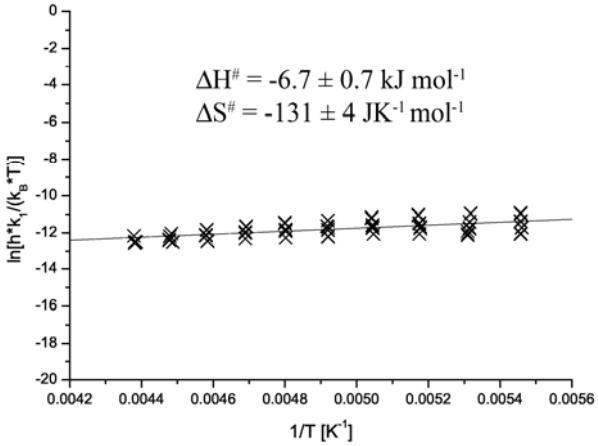

Figure 5-9: Eyring plot of k_1 for the reaction of $[Cu(Me_5dien)(CH_3CN)]ClO_4$ with dioxygen

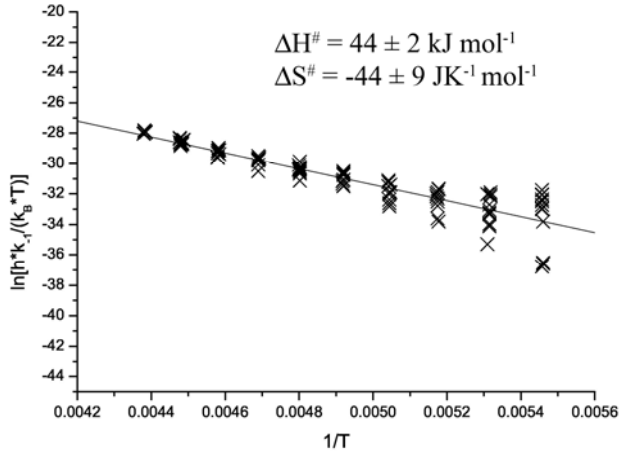

Figure 5-10: Eyring plot of k_{-1} for the reaction of $[Cu(Me_5dien)(CH_3CN)]ClO_4$ with dioxygen

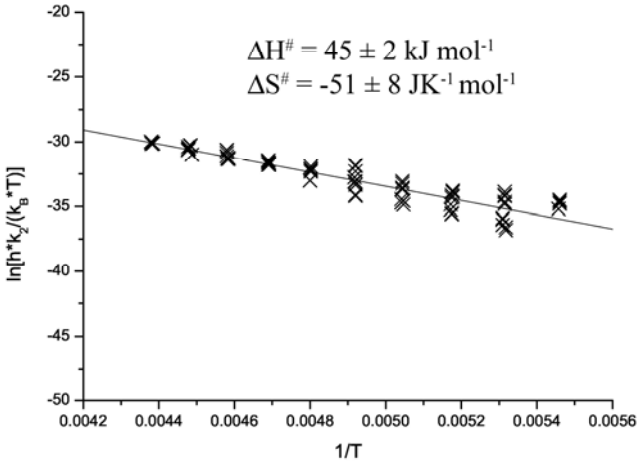

Figure 5-11: Eyring plot of k_2 for the reaction of $[Cu(Me_5dien)(CH_3CN)]ClO_4$ with dioxygen

Table 5-3: Kinetic and thermodynamic parameters for the reaction of O_2 with $[Cu(Me_5dien)CH_3CN]^+$ and related copper(I) complexes

Solvent	Temperature [K]	Me_5dien	AN[217]	MeAN[217]	PYAN[214]	MePY2[218]	^{iPr3}TACN[219,220]
		Acetone	CH_2Cl_2	CH_2Cl_2	Acetone	Acetone	Acetone
Product		Bis(μ)oxo	Bis(μ)oxo	Peroxo	Mixture	Peroxo	Mixture
k_1 ($M^{-2}s^{-1}$)	183.15	$4.1x10^7$	$2.7x10^4$	690			
	193						0.191 ($M^{-1}s^{-1}$)
	203				$1.5\ x10^5$		
	223.15	$2.3x10^7$					5.02
	253.16					$1.91x10^4$	
$\Delta H^{\#}$ ($kJmol^{-1}$)		-6.7 ± 0.7	-9.9 ± 0.6	-27 ± 3	-13.8 ± 0.2	-0.7 ± 1	37.2 ± 0.5
$\Delta S^{\#}$ ($JK^{-1}mol^{-1}$)		-131 ± 4	-210 ± 3	-335 ± 16	-211 ± 1	-164 ± 4	-62 ± 2
k_{-1} (s^{-1})	183.15	$2.4x10^{-2}$					
	223.15	1.8					
	203				$5x10^{-5}$		
$\Delta H^{\#}$ ($kJmol^{-1}$)		44 ± 2			66 ± 1		
$\Delta S^{\#}$ ($JK^{-1}mol^{-1}$)		-44 ± 9			-1 ± 6		
k_2 (s^{-1})	183.15	$2.8x10^{-3}$		-			-
	203			-	$7.7x10^{-4}$		
	223.15	$2.6x10^{-1}$	0.3	-			$1.13x10^{-3}$
$\Delta H^{\#}$ ($kJmol^{-1}$)		45 ± 2	35 ± 2	-	39.9 ± 0.3		49.1 ± 0.6
$\Delta S^{\#}$ ($JK^{-1}mol^{-1}$)		-51 ± 8	-95 ± 11	-	-105 ± 1		-79 ± 2

During the reaction of $[Cu(i\text{-}Pr_3TACN)(CH_3CN)]^+$ with dioxygen in acetone at -78°C an approximate 4:1 mixture of the μ-η^2:η^2-peroxo and the bis(μ-oxo) complex was formed.[122,178] Accordingly the model used for this reaction, the 1:1 Cu:O_2 adduct formation is followed by intermolecular trapping by a second copper(I) complex to

yield a bis(μ-oxo) complex which rapidly equilibrates with the μ-η^2:η^2-peroxo species[122]. Therefore, a direct comparison between the kinetic results of [Cu(i-Pr_3TACN)(CH_3CN)]$^+$ and the other complexes in Table 5-3 is difficult because k_{on} for the formation of the dinuclear dioxygen adduct of [Cu(i-Pr_3TACN)(CH_3CN)]$^+$ describes the formation of the superoxo complex that could not be determined for the other complexes and leads to different units for k_{on} ($M^{-2}s^{-1}$ vs. $M^{-1}s^{-1}$, Table 5-3). The activation parameters for the decay of [{(i-Pr_3TACN)Cu}$_2$(O_2)]$^{2+}$ are in line with the data of the open chain ligands.

5.3.8 Kinetic investigations of the reactions of dioxygen with the copper(I) complexes of the ligands Me-bpa and MeL and Et_5dien.

Most surprisingly and in contrast to our expectations discussed in the introduction (tmpa *vs.* Me_6tren), copper(I) complexes with the ligands Me-bpa and MeL did not show observable formation of bis(μ-oxo) species when reacted with dioxygen, under the same conditions as [Cu(Me_5dien)(CH_3CN)]ClO_4. Copper(I) complexes with the ligands Me-bpa and MeL were oxidised, however even at low temperatures during the stopped-flow experiments we could not observe the clear formation of a copper "dioxygen adduct complex": In contrast Itoh and coworkers could clearly demonstrate in recent publications that the copper(I) complex with the ligand $^{Ph}L^{Pym2}$ (*N,N*-di(2-pyridylmethyl)-2-phenylethlamine; a derivative of Me-bpa in which the methyl group is replaced by a phenylethyl group) reacts with dioxygen to form a bis(μ-oxo) complex at low temperatures (stopped-flow measurements showing the very fast increase of a absorbance maximum at 385 nm).[196,221] So far we cannot provide an explanation why we did not observe such intermediates for Me-bpa or Me-L.

Furthermore, it was surprising that during the oxidation of the copper(I) complex of Et_5dien we could not observe any "dioxygen intermediate complex" using the same conditions as for the studies with Me_5dien. Using this sterically more hindered ligand we had hoped to detect the 1:1 adduct (spectroscopically or during fitting of the kinetic data), the superoxo complex, prior to its further reaction to the 2:1 product (dinuclear bis(μ-oxo) or peroxo complex) if this dimerisation still can

occur. So far only a few crystal structures of copper(II) complexes with the ligand Et_5dien have been reported.[222-225]

5.4 Summary and Conclusions

Copper(I) complexes of the ligands Me_5dien, Et_5dien, Me-bpa and MeL have been investigated in regard to their oxidation with dioxygen. In that regard crystal structures of the copper(II) complexes of Me-bpa and MeL were solved. Crystals of copper(I) complexes could not be obtained, however Holm and coworkers previously described the crystal structure of $[Cu(Me_5dien)CH_3CN]^+$.[181] In contrast to our expectations we only succeeded in a detailed kinetic study on the reaction of $[Cu(Me_5dien)CH_3CN]^+$ with dioxygen during which a dinuclear bis(μ-oxo) copper complex was formed. Despite previous excellent work by the groups of Itoh, Karlin, Stack, Tolman and Zuberbühler related to our investigations described herein (and referred to above) at the current state we do not completely understand the different reactivity of copper(I) complexes with bidentate and tridentate ligands.

Chapter 6 - Summary

To provide a better understanding of the reactions of iron and copper proteins with dioxygen, the corresponding reactions of small molecule model complexes with dioxygen were analysed using spectroscopic and kinetic methods. Special attention focused upon the binding and activation of dioxygen by iron proteins such as hemerythrin (Hr) and protocatechuat-3,4-dioxygenase (3,4-PCD) and by copper proteins like hemocyanin (Hc) and tyrosinase.

Iron complexes of the ligand tmpa (tmpa = tris[(2-pyridyl)methyl]amine, also known as tpa in literature) were synthesised and modifications of the tmpa ligand were made. Increasing as well as decreasing chelate ring sizes in the highly active complex [Fe(tmpa)(dbc)]$B(C_6H_5)_4$ (dbc = 3,5-di-*tert*-butylcatecholate dianion), only resulted in decreased reactivity of the investigated compounds (see Figure 6-1, left). A detailed low-temperature stopped-flow investigation of the reaction of dioxygen with [Fe(tmpa)(dbc)]$B(C_6H_5)_4$ was performed and activation parameters of $\Delta H^{\ddagger}$ = 23 $\pm$ 1 kJ mol^{-1} and $\Delta S^{\ddagger}$ = –199 $\pm$ 4 J mol^{-1} K^{-1} were obtained (in Figure 6-1, right, time resolved UV-vis spectra of the reaction of iron complex with O_2 are shown).

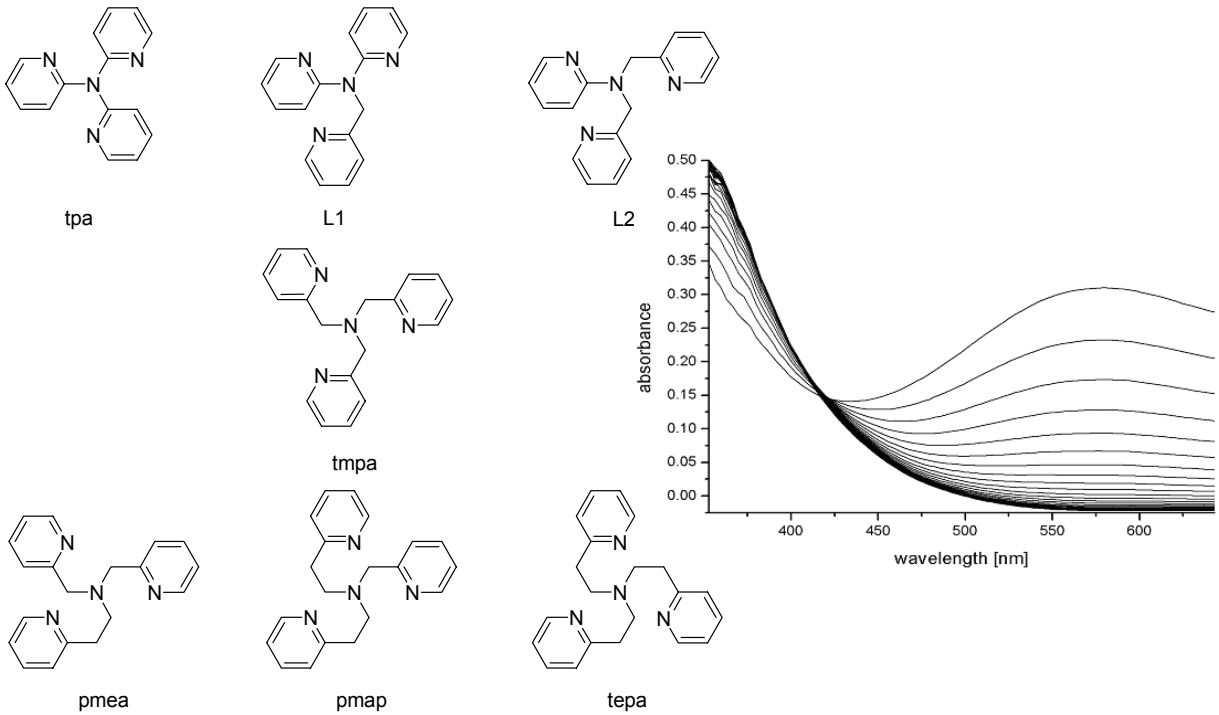

Figure 6-1: ligands related to tmpa and time resolved UV-vis spectra of reaction of iron complex with O_2

Crystal structures of bromo-(tetrachlorocatecholato-O,O')(bis((2-pyridyl)methyl)-2-pyridylamine-*N*,*N*',*N*'')-iron(III) (**2**), (μ-oxo)-bis(bromo)(bis((2-pyridyl) methyl)-2-pyridylamine-*N*,*N*',*N*'',*N*''')-diiron(III) (**3**), dichloro-((2-(2-pyridyl)ethyl)bis((2-pyridyl)methyl)amine-*N*,*N*',*N*'',*N*''')-iron(III) (**4**) and (tetrabromocatecholato-O,O')((2-(2-pyridyl)ethyl)bis((2-pyridyl)methyl)amine-*N*,*N*',*N*'',*N*''')-iron(III) (**5**) are reported (Chapter 2).

Besides altering the chelate ring size the influence of the donor atoms of the ligand on catechol dioxygenase reactivity was investigated. Two derivatives of the tmpa ligand (uns-penp and acetyl-uns-penp) were synthesised, where one aromatic nitrogen donor was replaced by an aliphatic nitrogen donor (see Figure 6-2). The iron(III) complexes of the tripodal ligands *N*',*N*'-bis[(2-pyridyl)methyl]ethylenediamine (uns-penp), $[Fe(uns\text{-}penp)Cl_2]ClO_4$ x CH_3CN, $[\{Fe(uns\text{-}penp)Cl\}_2O](ClO_4)_2$ x $2CH_3CN$ and the amide derivative *N*-Acetyl-*N'*,*N'*-bis[(2-pyridyl)methyl]ethylenediamine (acetyl-uns-penp), $[Fe_2(acetyl\text{-}uns\text{-}penp)_2O](ClO_4)_2$ x H_2O, [Fe(acetyl-uns-penp)(tcc)Br] x $(C_2H_5)_2O$ and $[\{Fe(acetyl\text{-}uns\text{-}penp)(tcc)\}_2O]$ x $(C_2H_5)_2O{\cdot}CH_3OH$ were synthesised and characterised. Catechol dioxygenase reactivity of *in situ* prepared complex solutions only showed slower reactions in comparison with the iron tmpa system (Chapter 3).

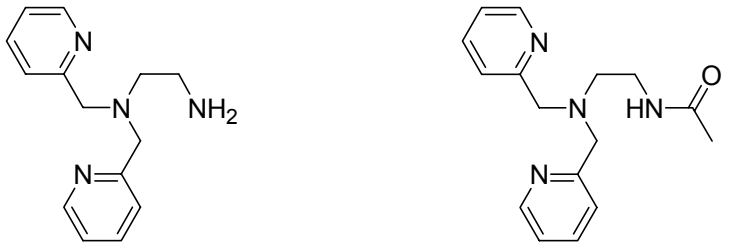

Figure 6-2: ligands uns-penp and acetyl-uns-penp

Corresponding ligand system variations in the small molecule model complexes of copper proteins were made and analysed with respect to dioxygen reactivity.

Intramolecular ligand hydroxylation was observed during the reactions of dioxygen with the dicopper(I) complexes of the ligands L^3 (L^3 = α,α′-bis[(2-pyridylethyl)amino]-*m*-xylene) and L^5 (L^5 = α,α′-bis[*N*-(2-pyridylethyl)-*N*-(2-pyridyl-methyl)-amino]-*m*-xylene). The dinuclear copper(I) complex $[Cu_2L^5](ClO_4)_2$ and the dicopper(II) complex $[Cu_2(L^3\text{-}O)(OH)(ClO_4)]ClO_4$ were characterised by single-crystal X-ray structure analysis. Furthermore, phenolate-bridged complexes were synthesised with the ligand L^4-OH and Me-L^5-OH (structurally characterised:

$[Cu_2(L^4\text{-}O)Cl_3]$ with L^4 = α,α'-bis[*N*-methyl-*N*-(2-pyridylethyl)amino]-*m*-xylene and $[Cu_2(Me\text{-}L^5\text{-}O)(\mu\text{-}X)](ClO_4)_2 \cdot nH_2O$ with Me-L^5-OH = 2,6-bis[*N*-(2-pyridylethyl)-*N*-(2-pyridylmethyl)amino]-4-methylphenol and X = $C_3H_3N_2^-$ (prz), $MeCO_2^-$ and N_3^-; ligands see Figure 6-3). Temperature-dependent magnetic studies revealed the antiferromagnetic coupling of the copper ions of these complexes (Chapter 4).

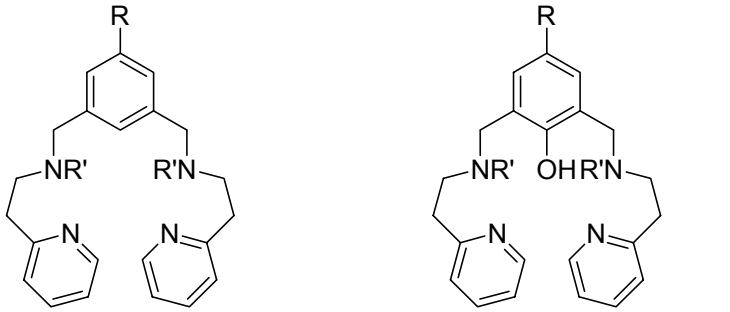

L^3: R' = H, R = H
L^4: R' = CH_3, R = H
L^5: R' = CH_2py, R = H

L^3-OH: R' = H, R = H
L^4-OH: R' = CH_3, R = H
Me-L^5-OH: R' = CH_2py, R = H

Figure 6-3: ligands L^3, L^4, L^5 and L^3-OH, L^4-OH and Me-L^5-OH

The reactions of dioxygen with copper(I) complexes of the tridentate ligands 1,1,4,7,7-pentamethyldiethylethylenetriamine (Me_5dien), 1,1,4,7,7-pentaethyldiethylethylenetriamine (Et_5dien), *N*-methyl-[bis(2-pyridyl)methyl]amine (Me-bpa) and *N*-methyl-[(2-pyridyl)ethyl(2-pyridyl)methyl]amine (MeL) have been investigated using low-temperature stopped-flow techniques. The formation of a bis(μ–oxo) copper complex as a reactive intermediate could only be detected spectroscopically at low temperatures for $[Cu(Me_5dien)(CH_3CN)]ClO_4$ and allowed a quantitative kinetic analysis to be performed. Crystal structures of the copper(II) complexes $[(Me\text{-}bpa)Cu(Cl)_2]$, $[\{(Me\text{-}bpa)Cu(Cl)(ClO_4)\}_2]$, $[\{(MeL)Cu(Cl)(ClO_4)\}_2]$ and $[(MeL)Cu(NCS)_2]$ are reported. (Ligands see Figure 6-4 and Figure 6-5; Chapter 5)

Figure 6-4: Ligands Me_5dien and Et_5dien

Figure 6-5: Ligands MeL and Me-bpa

Kapitel 7 - Zusammenfassung

Zum besseren Verständnis der Reaktionen von Eisen- und Kupferproteinen mit elementarem Sauerstoff wurden im Rahmen dieser Arbeit für Eisen- und Kupferproteine Modellkomplexe mit geringer Molekularmasse mit spektroskopischen oder kinetischen Methoden untersucht. Besondere Aufmerksamkeit wurde hierbei der Bindung und der Aktivierung von elementarem Sauerstoff durch die Eisenproteine, wie z. B. Hämerythrin (Hr) und Protocatechuat-3,4-dioxygenase (3,4-PCD), und die Kupferproteine, wie z. B. Hämocyanin (Hc) und Tyrosinase, gewidmet.

Bezüglich der Modelle für Eisenenzyme wurde der Ligand tmpa (tmpa = tris[(2-pyridyl)methyl]amin; in der Literatur auch mit tpa abgekürzt) untersucht und systematisch variiert. Die Vergrößerung und Verkleinerung der Chelatringgröße im hochreaktiven Komplex [Fe(tmpa)(dbc)] $B(C_6H_5)_4$ (dbc = 3,5-Di-*tert*-butylcatecholat Dianion) führte nur zu einer verringerten Reaktivität der untersuchten Verbindungen (Liganden siehe linke Seite der Abbildung 7-1). Die Reaktion von elementaren Sauerstoff mit [Fe(tmpa)(dbc)]$B(C_6H_5)_4$ wurde mittels der Tieftemperatur-„stopped-flow"-Technik untersucht und ergab die Aktivierungsparameter $\Delta H^{\ddagger}$ = 23 $\pm$ 1 kJ mol^{-1} und $\Delta S^{\ddagger}$ = –199 $\pm$ 4 J mol^{-1} K^{-1} (rechte Seite der Abbildung 7-1: zeitaufgelöste UV-Vis Spektren der Reaktion des Eisnekomplexes mit O_2).

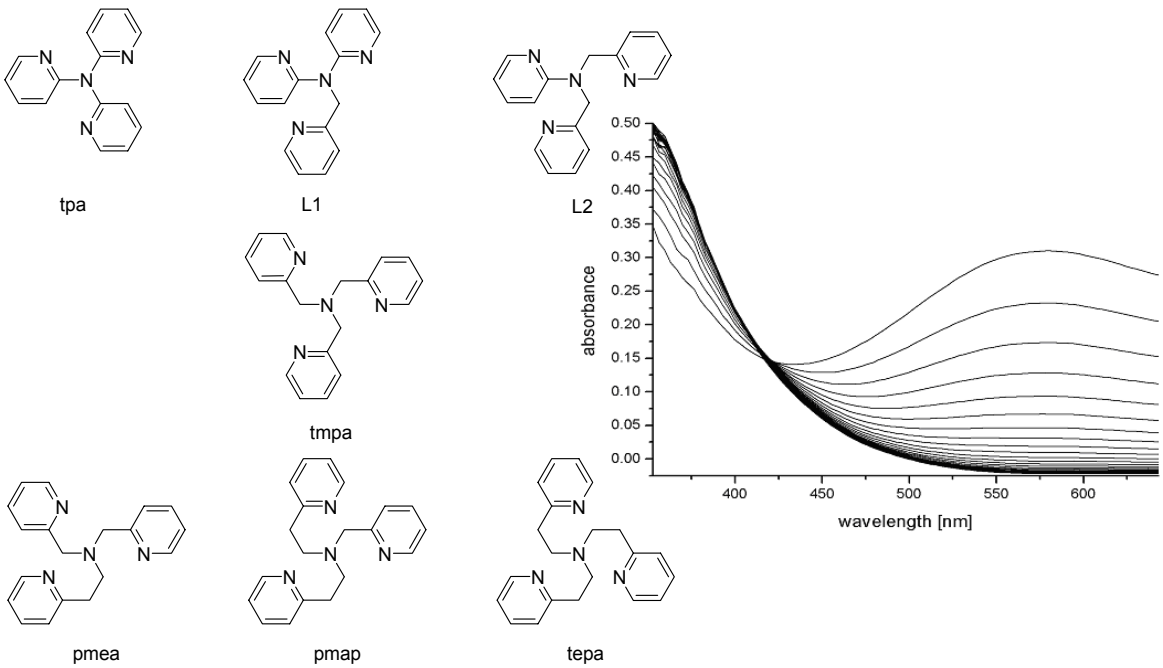

Abbildung 7-1: Liganden abgeleitet von tmpa und UV-Vis Spektrenschar des Eisenkomplexes mit O_2

Weiterhin wurden die Kristallstrukturanalysen der Verbindungen bromo-(tetra-chlorocatecholato-O,O')(bis((2-pyridyl)methyl)-2-pyridylamine-*N*,*N*',*N*'')-eisen(III) (**2**), (μ-oxo)-bis(bromo)(bis((2-pyridyl)methyl)-2-pyridylamine-*N*,*N*',*N*'',*N*''')-dieisen (III) (**3**), dichloro-((2-(2-pyridyl)ethyl)bis((2-pyridyl)methyl)amine-*N*,*N*',*N*'',*N*''')-eisen (III) (**4**) und (tetrabromocatecholato-O,O')((2-(2-pyridyl)ethyl)bis((2-pyridyl)methyl) amine-*N*,*N*',*N*'',*N*''')-eisen (III) (**5**) beschrieben (Kapitel 2).

Neben der Änderung der Chelatringgröße wurde auch der Einfluss der Donoratome des Liganden untersucht. Dazu wurden abgeleitet vom tmpa zwei Liganden (uns-penp und acteyl-uns-penp) synthetisiert, bei denen ein aromatischer Stickstoff durch einen aliphatischen Stickstoff ersetzt wurde (siehe Abbildung 7-2). Die Eisen(III) Komplexe mit den tripodalen Liganden N',N'-bis[(2-pyridyl)methyl]ethylenediamin (uns-penp), $[Fe(uns\text{-}penp)Cl_2]ClO_4$ x CH_3CN, $[\{Fe(uns\text{-}penp)Cl\}_2O](ClO_4)_2$ x $2CH_3CN$ und dem Amidderivat *N*-Acetyl-*N'*,*N'*-bis[(2-pyridyl)methyl]ethylenediamin (acetyl-uns-penp), $[Fe_2(acetyl\text{-}uns\text{-}penp)_2O](ClO_4)_2$ x H_2O, $[Fe(acetyl\text{-}uns\text{-}penp)(tcc)Br]$ x $(C_2H_5)_2O$ und $[\{Fe(acetyl\text{-}uns\text{-}penp)(tcc)\}_2O]$ x $(C_2H_5)_2O{\cdot}CH_3OH$ wurden synthetisiert und charakterisiert. Untersuchungen zur Catecholdioxygenasereaktivität der *in situ* dargestellten Komplexlösungen zeigten nur langsamere Reaktionen im Vergleich zu dem Eisen-tmpa-System (Kapitel 3).

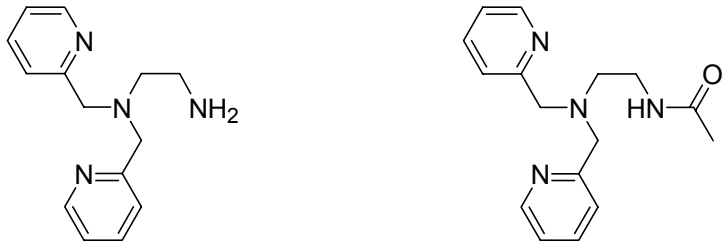

Abbildung 7-2: Die Liganden uns-penp und acetyl-uns-penp

Die Ligandensysteme für Modelle von Kupferproteinen wurden nach denselben Gesichtspunkten verändert wie bei den Modellen für die Eisenproteine.

Intramolekulare Hydroxylierung des Liganden war bei der Reaktion von elementaren Sauerstoff mit Dikupfer(I)-Komplexen der Liganden L^3 (L^3 = α,α′-bis[(2-pyridylethyl)amino]-*m*-xylol) und L^5 (L^5 = α,α′-bis[*N*-(2-pyridylethyl)-*N*-(2-pyridylmethyl)-amino]-*m*-xylol) zu beobachten. Der dinukleare Kupfer(I)-Komplex $[Cu_2L^5](ClO_4)_2$

und der Dikupfer(II)-Komplex $[Cu_2(L^3\text{-}O)(OH)(ClO_4)]ClO_4$ konnten durch Einkristallröntgenstrukturanalyse charakterisiert werden. Zusätzlich wurden Phenolat-verbrückte Komplexe mit den Liganden L^4-OH und Me-L^5-OH synthetisiert (Strukturlösungen für $[Cu_2(L^4\text{-}O)Cl_3]$ mit L^4 = α,α'-bis[*N*-methyl-*N*-(2-pyridylethyl)amino]-*m*-xylol und $[Cu_2(Me\text{-}L^5\text{-}O)(\mu\text{-}X)](ClO_4)_2 \cdot nH_2O$ (Me-L^5-OH = 2,6-bis[*N*-(2-pyridylethyl)-*N*-(2-pyridylmethyl)amino]-4-methylphenol und X = $C_3H_3N_2^-$ (prz), $MeCO_2^-$ und N_3^-); Liganden siehe Abbildung 7-3). Temperaturabhängige magnetische Untersuchungen zeigten antiferromagnetische Kopplung der Kupferionen in diesen Komplexen (Kapitel 4).

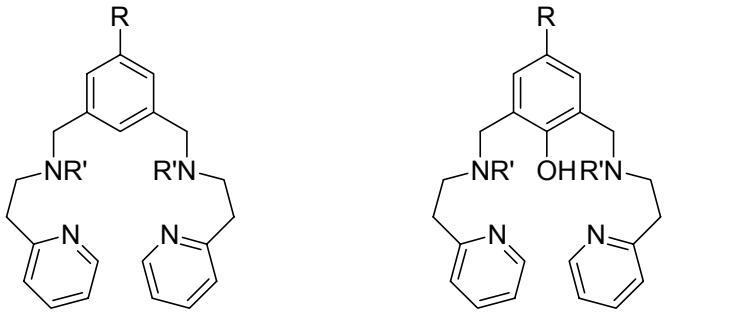

L^3: R' = H, R = H
L^4: R' = CH_3, R = H
L^5: R' = CH_2py, R = H

L^3-OH: R' = H, R = H
L^4-OH: R' = CH_3, R = H
Me-L^5-OH: R' = CH_2py, R = H

Abbildung 7-3: Die Liganden L^3, L^4, L^5 und L^3-OH, L^4-OH und Me-L^5-OH

Die Reaktionen von elementaren Sauerstoff mit Kupfer(I)-Komplexen der dreizähnigen Liganden 1,1,4,7,7-pentamethyldiethylethylenetriamin (Me_5dien), 1,1,4,7,7-pentaethyldiethylethylenetriamin (Et_5dien), *N*-methyl-[bis(2-pyridyl) methyl]amin (Me-bpa) und *N*-methyl-[(2-pyridyl)ethyl(2-pyridyl)methyl]amin (MeL) mit Hilfe der Tieftemperatur-„stopped-flow"-Technik untersucht. Die Bildung eines bis(μ–oxo)-Kupferkomplexes konnte dabei bei tiefen Temperaturen nur für den Komplex $[Cu(Me_5dien)(CH_3CN)]ClO_4$ spektroskopisch beobachtet und quantitativ kinetisch analysiert werden. Die Komplexe $[(Me\text{-}bpa)Cu(Cl)_2]$, $[\{(Me\text{-}bpa)Cu(Cl)(ClO_4)\}_2]$, $[\{(MeL)Cu(Cl)(ClO_4)\}_2]$ und $[(MeL)Cu(NCS)_2]$ konnten kristallographisch charakterisiert werden. (Liganden sieheAbbildung 7-4und Abbildung 7-5; Kapitel 5)

Abbildung 7-4: Die Liganden Me_5dien und Et_5dien

Abbildung 7-5: Die Liganden MeL und Me-bpa

Publications

- Merkel, M.; Pascaly, M.; Krebs, B.; Astner, J.; Foxon, S. P.; Schindler, S., Chelate Ring Size Variations and their Effects on Coordination Chemistry and Catechol Dioxygenase Reactivity of Iron(III) Complexes. *Inorg. Chem.* **2005,** 44, (21), 7582-7589

- Xu, J.-Y.; Astner, J.; Walter, O.; Heinemann, F. W.; Schindler, S.; Merkel, M.; Krebs, B., Iron(III) Complexes with the Ligands *N*',*N*'-bis[(2-pyridyl)methyl]ethylenediamine (uns-penp) and the Amide *N*-Acetyl-*N*'*N*'-bis[(2-pyridyl)methyl]ethylenediamine (acetyl-uns-penp). *Accepted from Eur. J. Inorg. Chem.*

- Foxon, S. P.; Utz, D.; Astner, J.; Schindler, S.; Thaler, F.; Heinemann, F. W.; Liehr, G.; Mukherjee, J.; Balamurugan, V.; Ghosh, D.; Mukherjee, R., Reaction behavior of dinuclear copper(I) complexes with m-xylyl-based ligands towards dioxygen. *J. Chem. Soc., Dalton Trans.* **2004,** 15, 2321-2328

- Astner, J.; Weitzer, M.; Foxon, S. F.; Schindler, S.; Heinemann, F. W.; Mukherjee, J.; Gupta, R.; Mahadevan, V.; Mukherjee, R.; Copper(I) Complexes with Tridentate Ligands and their Reactivity towards Dioxygen. *Submitted to Inorg. Chem.*

Curriculum Vitae

Jörg Rudolf Astner

geboren am 6. August 1974

in Erlangen

ledig

Ausbildung

Adalbert-Stifter-Grundschule, Erlangen	09/81 – 07/85
Emil-von-Behring-Gymnasium, Spardorf	09/85 – 07/94 Allgemeine Hochschulreife
Friedrich-Alexander-Universität, Erlangen-Nürnberg	11/94 – 01/02 Studium der Chemie Thema der Diplomarbeit bei Prof. Dr. S. Schindler: „Kinetische Untersuchungen an Modellkomplexen der Catecholdioxygenase“
Justus-Liebig-Universität, Gießen Institut für Anorganische und Analytische Chemie	01/02 – 01/06 Promotion bei Prof. Dr. S. Schindler mit dem Thema: „Reaction behavior of Iron and Copper Complexes towards Dioxygen“;

Berufstätigkeit

Siemens AG, Erlangen	08/95 – 09/95; 08/97 – 09/97 und 03/98 – 04/98 Werksstudent
DIW Instandhaltung GmbH, Nürnberg	04/00 – 12/00 Reiniger
FAU Erlangen-Nürnberg	1999-2002 Wissenschaftlicher Mitarbeiter
JLU Gießen Institut für Anorganische und Analytische Chemie,	05/02 – 07/05 Wissenschaftlicher Mitarbeiter in den Praktika für Haupt-, Real- und Gymnasiallehramtsstudenten und im Fortgeschrittenenpraktikum für Chemiker

Ausbildungsbegleitende Tätigkeiten

Studentenvertretung,	1995 – 2001
FAU Erlangen-Nürnberg	Kassenwart, studentischer Vertreter in der Fachgruppe und im Fachbereichsrat, Zusatzseminare für Studenten
FAU Erlangen-Nürnberg und	09/98 – 10/98
TU München	Ferienakademie „Katalyse in der Anwendung und Forschung“
Collegium Alexandrinum der	09/00 – 11/00
FAU Erlangen-Nürnberg	Planung und Teilnahme an der experimentellen Vorlesung „Chemische Zaubertricks“ von Prof. van Eldik
FAU Erlangen-Nürnberg und	05/02 – 11/02
JLU Gießen	Organisation und Durchführung des Umzugs der Arbeitsgruppe von Prof. Schindler
Indian Institute of Technology,	02/04 – 04/04
Kanpur, Indien	6 wöchiger Forschungsaufenthalt im Rahmen der Promotion

Bibliography

1. *Star Trek, The Original Series*, Journey to Babel, Season 2, Episode 10 **1967**.

2. Solomon, E. I.; Chen, P.; Metz, M.; Lee, S.-K.; Palmer, A. E., *Angew. Chem.* **2001,** 113, (24), 4702-4724.

3. Lippard, S.; Berg, J., *Bioanorganische Chemie*, Spektrum, Akad. Verlag: Heidelberg, **1995**.

4. Mirica, L. M.; Ottenwaelder, X.; Stack, T. D. P., *Chem. Rev.* **2004,** 104, (2), 1013-1045.

5. Stenkamp, R. E., *Chem. Rev.* **1994,** 94, (3), 715-726.

6. Kaim, W.; Rall, J., *Angew. Chem.* **1996,** 108, 47-64.

7. Jolley, R. L.; Evans, L. H.; Makino, N.; Mason, H. S., *J. Biol. Chem.* **1974,** 249, 335.

8. Costas, M.; Mehn, M. P.; Jensen, M. P.; Que junior, L., *Chem. Rev.* **2004,** 104, (2), 939-986.

9. Que junior, L.; Ho, R. Y. N., *Chem. Rev.* **1996,** 96, (7), 2607-2624.

10. Bugg, T. D. H.; Winfield, C. J., *Nat. Prod. Rep.* **1998,** 15, (5), 513-530.

11. Yamahara, R.; Ogo, S.; Masuda, H.; Watanabe, Y., *Inorg. Biochem* **2002,** 88, (3-4), 284-294.

12. Ohlendorf, D. H.; Lipscomb, J. D.; Weber, P. C., *Nature* **1988,** 336, (6197), 403-405.

13. Ohlendorf, D. H.; Orville, A. M.; Lipscomb, J. D., *J. Mol. Biol.* **1994,** 244, (5), 586-608.

14. Orville, A. M.; Lipscomb, J. D.; Ohlendorf, D. H., *Biochem.* **1997,** 36, (33), 10052-10066.

15. Elgren, T. E.; Orville, A. M.; Kelly, K. A.; Lipscomb, J. D.; Ohlendorf, D. H.; Que junior, L., *Biochem.* **1997,** 36, (38), 11504-11513.

16. Orville, A. M.; Elango, N.; Lipscomb, J. D.; Ohlendorf, D. H., *Biochem.* **1997,** 36, (33), 10039-10051.

17. Fujii, H.; Funahashi, Y., *Angew. Chem. Int. Ed.* **2002,** 41, (19), 3638-3641.

18. Funabiki, T.; Sakamoto, H.; Yoshida, S.; Tamara, L., *J. Chem. Soc., Chem. Commun.* **1979,** 17, 754-755.

19. Funabiki, T.; Mizoguchi, A.; Sugimoto, T.; Tada, S.; Tsuji, M.; Sakamoto, H.; Yoshida, S., *J. Am. Chem. Soc.* **1986,** 108, (11), 2921-2932.

20. Jang, H. G.; Cox, D. D.; Que junior, L., *J. Am. Chem. Soc.* **1991,** 113, (24), 9200-9204.

21. Cox, D. D.; Que junior, L., *J. Am. Chem. Soc.* **1988,** 110, (24), 8085-8092.

22. Cox, D. D.; Benkovic, S.; Bloom, L. M.; Bradley, F. C.; Nelson, M. J.; Que junior, L.; Wallick, D. E., *J. Am. Chem. Soc.* **1988,** 110, (7), 2026-2032.

23. Pascaly, M.; Duda, M.; Schweppe, F.; Zurlinden, K.; Müller, F. K.; Krebs, B., *J. Chem. Soc., Dalt. Trans.* **2001**, (6), 828-838.

24. Dietrich, J.; Heinemann, F. W.; Schrodt, A.; Schindler, S., *Inorg. Chim. Acta* **1999,** 288, (2), 206-209.

25. Schatz, M.; Becker, M.; Thaler, F.; Hampel, F.; Schindler, S.; Jacobson, R. R.; Tyeklár, Z.; Murthy, N. N.; Gosh, P.; Chen, Q.; Zubieta, J.; Karlin, K. D., *Inorg. Chem.* **2001,** 40, (10), 2312-2322.

26. Foxon, S. P.; Walter, O.; Schindler, S., *Eur. J. Inorg. Chem.* **2002**, (1), 111-121.

27. Battino, R., Ed., *Solubility Data Series, Vol. 7: Oxygen and Ozone*, Pergamon Press: New York, **1981**; 519 pp.

28. Yang, W.; Schmider, H.; Wu, Q.; Zhang, Y.; Wang, S., *Inorg. Chem.* **2000,** 39, (11), 2397-2404.

29. Oki, A. R.; Glerup, J.; Hodgson, D. J., *Inorg. Chem.* **1990,** 29, (13), 2435-2441.

30. Hojland, F.; Toftlund, H.; Yde Andersen, S., *Acta Chem. Scand., Series A* **1983,** A37, (3), 251-257.

31. SADABS, *Siemens Area Detector Absorption Correction*, Siemens.

32. Sheldrick, G. M., *SHELX-97*, Universität Göttingen: **1997**.

33. Karlin, K. D.; Kaderli, S.; Zuberbühler, A. D., *Acc. Chem. Res.* **1997,** 30, (3), 139-147.

34. Duda, M.; Pascaly, M.; Krebs, B., *Chem. Comm.* **1997**, (9), 835-836.

35. Merkel, M.; Schnieders, D.; Baldeau, S. M.; Krebs, B., *Eur. J. Inorg. Chem.* **2004**, (4), 783-790.

36. Raffard, N.; Carina, R.; Simaan, A. J.; Sainton, J.; Riviere, E.; Tchertanov, L.; Bourcier, S.; Bouchoux, G.; Delroisse, M.; Banse, F.; Girerd, J.-J., *Eur. J. Inorg. Chem.* **2001**, (9), 2249-2254.

37. Koch, W. O.; Krüger, H.-J., *Angew. Chem. Int. Ed.* **1996,** 34, (23-24), 2671-2674.

38. Feig, A. L.; Becker, M.; Schindler, S.; van Eldik, R.; Lippard, S., *Inorg. Chem.* **1996,** 35, (9), 2590-2601.

39. Becker, M.; Schindler, S.; Karlin, K. D.; Kaden, T. A.; Kaderli, S.; Palanché, T.; Zuberbühler, A. D., *Inorg. Chem.* **1999,** 38, (9), 1989-1995.

40. Schindler, S., *Eur. J. Inorg. Chem.* **2000**, (11), 2311-2326.

41. Merkel, M.; Pascaly, M.; Wieting, M.; Duda, M.; Rompel, A., *Z. Anorg. Allg. Chem.* **2003,** 629, (12-13), 2216-2221.

42. Kojima, T.; Leising, R. A.; Shiping, Y.; Que junior, L., *J. Am. Chem. Soc.* **1993,** 115, (24), 11328-11335.

43. Kucharski, E. S.; R., M. W.; White, A. H., *Aust. J. Chem.* **1978,** 31, (1), 53-56.

44. Kryatov, S. V.; Rybak-Akimova, E. V.; Schindler, S., *Chem. Rev.* **2005,** 105, (6), 2175-2226.

45. Lewis, E. A.; Tolman, W. B., *Chem. Rev.* **2004,** 104, (2), 1047-1076.

46. Simaan, A. J.; Döpner, S.; Banse, F.; Bourcier, S.; Bouchoux, G.; Boussac, A.; Hildebrandt, P.; Girerd, J.-J., *Eur. J. Inorg. Chem.* **2000**, (7), 1627-1633.

47. Simaan, A. J.; Banse, F.; Mialane, P.; Boussac, A.; Un, S.; Kargar-Grisel, T.; Bouchoux, G.; Girerd, J.-J., *Eur. J. Inorg. Chem.* **1999**, (6), 993-996.

48. Hazell, A.; McKenzie, C. J.; Nielsen, L. P.; Schindler, S.; Weitzer, M., *J. Chem. Soc., Dalt. Trans.* **2002**, (3), 310-317.

49. Duelund, L.; Hazell, R.; McKenzie, C. J.; Preuss Nielsen, L.; Toftlund, H., *J. Chem. Soc., Dalt. Trans.* **2001**, (2), 152-156.

50. Bernal, I.; Jensen, I. M.; Jensen, K. B.; McKenzie, C. J.; Toftlund, H.; Tuchagues, J.-P., *J. Chem. Soc., Dalt. Trans.* **1995**, (22), 3667-3675.

51. Kaizer, J.; Klinker, E. J.; Oh, N. Y.; Rohde, J.-U.; Song, W. J.; Stubna, A.; Kim, J.; Münck, E.; Nam, W.; Que junior, L., *J. Am. Chem. Soc.* **2004,** 126, (2), 472-473.

52. Mandel, J.; Maricondi, C.; Douglas, B., *Inorg. Chem.* **1988,** 27, (17), 2990-2996.

53. Schatz, M.; Leibold, M.; Foxon, S. P.; Weitzer, M.; Heinemann, F. W.; Hampel, F.; Walter, O.; Schindler, S., *J. Chem. Soc., Dalt. Trans.* **2003**, (8), 1480-1487.

54. Matouzenko, G. S.; Bousseksou, A.; Lecocq, S.; van Koningsbruggen, P. J.; Perrin, M.; Kahn, O.; Collet, A., *Inorg. Chem.* **1997,** 36, (14), 2975-2981.

55. Davies, C. J.; Fawcett, J.; Shutt, R.; Solan, G. A., *J. Chem. Soc., Dalt. Trans.* **2005**, (15), 2630-2640.

56. Hanaoka, K.; Kikuchi, K.; Urano, Y.; Nagano, T., *J. Chem. Soc., Perkin Trans. 2* **2001**, (9), 1840-1843.

57. Incarvito, C.; Lam, M.; Rhatigan, B.; Rheingold, A. L.; Quin, C. J.; Gavrilova, A. L.; Bosnich, B., *J. Chem. Soc., Dalt. Trans.* **2001**, (23), 3478-3488.

58. Horner, O.; Charlot, M.-F.; Boussac, A.; Un, S.; Kargar-Grisel, T.; Bouchoux, G.; Girerd, J.-J., *Inorg. Chem.* **1999,** 38, (6), 1222-1232.

59. Mandel, J.; Douglas, B., *Inorg. Chim. Acta* **1989,** 155, (1), 55-69.

60. Sigel, H.; Martin, R. B., *Chem. Rev.* **1982,** 82, (4), 385-426.

61. Guajardo, R. J.; Hudson, S. E.; Brown, S. J.; Mascharak, P. K., *J. Am. Chem. Soc.* **1993,** 115, (18), 7971-7977.

62. Marlin, D. S.; Mascharak, P. K., *Chem. Soc. Rev.* **2000,** 29, (1), 69-74.

63. Noveron, J. C.; Olmstead, M. M.; Mascharak, P. K., *J. Am. Chem. Soc.* **2001,** 123, (14), 3247-3259.

64. Huang, W.; Jia, J.; Cummings, J.; Nelson, M.; Schneider, G.; Lindqvist, Y., *Structure* **1997,** 5, (5), 691-699.

65. Nagashima, S.; Nakasako, M.; Dohmae, N.; Tsujimura, M.; Takio, K.; Odaka, M.; Yohda, M.; Kamiya, N.; Endo, I., *Nat. Struct. Biol.* **1998,** 5, (5), 347-351.

66. Afshar, R.; Patra, A. K.; Olmstead, M. M.; Mascharak, P. K., *Inorg. Chem.* **2004,** 43, (18), 5736-5743.

67. Patra, A. K.; Afshar, R.; Rowland, J. M.; Olmstead, M. M.; Mascharak, P. K., *Angew. Chem. Int. Ed.* **2003,** 42, (37), 4517-4521.

68. Patra, A. K.; Rowland, J. M.; Marlin, D. S.; Bill, E.; Olmstead, M. M.; Mascharak, P. K., *Inorg. Chem.* **2003,** 42, (21), 6812-6823.

69. Marlin, D. S.; Olmstead, M. M.; Mascharak, P. K., *Eur. J. Inorg. Chem.* **2002**, (4), 859-865.

70. Patra, A. K.; Afshar, R.; Olmstead, M. M.; Mascharak, P. K., *Angew. Chem. Int. Ed.* **2002,** 41, (14), 2512-2515.

71. Guajardo, R. J.; Chavez, F.; Farinas, E. T.; Mascharak, P. K., *J. Am. Chem. Soc.* **1995,** 117, (13), 3883-3884.

72. Rowland, J. M.; Olmstead, M. M.; Mascharak, P. K., *Inorg. Chim. Acta* **2002,** 332, (1), 37-40.

73. Patra, A. K.; Mascharak, P. K., *Inorg. Chem.* **2003,** 42, (23), 7363-7365.

74. Müller, H.; Seidel, W.; Görls, H., *J. Organomet. Chem.* **1994,** 472, (1-2), 215-220.

75. Kryatov, S. V.; Nazarenko, A.; Robinson, P. D.; Rybak-Akimova, E. V., *Chem. Comm.* **2000**, (11), 921-922.

76. Kurtz junior, D. M., *Chem. Rev.* **1990,** 90, (4), 585-606.

77. Bugg, T. D. H.; Lin, G., *Chem. Comm.* **2001**, (11), 941-952.

78. Yamahara, R.; Ogo, S.; Masuda, H.; Watanabe, Y., *J. Inorg. Biochem.* **2002,** 91, (1), 151-158.

79. Jo, D.-H.; Que junior, L., *Angew. Chem. Int. Ed.* **2000,** 39, (23), 4284-4287.

80. Velusamy, M.; Palaniandavar, M., *Inorg. Chem.* **2003,** 42, (25), 8283-8293.

81. Viswanathan, R.; Palaniandavar, M.; Balasubramanian, T.; Muthiah, T. P., *Inorg. Chem.* **1998,** 37, (12), 2943-2951.

82. Merkel, M.; Müller, F. K.; Krebs, B., *Inorg. Chim. Acta* **2002,** 337, (all), 308-316.

83. Mialane, P.; Anxolabéhère-Mallart, E.; Blondin, G.; Nivorojkine, A.; Guilhem, J.; Tchertanova, L.; Cesario, M.; Ravi, N.; Bominaar, E.; Girerd, J.-J.; Münck, E., *Inorg. Chim. Acta* **1997,** 263, (1-2), 367-378.

84. Spartalian, K.; Carrano, C. J., *Inorg. Chem.* **1989,** 28, (1), 19-24.

85. Heistand II, R. H.; Roe, L. A.; Que junior, L., *Inorg. Chem.* **1982,** 21, (2), 676-681.

86. Heistand II, R. H.; Lauffer, R. B.; Fikrig, E.; Que junior, L., *J. Am. Chem. Soc.* **1982,** 104, (10), 2789-2796.

87. Merkel, M.; Pascaly, M.; Krebs, B.; Astner, J.; Foxon, S. P.; Schindler, S., *Inorg. Chem.* **2005,** 44, (21), 7582-7589.

88. Vetting, M. W.; D' Argenio, D. A.; Ornston, L. N.; Ohlendorf, D. H., *Biochem.* **2000,** 39, (27), 7943-7955.

89. Davis, M. I.; Orville, A. M.; Neese, F.; Zaleski, J. M.; Lipscomb, J. D.; Solomon, E. I., *J. Am. Chem. Soc.* **2002,** 124, (4), 602-614.

90. Moon, D.; Lah, M. S.; Sesto, R. E. D.; Miller, J. S., *Inorg. Chem.* **2002,** 41, (18), 4708-4714.

91. Pascaly, M.; Duda, M.; Rompel, A.; Sift, B. H.; Meyer-Klaucke, W.; Krebs, B., *Inorg. Chim. Acta* **1999,** 291, (1-2), 289-299.

92. Nishida, Y.; Okuno, T.; Ito, S.; Harada, A.; Ohba, S.; Matsushima, H.; Tokii, T., *Chem. Lett.* **1995**, (10), 885-886.

93. Wilkinson, E. C.; Dong, Y.; Que junior, L., *J. Am. Chem. Soc.* **1994,** 116, (18), 8394-8395.

94. Kwak, B.; Cho, K. W.; Pyo, M.; Lah, M. S., *Inorg. Chim. Acta* **1999,** 290, (1), 21-27.

95. Whittlesey, B. R.; Pang, Z.; Holwerda, R. A., *Inorg. Chim. Acta* **1999,** 284, (1), 124-126.

96. Itoh, S.; Okuno, T.; Matsushima, H.; Tokii, T.; Nishida, Y., *J. Chem. Soc., Dalt. Trans.* **1996**, (23), 4479-4484.

97. Hazell, A.; Jensen, K. B.; McKenzie, C. J.; Toftlund, H., *Inorg. Chem.* **1994,** 33, (14), 3127-3134.

98. Buchanan, R. M.; Chen, S.; Richardson, J. F.; Bressan, M.; Forti, L.; Morvillo, A.; Fish, R. H., *Inorg. Chem.* **1994,** 33, (15), 3208-3209.

99. Dong, Y.; Fujii, H.; Hendrich, M. P.; Leising, R. A.; Pan, G.; Randall, C. R.; Wilkinson, E. C.; Zang, Y.; Que junior, L., *J. Am. Chem. Soc.* **1995,** 117, (10), 2778-2792.

100. Norman, R. E.; Yan, S.; Que junior, L.; Backes, G.; Ling, J.; Sanders-Loehr, J.; Zhang, J. H.; O'Connor, C. J., *J. Am. Chem. Soc.* **1990,** 112, (4), 1554-1562.

101. Yan, S.; Cox, D. D.; Pearce, L. L.; Juarez-Garcia, C.; Que junior, L.; Zhang, J. H.; O'Connor, C. J., *Inorg. Chem.* **1989,** 28, (13), 2507-2509.

102. Musie, G.; Lai, C.-H.; Reibenspies, J. H.; Sumner, L. W.; Darensbourg, M. Y., *Inorg. Chem.* **1998,** 37, (16), 4086-4093.

103. Rowland, J. M.; Olmstead, M. M.; Mascharak, P. K., *Inorg. Chem.* **2001,** 40, (12), 2810-2817.

104. Hanaoka, K.; Kikuchi, K.; Kojima, H.; Urano, Y.; Nagano, T., *Angew. Chem. Int. Ed.* **2003,** 42, (26), 2996-2999.

105. Ghosh, K.; Eroy-Reveles, A. A.; Avila, B.; Holman, T. R.; Olmstead, M. M.; Mascharak, P. K., *Inorg. Chem.* **2004,** 43, (9), 2988-2997.

106. Coppens, P., *Crystallographic Computing*, Eds. Ahmed, F. R.; Hall, S. R.; Huber, C. P., Munksgard, Copenhagen, **1970**; 255-270.

107. SHELXTL NT 6.12; Bruker AXS, Inc.: Madison, WI, U.S.A., 2002.

108. Decker, H.; Dillinger, R.; Tuczek, F., *Angew. Chem. Int. Ed.* **2000,** 39, (9), 1591-1595.

109. Solomon, E. I.; Sundaram, U. M.; Machonkin, T. E., *Chem. Rev.* **1996,** 96, (7), 2563-2606.

110. Lerch, K., *ACS Symp. Ser.* **1995,** 600, 64-80.

111. Sánchez-Ferrer, Á.; Rodriguéz-López, J. N.; García-Cánovas, F.; García-Carmona, F., *Biochim. Biophys. Acta* **1995,** 1247, (1), 1-11.

112. Karlin, K. D.; Hayes, J. C.; Gultneth, Y.; Cruse, R. W.; McKnown, J. W.; Hutchinson, J. P.; Zubieta, J., *J. Am. Chem. Soc.* **1984,** 106, (7), 2121-2128.

113. Karlin, K. D.; Dahlstrom, P. L.; Cozzette, S. N.; Scensny, P. M.; Zubieta, J., *J. Chem. Soc., Chem. Commun.* **1981**, (17), 881-882.

114. Pidcock, E.; DeBeer, S.; Obias, H. V.; Hedman, B.; Hodgson, K. O.; Karlin, K. D.; Solomon, E. I., *J. Am. Chem. Soc.* **1999,** 121, (9), 1870-1878.

115. Karlin, K. D.; Nasir, M. S.; Cohen, B. I.; Cruse, R. W.; Kaderli, S.; Zuberbühler, A. D., *J. Am. Chem. Soc.* **1994,** 116, (4), 1324-1336.

116. Cruse, R. W.; Kaderli, S.; Karlin, K. D.; Zuberbühler, A. D., *J. Am. Chem. Soc.* **1988,** 110, (20), 6882-6883.

117. Holland, P. L.; Rodgers, K. R.; Tolman, W. B., *Angew. Chem. Int. Ed.* **1999,** 38, (8), 1139-1142.

118. Battaini, G.; Casella, L.; Gullotti, M.; Monzani, E.; Nardin, G.; Perotti, A.; Randaccio, L.; Santagostini, L.; Heinemann, F. W.; Schindler, S., *Eur. J. Inorg. Chem.* **2003**, (6), 1197-1205.

119. Blackman, A. G.; Tolman, W. B., *Struct. Bonding (Berlin)* **2000,** 97, 179-211.

120. Karlin, K. D.; Tyeklár, Z.; Zuberbühler, A. D., *Bioinorganic Catalysis*, Ed. Reedijk, J., Marcel Dekker, Inc., **1993**.

121. Sorrell, T. N., *Tetrahedron* **1989,** 45, (1), 3-68.

122. Mahapatra, S.; Kaderli, S.; Llobet, A.; Neuhold, Y.-M.; Palanché, T.; Halfen, J. A.; Young junior, V. G.; Kaden, T. A.; Que junior, L.; Zuberbühler, A. D.; Tolman, W. B., *Inorg. Chem.* **1997,** 36, (27), 6343-6356.

123. Casella, L.; Gullotti, M.; Bartosek, M.; Pallanza, G.; Laurenti, E., *J. Chem. Soc., Chem. Commun.* **1991**, (18), 1235-1237.

124. Sorrell, T. N.; Vankai, V. A.; Garrity, M. L., *Inorg. Chem.* **1991,** 30, (2), 207-210.

125. Sorrell, T. N.; Garrity, M. L., *Inorg. Chem.* **1991,** 30, (2), 210-215.

126. Ma, H.; Allmendinger, M.; Thewalt, U.; Lentz, A.; Klinga, M.; Rieger, B., *Eur. J. Inorg. Chem.* **2002**, (11), 2857-2867.

127. Utz, D.; Heinemann, F. W.; Hampel, F.; Richens, D. T.; Schindler, S., *Inorg. Chem.* **2003,** 42, (5), 1430-1436.

128. Ryan, S.; Adams, H.; Fenton, D. E.; Becker, M.; Schindler, S., *Inorg. Chem.* **1998,** 37, (9), 2134-2140.

129. Becker, M.; Schindler, S.; van Eldik, R., *Inorg. Chem.* **1994,** 33, (24), 5370-5371.

130. Menif, R.; Martell, A. E.; Squattrito, P. J.; Clearfield, A., *J. Am. Chem. Soc.* **1990,** 29, (23), 4723-4729.

131. Menif, R.; Martell, A. E., *J. Chem. Soc., Chem. Commun.* **1989**, (20), 1521-1523.

132. Gelling, O. J.; van Bolhuis, F.; A., M.; Feringa, B. L., *J. Chem. Soc., Chem. Commun.* **1988**, (8), 552-554.

133. Casella, L.; Gullotti, M.; Pallanza, G.; Rigoni, L., *J. Am. Chem. Soc.* **1988,** 110, (13), 4221-4227.

134. Casella, L.; Gullotti, M.; Pallanza, G., *Biochem. Soc. Trans.* **1988,** 16, (5), 821-822.

135. Casella, L.; Rigoni, L., *Rev. Port. Quim.* **1985,** 27, 301.

136. Drew, M. G. B.; Trocha-Grimshaw, J.; McKillop, K. P., *Polyhedron* **1989,** 8, (20), 2513-2515.

137. Schindler, S.; Elias, H., *Z. Naturforsch.* **1990,** 45b, 607-618.

138. Lorösch, J.; Haase, W., *Inorg. Chim. Acta* **1985,** 108, (1), 35-40.

139. Mandal, S. K.; Nag, K., *J. Chem. Soc., Dalt. Trans.* **1984**, (10), 2141-2149.

140. Grzybowski, J. J.; Merell, P. H.; Urbach, F. L., *Inorg. Chem.* **1978,** 17, (11), 3078-3082.

141. Dickson, I. E.; Robson, R., *Inorg. Chem.* **1974,** 13, (6), 1301-1306.

142. Abdel-Magid, A. F.; Carson, K. G.; Harris, B. D.; Maryanoff, C. A.; Shah, R. D., *J. Org. Chem.* **1996,** 61, (11), 3849-3862.

143. Ghosh, D.; Mukherjee, R., *Inorg. Chem.* **1998,** 37, (26), 6597-6605.

144. Ghosh, D.; Lal, T. K.; Ghosh, S.; Mukherjee, R., *J. Chem. Soc., Chem. Commun.* **1996**, (1), 13-14.

145. Farrugia, L. J., *J. Appl. Cryst.* **1997,** 30, (5 Pt. 1), 565.

146. Addison, W.; Rao, T. N.; Reedijk, J.; van Rijn, J.; Verschoor, G. C., *J. Chem. Soc., Dalt. Trans.* **1984**, (7), 1349-1356.

147. Karlin, K. D.; Hayes, J. C.; Hutchinson, J. P.; Zubieta, J., *Inorg. Chim. Acta* **1983,** 78, (4), L45-L46.

148. Murthy, N. N.; Mahroof-Tahir, M.; Karlin, K. D., *Inorg. Chem.* **2001,** 40, (4), 628-635.

149. Belle, C.; Beguin, C.; Gautier-Luneau, I.; Hamman, S.; Philouze, C.; Pierre, J.-L.; Thomas, F.; Torelli, S.; Saint-Aman, E.; Bonin, M., *Inorg. Chem.* **2002,** 41, (3), 479-491.

150. Majeste, R. J.; Klein, C. L.; Stevens, E. D., *Acta Cryst. Sect. C, Cryst. Struct. Commun.* **1983,** C39, (1), 52-54.

151. Karlin, K. D.; Farooq, A.; Hayes, J. C.; Cohen, B. I.; Rowe, T. M.; Sinn, E.; Zubieta, J., *Inorg. Chem.* **1987,** 26, (8), 1271-1280.

152. Kamaras, P.; Cajulis, M. C.; Rapta, M.; Brewer, G.; Jameson, G. B., *J. Am. Chem. Soc.* **1994,** 16, (22), 10334-10335.

153. Gupta, R.; Mukherjee, R., *Polyhedron* **2000,** 19, (6), 719-724.

154. Mukherjee, R., *Chapter on Copper*, Eds. McCleverty, J. A.; Meyer, T. J., Volume Ed: Fenton, D. E., Comprehensive Coordination Chemistry-II: From Biology to NanotechnologyElsevier/Pergamon, Amsterdam, **2003**; Vol. 6, 747-910.

155. Ghosh, D.; Lal, T. K.; Ghosh, S.; Mukherjee, R., *Chem. Commun.* **1996**, 13.

156. Karlin, K. D.; Cohen, B. I.; Hayes, J. C.; Farooq, A.; Zubieta, J., *Inorg. Chem.* **1987,** 26, (1), 147-153.

157. Kubas, G. J.; Monzyk, B.; Crumbliss, A. L., *Inorg. Synth.* **1979,** 19, 90-92.

158. Evans, D. F., *J. Chem. Soc., Abstracts* **1959**, 2003-2005.

159. O'Connor, C. J., *Prog. Inorg. Chem.* **1982,** 29, 203-283.

160. Weitzer, M.; Schatz, M.; Hampel, F.; Heinemann, F. W.; Schindler, S., *J. Chem. Soc., Dalt. Trans.* **2002**, (5), 686-694.

161. Mahapatra, S.; Gupta, N.; Mukherjee, R., *J. Chem. Soc., Dalt. Trans.* **1992**, (20), 3041-3045.

162. Geary, W. J., *Coord. Chem. Rev.* **1971,** 7, (1), 81-122.

163. Farrugia, L. J., *J. Appl. Cryst.* **1999,** 32, (4), 837-838.

164. SADABS, *Bruker-AXS, Inc.*, Madison, WI, U.S.A., **2002**.

165. Reedijk, J.; Bouwman, E.; Editors, *Bioinorganic Catalysis, Second Edition, Revised and Expanded*, **1999**; 606 pp.

166. Schatz, M.; Raab, V.; Foxon, S. P.; Brehm, G.; Schneider, S.; Reiher, M.; Holthausen, M. C.; Sundermeyer, J.; Schindler, S., *Angew. Chem. Int. Ed.* **2004,** 43, (33), 4360-4363.

167. Hatcher, L. Q.; Karlin, K. D., *J. Biol. Inorg. Chem.* **2004,** 9, (6), 669-683.

168. Jacobson, R. R.; Tyeklár, Z.; Farooq, A.; Karlin, K. D.; Liu, S.; Zubieta, J., *J. Am. Chem. Soc.* **1988,** 110, (11), 3690-3692.

169. Holland, P. L.; Cramer, P. J.; Wilkinson, E. C.; Mahapatra, S.; Rodgers, K. R.; Itoh, S.; Taki, M.; Fukuzumi, S.; Que junior, L.; Tolman, W. B., *J. Am. Chem. Soc.* **2000,** 122, (5), 792-802.

170. Kitajima, N.; Fujisawa, K.; Fujimoto, C.; Moro-oka, Y.; Hashimoto, S.; Kitegawa, T.; Toriumi, K.; Tatsumi, K.; Nakamura, A., *J. Am. Chem. Soc.* **1992,** 114, (4), 1277-1291.

171. Obias, H. V.; Lin, Y.; Murthy, N. N.; Pidcock, E.; Solomon, E. I.; Ralle, M.; Blackburn, N. J.; Neuhold, Y.-M.; Zuberbühler, A. D.; Karlin, K. D., *J. Am. Chem. Soc.* **1998,** 120, (49), 12960-12961.

172. Cole, A. P.; Mahadevan, V.; Mirica, L. M.; Ottenwaelder, X.; Stack, T. D. P., *Inorg. Chem.* **2005,** 44, (21), 7345-7364.

173. Sanyal, I.; Mahroof-Tahir, M.; Nasir, M. S.; Ghosh, P.; Cohen, B. I.; Gultneth, Y.; Cruse, R. W.; Farrugia, L. J.; Karlin, K. D.; Liu, S.; Zubieta, J., *Inorg. Chem.* **1992,** 31, (21), 4322-4332.

174. Itoh, S.; Taki, M.; Nakao, H.; Holland, P. L.; Tolman, W. B.; Que junior, L.; Fukuzumi, S., *Angew. Chem. Int. Ed.* **2000,** 39, (2), 398-400.

175. Cole, A. P.; Root, D. E.; Mukherjee, P.; Solomon, E. I.; Stack, T. D. P., *Science* **1996,** 273, (5283), 1848-1850.

176. Osako, T.; Tachi, Y.; Taki, M.; Fukuzumi, S.; Itoh, S., *Inorg. Chem.* **2001,** 40, (26), 6604-6609.

177. Que junior, L.; Tolman, W. B., *Angew. Chem. Int. Ed.* **2002,** 41, (7), 1114-1137.

178. Halfen, J. A.; Mahapatra, S.; Wilkinson, E. C.; Kaderli, S.; Young junior, V. G.; Que junior, L.; Zuberbühler, A. D.; Tolman, W. B., *Science* **1996,** 271, (5254), 1397-1400.

179. Weitzer, M.; Schindler, S.; Brehm, G.; Schneider, G.; Hörmann, E.; Jung, B.; Kaderli, S.; Zuberbühler, A. D., *Inorg. Chem.* **2003,** 42, (6), 1800-1806.

180. Becker, M.; Heinemann, F. W.; Schindler, S., *Chem. Eur. J.* **1999,** 5, (11), 3124-3129.

181. Scott, M. J.; Holm, R. H., *J. Am. Chem. Soc.* **1994,** 116, (25), 11357-11367.

182. Gampp, H.; Maeder, M.; Meyer, C. J.; Zuberbühler, A. D., *Talanta* **1985,** 32, (2), 95-101.

183. North, A. C. T.; Phillips, D. C.; Mathews, F. S., *Acta Cryst. Sect. A, Foundations of Crystallography* **1968,** A24, (3), 351-359.

184. Coppens, P., *Evaluation of absorption and extinction in single-crystal structure analysis*, Eds. Ahmed, F. R.; Hall, S. R.; Huber, C. P., Crystallogr. Comput., Proc. Int. Summer Sch.Munksgard, Copenhagen, **1970**; 255-270.

185. Farrugia, L. J. WINGX ver 1.61, An Integrated Systems of Windows programs for the Solution, Refinement and Analysis of Single-Crystal X-ray Diffraction data; Department of Chemistry, University of Glasgow, 2004.

186. Gupta, R.; Mukherjee, S.; Mahapatra, S.; Ray, M.; Mukherjee, R., *Inorg. Chem.* **1992,** 31, (1), 139-141.

187. Romary, J. K.; Zachariasen, R. D.; Barger, J. D.; Schiesser, H., *J. Chem. Soc. C* **1968**, (23), 2884-7.

188. de Bruin, B.; Verhagen, J. A. W.; Schouten, C. H. J.; Gal, A. W.; Feichtinger, D.; Plattner, D. A., *Chem. Eur. J.* **2001,** 7, (2), 416-422.

189. Mukherjee, J.; Balamurugan, V.; Gupta, R.; Mukherjee, R., *J. Chem. Soc., Dalt. Trans.* **2003**, (19), 3686-3692.

190. Jensen, K. B.; McKenzie, C. J.; Simonsen, O.; Toftlund, H.; Hazell, A., *Inorg. Chim. Acta* **1997,** 257, (2), 163-172.

191. Houben, J.; Weyl, T., *Methoden der Organischen Chemie*, 4 ed.; G. Thieme Verlag, Stuttgart, **1957**; Vol. XI(I), 650-654.

192. Clarke, H. T.; Gillespie, H. B.; Weisshaus, S. Z., *J. Am. Chem. Soc.* **1933,** 55, (11), 4571-4587.

193. Moore, M. L., *Org. Reactions* **1949,** 5, 301-330.

194. Eschweiler, W., *Ber. Deutsch. Chem. Gesell.* **1905,** 38, 880-882.

195. Abdel-Magid, A. F.; Carson, K. G.; Harris, B. D.; Maryanoff, C. A.; Shah, R. D., *J. Org. Chem.* **1996,** 61, 3849-3862.

196. Osako, T.; Ueno, Y.; Tachi, Y.; Itoh, S., *Inorg. Chem.* **2003,** 42, (24), 8087-8097.

197. Lee, D. H.; Murthy, N. N.; Lin, Y.; Nasir, N. S.; Karlin, K. D., *Inorg. Chem.* **1997,** 36, (27), 6328-6334.

198. Liang, H.-C.; Zhang, C. X.; Henson, M. J.; Sommer, R. D.; Hatwell, K. R.; Kaderli, S.; Zuberbühler, A. D.; Rheingold, A. L.; Solomon, E. I.; Karlin, K. D., *J. Am. Chem. Soc.* **2002,** 124, (16), 4170-4171.

199. Liang, H.-C.; Henson, M. J.; Hatcher, L. Q.; Vance, M. A.; Zhang, C. X.; Lahti, D.; Kaderli, S.; Sommer, R. D.; Rheingold, A. L.; Zuberbühler, A. D.; Solomon, E. I.; Karlin, K. D., *Inorg. Chem.* **2004,** 43, (14), 4115-4117.

200. Balamurugan, V.; Mukherjee, J.; Hundal, M. S.; Mukherjee, R., *J. Mol. Struct.* **2005,** in press.

201. Mukherjee, J.; Gupta, R.; Mallah, T.; Mukherjee, R., *Inorg. Chim. Acta* **2005,** 358, (9), 2711-2717.

202. Mukherjee, J.; Balamurugan, V.; Hundal, M. S.; Mukherjee, R., *J. Chem. Sci.* **2005,** 117, (2), 111-116.

203. Scott, M. J.; Zhang, H. H.; Lee, S. C., *J. Am. Chem. Soc.* **1995,** 117, (1), 568-569.

204. Breeze, S. R.; Wang, S., *Inorg. Chem.* **1996,** 35, (11), 3404-3408.

205. Scott, M. J.; Goddard, C. A.; Holm, R. H., *Inorg. Chem.* **1996,** 35, (9), 2558-2567.

206. Kickelbick, G., *Acta Cryst. Sect. E, Struct. Rep. Online* **2001,** E57, (8), m365-m367.

207. Brennan, T. F.; Davies, G.; El-Sayed, M. A.; El-Shazly, M. F.; Rupich, M. W.; Veidis, M., *Inorg. Chim. Acta* **1981,** 51, (1), 45-48.

208. Scott, M. J.; Lee, S. C.; Holm, R. H., *Inorg. Chem.* **1994,** 33, (21), 4651-4662.

209. Elder, M.; McKenzie, E. D., *Inorg. Chim. Acta* **1978,** 31, 211-215.

210. Lee, D. H.; Murthy, N. N.; Karlin, K. D., *Inorg. Chem.* **1996,** 35, (4), 804-805.

211. Bürger, K.-S.; Chauduri, P.; Wieghardt, K., *Inorg. Chem.* **1996,** 35, (9), 2704-2707.

212. Jiang, F.; Conry, R. R.; Bubacco, L.; Tyeklár, Z.; Jacobson, R. R.; Karlin, K. D.; Peisach, J., *J. Am. Chem. Soc.* **1993,** 115, (6), 2093-2102.

213. Tolman, W. B., *Acc. Chem. Res.* **1997,** 30, (6), 227-237.

214. Liang, H.-C.; Henson, M. J.; Hatcher, L. Q.; Vance, M. A.; Zhang, C. X.; Lahti, D.; Kaderli, S.; Sommer, R. D.; Rheingold, A. L.; Zuberbühler, A. D.; Solomon, E. I.; Karlin, K. D., *Inorg. Chem.* **2004,** 43, 4115-4117.

215. Liang, H.-C.; Karlin, K. D.; Dyson, R.; Kaderli, S.; Jung, B.; Zuberbühler, A. D., *Inorg. Chem.* **2000,** 39, (26), 5884-5894.

216. Henson, M. J.; Vance, M. A.; Zhang, C. X.; Liang, H.-C.; Karlin, K. D.; Solomon, E. I., *J. Am. Chem. Soc.* **2003,** 125, (17), 5186-5192.

217. Liang, H.-C.; Zhang, C. X.; Henson, M. J.; Sommer, R. D.; Hatwell, K. R.; Kaderli, S.; Zuberbühler, A. D.; Rheingold, A. L.; Solomon, E. I.; Karlin, K. D., *J. Am. Chem. Soc.* **2002,** 124, 4170-4171.

218. Obias, H. V.; Lin, Y.; Murthy, N. N.; Pidcock, E.; Solomon, E. I.; Ralle, M.; Blackburn, N. J.; Neuhold, Y.-M.; Zuberbühler, A. D.; Karlin, K. D., *J. Am. Chem. Soc.* **1998,** 120, 12960-12961.

219. Halfen, J. A.; Mahapatra, S.; Wilkinson, E. C.; Kaderli, S.; Young Jr., V. G.; Que Jr., L.; Zuberbühler, A. D.; Tolman, W. B., *Science* **1996,** 271, 1397-1400.

220. Mahapatra, S.; Kaderli, S.; Llobet, A.; Neuhold, Y.-M.; Palanché, T.; Halfen, J. A.; Young Jr., V. G.; Kaden, T. A.; Que Jr., L.; Zuberbühler, A. D.; Tolman, W. B., *Inorg. Chem.* **1997,** 36, 6343-6356.

221. Osako, T.; Terada, S.; Tosha, T.; Nagatomo, S.; Furutachi, H.; Fujiunami, S.; Kitagawa, T.; Suzuki, M.; Itoh, S., *J. Chem. Soc., Dalt. Trans.* **2005**, (21), 3514-3521.

222. Verdaguer, M.; Gouteron, J.; Jeannin, S.; Jeannin, Y.; Kahn, O., *Inorg. Chem.* **1984,** 23, (25), 4291-4296.

223. Escuer, A.; Font-Bardia, M.; Penalba, E.; Solans, X.; Vicente, R., *Inorg. Chim. Acta* **1999,** 286, (2), 189-196.

224. Sletten, J.; Hope, H.; Julve, M.; Kahn, O.; Verdaguer, M.; Dvorkin, A., *Inorg. Chem.* **1988,** 27, (3), 542-549.

225. Escuer, A.; Font-Bardia, M.; Penalba, E.; Solans, X.; Vicente, R., *Inorg. Chim. Acta* **2000,** 298, (2), 195-201.